NASA CR-166789

BTS → BUSINESS AND TECHNOLOGICAL SYSTEM
AEROSPACE BUILDING
10210 GREENBELT ROAD
SEABROOK, MARYLAND 20801

For: 253.1

Publication Branch, Code ~~251~~
NASA/Goddard Space Flight Center
Greenbelt, Maryland 20771

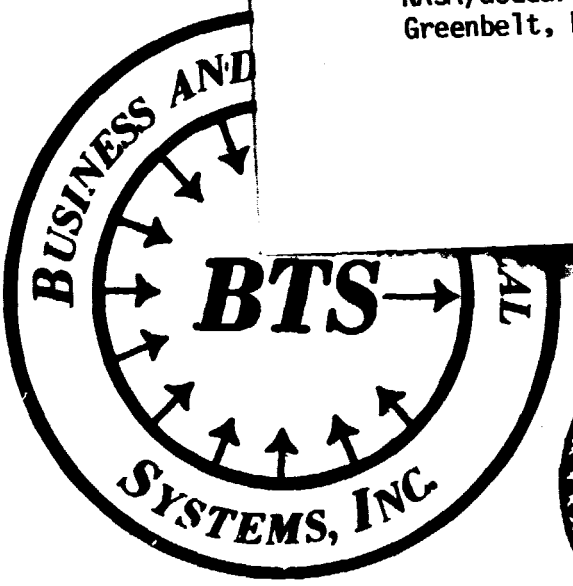

(NASA-CR-166789) CONTEXT SENSITIVE FORMULATIONS OF ANTENNA PATTERN CORRECTION AND SIDE LOBE COMPENSATION FOR NOSS/LAMMR REAL TIME PROCESSING Final Report (Business and Technological Systems, Inc.) 157 p

N82-21457

HC A08/MF A01

G3/32

Unclas
18303

BTS-FR-81-165

October 7, 1981

CONTEXT SENSITIVE FORMULATIONS OF ANTENNA PATTERN CORRECTION AND SIDE LOBE COMPENSATION FOR NOSS/LAMMR REAL TIME PROCESSING

BY

Dr. Roland T. Chin

Dr. Paul R. Beaudet

IN RESPONSE TO

Contract No. NAS 5-26541

SUBMITTED TO

NATIONAL AERONAUTICS AND SPACE ADMINISTRATION

Goddard Space Flight Center

Greenbelt, Maryland 20771

SUBMITTED BY

BUSINESS AND TECHNOLOGICAL SYSTEMS, INC.

Aerospace Building, Suite 440

10210 Greenbelt Road

Seabrook, Maryland 20706

TABLE OF CONTENTS

TABLE OF CONTENTS CONTINUED

1.0 INTRODUCTION

The Large Antenna Multi-channel Microwave Radiometer (LAMMR) is a mechanically scanned multi-frequency passive microwave sensor that receives power emanating from the surface of the earth in seven spectral channels for both horizontal and vertical polarizations. The seven microwave frequency bands lie between 4.3 and 36.5 GHz and are extracted using a single high-gain antenna which scans the earth at one revolution per second, mapping its surface and atmosphere. The geophysical properties of sea surface temperature, oceanic wind speed, precipitation, water vapor, sea ice concentration, snow and land presence can be inferred from the antenna brightness temperatures. The finite parabolic antenna receives significant energy within .26 to 1.3 degrees depending upon microwave frequency, but also receives some non-negligible side lobe energy. The LAMMR embodies a 4.0 meter aperture antenna which scans the earth in a circle of 43.6° half cone angle from nadir. Data sampling occurs during the forward 150° of rotation as shown in Figure 1.1. Table 1.1 shows the major LAMMR characteristics.

LAMMR software specifications have been written for LAMMR ground processing. There is a need to determine more computationally-efficient antenna temperature correction methods in compensating side lobe contributions especially near continents, islands, and weather fronts. In a previous study,[+] antenna patterns were shown to be digitally modifiable and alternative philosophies were established for Antenna Pattern Corrections (APC). One of the major realizations of this study was that APC processes did not accomplish the implied goals of compensating for the antenna side lobe influences on brightness temperature. A-priori knowledge of land/water locations was shown to be needed and had to be incorporated in a context sensitive APC process if the artifacts caused by land presence is to be avoided. The high temperatures in land regions

[+]Alternative Formulations of Antenna Pattern Correction For NOSS/LAMMR Real Time Processing, BTS Report BTS-FR-81-153 under contract No. NAS 5-26280.

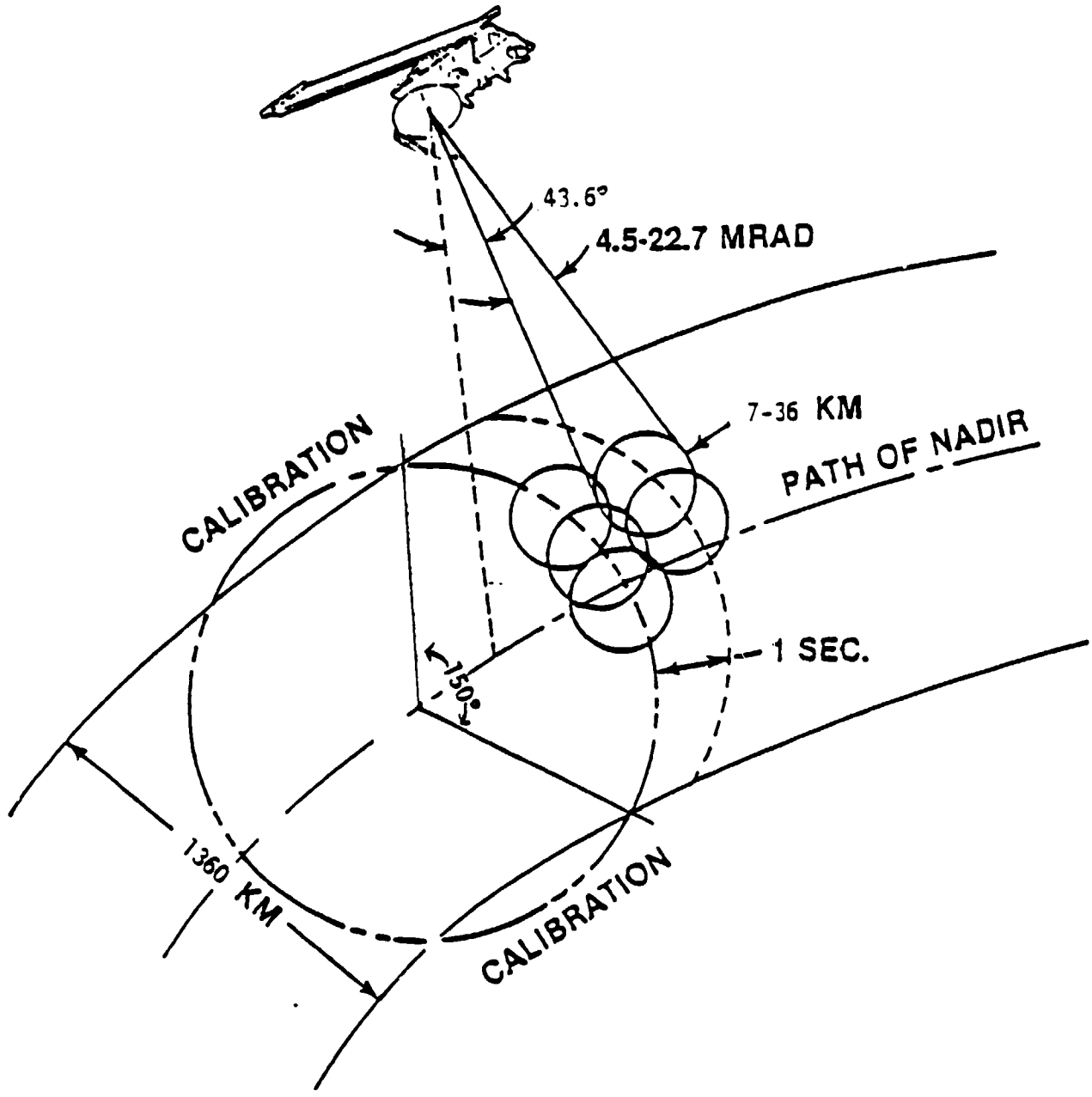

Figure 1.1 LAMMR Scan Geometry

PERFORMANCE

- Sea Surface Temperature accurate to within ± 1.5° at 25 km resolution
- Wind Speed 0-50 m/s, accurate to within ± 2 m/s or 10%, whichever is greater at 17 km resolution
- Sea Ice Concentration to within ± 15% at 9 km resolution
  - Type classification - first-year, multi-year
  - Age - inferred thickness to within ± 2 m
- Atmospheric Water Vapor to within ± 0.2 g/cm^2 at 9 km resolution

LAMMR TECHNICAL CHARACTERISTICS

• Orbital Altitude	700 km						
• Weight	320 kg						
• Digitization	12 bits						
• Data Rate	64 kb/s						
• Power (nominal-average)	350 W (Nominal Average)						
• Frequency (GHz)	4.3	5.1	6.6	10.65	18.7	21.3	36.5
• Wavelength (cm)	7.0	5.9	4.5	2.8	1.6	1.4	0.8
• Antenna Aperture	4.0 m						
• Polarization	HORIZONTAL AND VERTICAL						
• Cross-Polarization Isolation	17 db minimum						
• 3 dB Beamwidth (deg)	1.3	1.1	0.9	0.6	0.3	0.25	0.25
• Beam Efficiency	90% minimum						
• Sensitivity Ta (K)	0.6	0.7	0.8	0.8	0.8	0.8	1.5
• Calibration Accuracy (K)	1.0	1.0	1.0	1.0	1.5	1.5	1.5
• Scan Nadir Angle	43.6°						
• Viewing Zenith Incidence Angle	50.0°						
• 2-Axis Viewing Angle Stability	0.02°						
• Footprint (km x km)	23x36	20x31	16x25	11x17	5x8	5x7	5x7
• Scan Rate	1 Hz						
• Active Scan ARC (Forward)	150°						
• Swath Width (150° Scan)	1360 km						
• IFOV's Sampled Per Scan (Each Channel)	256					512	

Table 1.1 LAMMR Baseline Technical Characteristics

can severly bias the lower ocean response even though the side lobe gain through which land and weather fronts are viewed may only be a few percent of the main beam gain. Linear context-free techniques fall short of achieving this goal. It is for that reason that this study of antenna pattern corrections and side lobe compensation was initiated to extend the results of the previous effort.

1.1 APC Processing Goals

There are two major goals associated with the context sensitive formulation of antenna pattern correction and side lobe compensation:

- An error analysis and assessment to show that the proposed context sensitive schemes are satisfactory, and

- Demonstration that acceptable error allowances can be achieved within reasonable computational loads.

In the error assessment area, a least squares error measure was defined under some reasonable underlying statistical assumptions concerning the signal characteristics relative to noise. The use of a priori knowledge in the processing of antenna temperatures compounds the issue with regard to error measures which this study resolves. A unified scheme and/or philosophy of processing was established. We highly recommend a context sensitive APC process which we believe yields a good tradeoff between contending factors and which significantly reduces the computational burden. This report demonstrates its effectiveness. In the demonstration area, the computation of APC coefficients under alternative signal-to-noise conditions, under various matrix truncation conditions, and under aliasing and non-aliasing sampling spacings were selected and applied to the unmodeled portion of the antenna temperature field. All analyses and supporting rationale were completed and the demonstration of their effectiveness using a synthetic image model was accomplished. Work was initiated on trying to apply the technique to SMMR data, but time did not permit us to complete this extention.

1.2 Error Assessment

Within our previous study an error assessment was made incorporating many error measures:

- Error variations due to geometry within the swath,
- Noise amplification resulting from the APC process,
- Alternative error measures associated with different signal auto-correlations,
- APC matrix truncation error,
- Error in being able to achieve correct brightness temperatures as a result of sensor noise, or data sampling limitations (aliasing errors), and
- Error reduction due tc incorporating a priori knowledge in a context-sensitive APC process.

Least squares error estimates were made under all of the alternative conditions, but little use can be made of these estimates in a context-free processing scheme since environmental conditions vary greatly in the real world.

Context sensitive APC processing adapts to varying environmental conditions. It incorporate a-priori knowledge about land mass, ice, and water locations and models the brightness temperatures in those areas. This brightness temperature model is used as a baseline from which an antenna temperature can be computed and compared with measured antenna temperatures T_A. The variation of T_A from the model can be corrected to variations of brightness temperature estimates δT_B from the brightness temperature model so that a final estimate of brightness temperatures can be made. Also, varying statistical correlations can be

used to reflect coherences that may be different over land than they are over water, etc. The main advantages of this approach are:

- Gibbs artifacts generated by correcting the finite spectral response of the antenna near land/water boundaries are overcome.

- The computational system is consistent in that no special attention has to be given to those pixels near each end of the swath traces as would otherwise be required and which is described in the algorithm freeze report.

- It utilizes more realistic statistical assumptions in establishing a matched filter for modulation transfer function compensation which can be different over different fields.

- The algorithm is computationally more efficient than the context-free cases.

In the theory, we found no need to deviate from a least squares error assessment model except to realize that the underlying statistical assumptions may not be context sensitive; differing over land, water, snow and ice.

1.3 Real Time Processing Constraints

Within the BTS study, concepts for reducing computational workloads are suggested. Some of these concepts are:

- Reduction of matrix size while meeting acceptable error allowances for modulation transfer function compensation of antenna temperature variation from the model,

- Use of world surface map features for adaptively processing the data,

- The use of a priori brightness temperature models for data interpretation, and

- Application of APC process in instrument coordinates.

This final report clearly identifies factors and assumptions used in the proposed schemes. It is recommended that APC be performed in instrument coordinates so that no geographically-referenced binning be required as in SMMR. Computer configuration requirements such as core, data representations and processing speeds are presumed. Other factors such as programming language, processing structure, algorithm descriptions, mathematical specifications, and data structures for both input and output are consistent with the LAMMR algorithm freeze specifications.

Our report is organized as follows. Section 2 contains our executive summary. Therein contained is a description of the context sensitive APC philosophy, the presentation of computational results, a discussion of pertinent findings, and a few recommendations. Section 3 consists of the analysis conducted during the course of this work. It also includes examples of some of the computations which were conducted. Related analysis needed for understanding this section are to be found in an appendix. Section 4 describes our software code in modular form and references several appendices containing the detailed runs and code listings. Section 5 gives our conclusions and recommendations, it identifies problem areas and delineates approaches to their solutions.

2.0 EXECUTIVE SUMMARY

This section describes the essential results of the context sensitive Antenna Pattern Correction (APC) and Side Lobe Compensation (SLC) study. It contains the objectives the rationale for selected philosophies, study approach, results and recommendations.

2.1 APC and SLC Objectives

There are two major objectives in this study.

- Alternative approaches to context sensitive antenna pattern corrections and side lobe compensation that are considered to be computationally viable are to be formulated utilizing a statistically rigorous derivation and geographic model information so as to establish alternative philosophies and/or assumptions needed in these theories. This analysis is to be an extension of work that had been previously performed.

- To perform some computational demonstration that are sufficient to establish the algorithmic feasibility of context sensitive antenna pattern corrections and to make recommendations for an approach to be used in LAMMR processing.

2.2 Rationale for Selected Philosophies

In previous work by BTS and others, the words "antenna pattern correction" implied a process by which antenna temperatures are converted to estimates of brightness temperatures over some spatial field. Linear convolusion processes were the only processes previously considered for this conversion. In our previous study, it was shown that the coefficient to be used in this estimate of brightness temperature can be

rigorously derived as long as there is knowledge of the brightness temperature auto-correlation function. That is, one requires statistical knowledge of the fluctuations to be expected in the brightness temperature field. In that study it was shown that the presence of land in the brightness temperature field causes a disturbance which is not adequately modeled by any reasonable statistical auto-correlation function assumption. Therefore, the underlying theory of linear convolutions for brightness temperature estimates are not suitable in the land/water boundary regions. Since it is precisely the coastal regions where accurate knowledge of brightness temperatures have their greatest utility, it becomes essential to solve the dilemma. In so doing, we have found it convenient to separate the brightness temperature estimation process into parts. The first part we call side lobe corrections, and the second part we call antenna pattern corrections.

It was previously thought that antenna pattern corrections would solve the problems associated with side lobe influences. It was known that when a bright island appeared under one of the major side lobe peaks, that brightness temperatures would radiate into the antenna thereby affecting its antenna temperature measurement; an erroneous reading in the surrounding waters is created. Since antenna pattern corrections modify the side lobe structures of the effective antenna pattern, it was thought that these influences could be subdued numerically and indeed such is the case, except that this reduction causes a significant widening of the main beam with a subsequent loss of resolution, i.e., the process of reducing side lobe influences blurs the imagery. Antenna characteristics already cause a blurring of the imagery; rapid spatial variations or high spatial frequencies are severely modulated as the antenna radiometer responds to these variations. The typical engineering process of modulation transfer function compensation would digitally amplify the higher frequency components, so as to compensate for their loss as a result of the antenna system characteristics. It is easy to show, however, that such a compensation which amplifies higher spatial freqencies will narrow the main beam of the effective antenna pattern but

simultaneously introduce a large number of relatively high amplitude (positive and negative) side lobes. The existence of a small island and/or a land water boundaries creates significant artifacts in the brightness field estimated by such an effective antenna pattern. Approaches which are based on optimum estimates of brightness temperature fields indicates that the modulation of the spatial response of antenna system should be compensated as previously described in a well known manner known as Weiner Filtering. However, this analysis must utilize an a priori estimate of the autocorrelation in brightness temperature fluctuations about some expected mean brightness temperature. The usual assumption that these brightness temperature fluctuations are spatially independent is valid in uniform regions, such as, over land or over ocean. That assumption is totally inadequate in the vacinity of land/water boundaries and the correction process generates artifacts. To avoid the artifacts, land presence must be explicitly or implicitly recognized. Several approaches were considered for incorporating our a priori knowledge of land/water differences in side lobe compensations.

- The geometric knowledge of land/water interfaces could be utilized to generate an a priori field of expected brightness temperatures over the surface of the Earth.

- The same model could be parameterized with two brightness temperatures; a parameter for the brightness temperature over water and a separate parameter for the brightness over land.

- An implicit approach could be taken in which areas above a set threshold would be considered land while those below the threshold would be considered water. In the implicit scheme land/water boundaries are extracted directly from the antenna temperature measurements.

As a result of our analysis it was concluded that the second of these two schemes was appropriate for LAMMR. The reasons for this choice are as follows:

An unparameterized model as in the first bullet would be expected to have erroneous a priori brightness temperature values over land and water within the model. The differences between these assumptions and the actual values would lead to a spatial discontinuity at the boundary causing some residual artifacts. The third bullet was rejected because, in the processing algorithm for LAMMR, knowledge of land/water locations are required outside the swath of observed data. A simple thresholding technique would not yield this information and so a world boundary map would be required. This requirement would cause the algorithm for pixels along the boundary of the swath to be different than those on the interior of the swathe complicating, therefore, the SLC process. Hence, it was decided that the second approach of a parameterized model utilizing a priori knowledge of land/water locations was most appropriate for LAMMR.

We must now show how such a model can be used to remove the influences of the side lobes; the process is called side lobe compensation (SLC). The side lobe compensation process is recognized as one which has an influence only in the presence of land; large oscillating side lobes with positive and/or negative contributions to the antenna temperature do not generate artifacts when the field of observation is relatively uniform. Side lobe influences can be removed in two ways.

- Removal of the side lobe structure and antenna pattern
- Removal of the influences caused by land

As previously described, the reduction of side lobes by affecting the antenna itself has two major disadvantages. First it causes the main beam which is already wide to be further widened, thereby, leading to image blur and loss of resolution. Secondly, the process of modifying

the antenna pattern to remove side lobes lead to large convolution matrices which are computationally expensive and needlessly complicates the system. Through modelling it is possible to remove the influences that the land/water boundaries have on brightness temperature estimates. In this process the parameterized model of brightness temperatures is convolved (a one time process) with the antenna pattern of the instrument generating a model antenna temperature field. This antenna temperature field is compared with the observed data to determine the values of the to brightness temperature parameters which best explain the observed data. Now differences between the observed antenna temperature and the modelled antenna temperatures are antenna temperature unexplained variation. These unexplained variations are no longer influenced by the presence of land and/or water; the gross mismatched between brightness temperatures over land and water have been removed. By moving to the space of unmodelled antenna temperatures, we have eliminated the influences of land beaming into the side lobes of the antenna pattern and have therefore performed a side lobe compensation function. Hence, we call the process of moving to the space of unexplained antenna temperature variations the process of side lobe compensation. Note that we have not yet corrected for the response function of the antenna system which is appropriately called antenna pattern corrections. The antenna pattern correction process is applied to the unexplained antenna temperature field to generate estimates of an unexplained brightness temperature field. This process must simply compensate for the loss of high frequencies that have been significantly modulated by the observation process. In our previous report, the methodology for linear APC processes have been extensively discussed. It was shown that most of the high frequency compensation process can be accomplished with a relatively small matrix. A 5×5 array of coefficients is adequate and it is even possible that a 3×3 APC process would be just as good. It must be recognized that the set of coefficients that are used for high frequency compensations do depend upon a priori assumptions in the spatial coherence of the unmodelled brightness temperature field. As a first step in this assumption, the unmodelled brightness temperature

field would be assumed spatially uncorrelated. This assumption can be tested over land, water, ice and snow once real data is obtained. Modifications to APC matrix coefficients could then be modified contexturally and applied to these separate categories. This refinement, however, is considered to be unessential as an initial system specification.

2.3 Study Approach

The approach used to accomplish the task associated with the context-sensitive antenna pattern correction and side lobe compensation study are embodied in Figure 2.1. Here the functional milestone chart of the antenna pattern correction study is presented for each of five tasks and associated subtasks. Also shown are tasks which have been completed in a previous study for context-free APC evaluation.

The tasks which were herein completed include:

- Analysis and planning
- APC benchmark software development
- APC weighting coefficients
- Verification testing and analysis
- Documentation and demonstration

In the analysis and planning tasks the APC/Data Bank Algorithms which are described in the LAMMR freeze report dated October 1980 were analyzed and checked for completeness, accuracy, adequacy and cumbersomeness. From our previous work it was determined that the algorithm as described had elements of a context-sensitive nature which had to be applied along the boundaries of the swath. In particular, land/water flags were needed in the region just outside the swath of available data so as to be able to perform an antenna pattern correction function for several pixels near the beginning and end of each scan line. This need for land/water flags coupled with the realization that

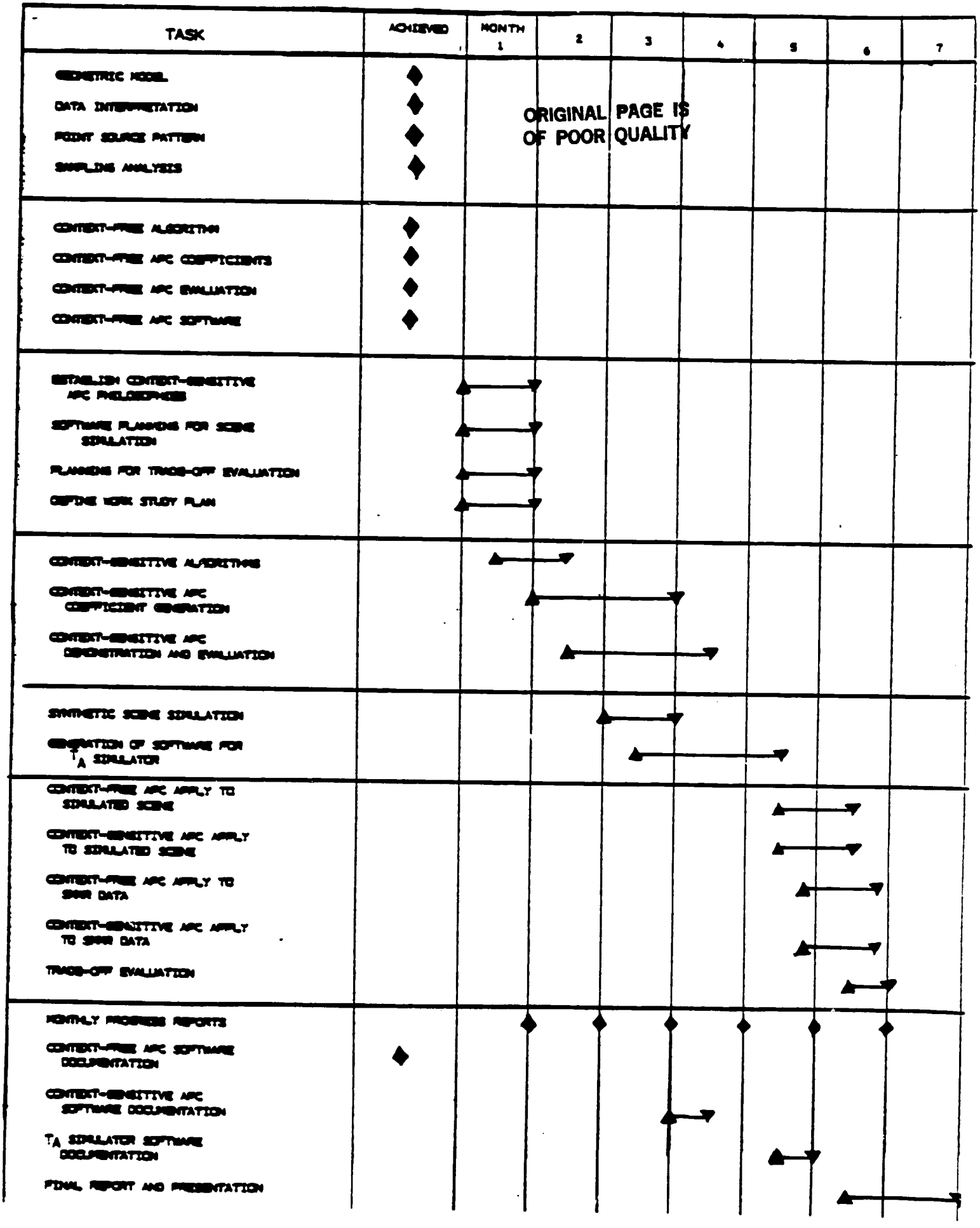

Figure 2.1 Functional Milestone Chart of Antenna Pattern Correction Study

the matrix multiplication process may not compensate for the influences of side lobe interferences has lead us to consider a unifying context sensitive APC process for LAMMR. The use of the land/water flags are needed to interpret the observed antenna temperatures so that artifacts free brightness temperatures can be drived from them. A unifying philosophy was established which treated the beginning and end of scan data no differently than the rest of the data and which took advantage everywhere of our knowledge of land/water boundaries. Software was then planned for developing a simulated scene and trade-off evaluation plans were established for utilizing this scene to demonstrate this context sensitive approach. A work study plan was generated.

In the APC weighting coefficients tasks, context-sensitive algorithms were studied and analyzed. The work on the generation of coefficients for antenna pattern corrections was extended so that we could better understand the trade-off between the modulation transfer function compensation and desires for reducing the amount of arithmetic needed in the performance of this function. Studies were conducted utilizing alternative sets of matrix coefficients for modifying the antenna pattern and the differences were evaluated in the context of the LAMMR instrument.

In the APC benchmark software development task, software was developed to synthetically simulate a scene consisting of land and water. This scene consisted of a rectangular island completely surrounded by water. The geometry of this island is such that the effects of the context-sensitive algorithms could be studied both in the vicinity of straight boundaries as well as along sharp curves. Software was also generated utilizing the synthetic scene to simulate the effects of the antenna viewing this scene. This simulator generated antenna temperatures from the given brightness temperatures of the land and water.

In the verification testing and analysis task, both context-free and context-sensitive antenna pattern correction and/or side lobe compensation algorithms were applied to the simulated scene. The results verified that context-sensitive algorithms outperformed context-free ones especially in the vicinity of land/water boundaries. Plans were made to apply these algorithms to SMMR data. A world scene was extracted for use as the land/water flags to replace the synthetic scene. Studies were made of available SMMR data which could be applied in a complex water/land environment. It was decided that the region of the mediteranian which included Italy would be ideally suited to show the advantages of context-sensitive processing. However, several problems arose that did not permit us to complete the simulation on SMMR data. These problems include:

- The Government furnished land boundary flaged software which was was coded in such a manner that the region between water and land had mixed pixels designations. This would have been okay if such a mixed pixel was a single pixel. However, for some reason this file blurred the land/water boundaries by as much as ten pixels so that the region of interest lacked the resolution needed to demonstrate the utility of our algorithms.

- In an effort to obtain raw antenna temperature measurements as observed by the SMMR instrument it was ascertained that such raw data did not exist in a format that would be easy enough for us to use. The only data set that was conveniently available for processing had been already "binned" and had therefore, totally destroyed relationships from which an antenna pattern correction function could be expected to give compensated results.

Efforts, however were extended to remedy these situations. For example, the land/water boundary flag algorithms were modified in an attempt to avoid the bluring function that is embeded in that algorithm. This proved to be a difficult task because there is no documentation of the raw data from which the land boundary information is extracted nor is there any documentation within the code which define the variables and the functions which are performed therein; reading the code makes one wonder what is going on and why. Efforts to modify this code to generate sharper boundaries have thus far failed and is perhaps the reason why the boundaries are blurred in the first place. Some effort was extended to understand the nature of available SMMR data. It was ascertained that the binning operation completely swamped the effects of the SMMR antenna pattern so that it was dubious that the SMMR context-sensitive simulation would prove anything useful for LAMMR. Because of difficulties that would be encountered in a proper simulation this effort was abandoned in favor of a more extended study of the simulated scene. As a result of work done on the simulated scene some trade-off evaluations were conducted which lead to the algorithm proposed in this documentation.

In the documentation and demonstration subtask context-free and context-sensitive software was documented. Final report was prepared and demonstration material was generated as required. This task also included the generation of monthly progress reports.

2.4 Study Results

A compilation of the essential results of our study follows:

- Alternative Approaches: Detailed analyses of the context sensitive antenna pattern correction and side lobe compensation processes indicated that some model assumptions and some statistical assumptions are absolutely required. Different assumptions in this detailed analysis

leads to alternative philosophical approaches to antenna pattern correction as well as to alternative approaches to the side lobe compensation functions.

- Alternative APC Coefficient Computations: For each of the alternative philosophies, additional approximations can be made in the computation of antenna pattern correction sets of coefficients. A matrix approach has been developed when the set of correction coefficients are truncated to a finite set. Fourier techniques are applicable when the antenna pattern rotation effects can be locally ignored. Techniques for computing coeffients using the Fourier approach have been demonstrated for both over-sampling and under-sampling conditions, and have been shown to agree quantitatively with the matrix truncation approach. In the context-sensitive approach, it was ascertained that the APC function is one of compensating for the modulation transfer function of the system and that this can adequately be done using a 5 x 5 matrix approach.

- Instrument Coordinates: It has been shown to be computationally efficient to perform the computations in instrument coordinates in that the raw data exists in this coordinate sysem. Resampling of the raw data to fit a priori selected geographic blocks on the surface of the earth as in SMMR processing hae been found to be unrealistic and undesireable. Hence, "Binning" should be avoided.

- Data Interpretive Techniques: A data interpretive technique has been developed whereby the discrete set of antenna pattern correction coefficients can be computed by solving a truncated system of linear equations. Because the antenna pattern varies significantly over the distance associated with a sample, it is necessary to retain a con-

tinuum representation of antenna patterns for the computation of matrix elements which enter into the system of linear equations for APC.

- Geometric Model: A complete geometric model which relates the instrument in nominal spacecraft coordinates to a geographically-referenced coordinate system with associated scanning geometry has been developed. Geographic referencing is needed to extract the land/water flags.

- K Space: Because of the finite aperture of the LAMMR antenna, it is strictly correct that the Fourier transform of the antenna pattern has a sharp spatial frequency cut-off. It has been determined that this statement is correct only in the K Space corresponding to the projection of the Poynting vector onto a plane orthogonal to the antenna axis. Spatial transforms from instrument coordinates to K Space have been derived so that Fourier transforms in K Space can be utilized, taking advantage of the sharp frequency cut-off that occurs in that space. This is useful for generating consistent antenna patterns and for performing convolutions with simulated scenes.

- Earth Rotation: It has been determined that earth rotation effects are significant in two respects. First, the ground velocity vector and the instrument axis corresponding to the center of the sampling angles do not coincide as a result of earth rotation; and second, the separation between lines alters as the ground velocity is modulated by earth rotation effects.

- Antenna Pattern Representation: It has been determined that adequate representation of antenna patterns are viable utilizing linear interpolation if four points per nominal

sampling interval are used to represent the antenna pattern with sequences of straight line segments. All simulated results utilize this approximation when convolution techniques are used.

- Error Measures: Several error measures have been defined in the context of this study. However, the least squares difference between the estimated brightness temperature and the corrected brightness temperature has been selected as the only reasonable criteria for measuring the effectiveness of alternative antenna pattern correction processes. It is realized, however, that this same error measure can be applied to alternative models. A discussion of an appropriate mix of models is to be found in our previous report.

- Noise Amplification: Each of the antenna correction processes enhances frequencies (or suppresses frequencies) that were modulated by the antenna pattern of the LAMMR instrument. As a result of the spatial frequency enhancement, noise at those frequencies are likewise enhanced so that a total merit of noise amplification is pertinent to the analysis. Codes for computing noise amplification have been developed and used in generating optimum APC matrix coefficients.

- Effective Power Spectra: In the truncated matrix approach to antenna pattern corrections, a linear combination of local data is chosen as a means to enhance the spatial frequencies of the unexplained antenna temperatures that have been modulated by the antenna. As a result of this linear combination, the resulting brightness temperature will have a corresponding point spread function and associated power spectra. Codes for computing both of these curves in both

one- and two-dimensions have been developed. The large side-lobe oscillations in these patterns are not important when applied to the "unexplained" antenna temperatures because the effects of land have been removed and can no longer have a large influence on the brightness temperature measurement.

- Aliasing Versus Signal-to-Noise: From our analysis, we find two competing sources of error which govern the choice of antenna pattern correction coefficients. These competing factors are signal-to-noise ratio and the degree to which the data has been undersampled. It has been demonstrated that when undersampling is such that the signal strength at the Nyquist frequency is larger or comparable to the noise power, then the affects of aliasing and errors associated thereto completely dominate the antenna pattern correction process independent of the signal-to-noise ratio. When the context sensitive SLC processes are invoked, the effects of aliasing do not appear to be significant.

- Truncation: In order to keep the number of computations in the antenna pattern correction process reasonable, it is necessary to truncate the array of coefficients to be applied to the data in converting antenna temperatures to brightness temperatures. It has been shown that there is little to be gained by considering large arrays for antenna pattern corrections when SLC processes are used. 5 x 5 sets of coefficients are recommended, but 3 x 3 compensation appears adequate.

- Undersampling: A model of the antenna pattern associated with a four-meter dish, its electronics, its motion and sampling strategy, as planned for the LAMMR instrument has

been developed. Although the three db points agree in general with those previously published for this instrument, it has nonetheless been determined that in the context of reasonable signal-to-noise ratios, and in the context of our ability to enhance spatial frequencies that had been modulated significantly, that the planned sampling strategy significantly undersamples the data over most of the frequency channels. As a result, aliasing is expected to occur, and limit the spatial resolution which could otherwise be acquired. Techniques for dealing with aliasing have been developed; aliasing is dominant in most cases but may not be significant when geometric models are used.

- Gibbs Phenomena: The discontinuity which occurs at the land/water interface contains unbounded spatial frequencies. Because of the finite dimensions of the antenna, only those spatial frequencies that are less than the cut-off frequency will be sensed by the antenna. Under ideal conditions where noise is insignificant relative to all or most of the observed spatial frequencies, compensation for the modulation of each frequency can be digitally implemented. Even if this were done, however, the resulting edge would show the characteristic "ringing" associated with Gibbs phenomena. It has been determined that additional a priori knowledge associated with the nature of land/water discontinuities must be utilized and incorporated within the antenna pattern correction process in order to avoid the Gibbs ringing. A method similar to one utilized by Dr. Schell for radio astronomy has been developed for this purpose, and is designated as a context-sensitive antenna pattern correction process. This process in effect compensates for the side lobe influences of land and is called side-lobe compensating (SLC).

- Context-Sensitive Processes: Context-sensitive antenna pattern correction processes have evolved during the course of these studies. One very simple process is to utilize a data base consisting of the difference between a modeled antenna temperature and its associated brightness temperature as a means of correcting observed antenna temperatures which appropriately incorporates the a priori knowledge of the location of land/water boundaries. A parameterized version is the one recommended for LAMMR.

- World Brightness Map: As a result of our investigation, it appeared feasible to utilize a world brightness map containing a priori knowledge of expected brightness temperatures over the surface of the earth. A model of the antenna could be applied to this world brightness data base, generating expected antenna temperatures associated with this model. Differences between antenna temperatures computed in this way and the modeled or statistically-observed brightness temperature constitutes a bias which should be utilized for antenna pattern correction. This bias has been determined to consist of two parts; first, a part resulting near discontinuities in brightness temperatures such as land/water interfaces, and second, biases resulting from the tails of the antenna pattern resulting from the amount of land to be found in the far tails of the distribution. These biases may have been observed in SMMR data, and may have been erroneously attributed to radio frequency interference. Attempts are being made to generate a World Brightness Map suitable for LAMMR processing.

2.5 Recommendations

There are two major recommendations to be made resulting from this study on alternative processes of context-sensitive antenna pattern correction and side lobe compensation. These recommendations are:

- That a parameterized context-sensitive antenna pattern correction process be implemented for LAMMR in that no single context-free process will adequately compensate for the antenna modulation of higher spatial frequencies while simultaneously avoiding the artifacts and errors generated by bright spots, glaring into the side lobes of the antenna pattern.

- That the LAMMR APC algorithm be separated into two functions. First is a side-lobe compensation function in which a parameterized World Brightness Map is used to estimate the expected antenna temperatures and an "unexplained" antenna temperature field is generated as a representation of the data. Second, a matrix method of compensation be applied to correct for the modulation transfer function of the antenna system.

3.0 ANALYTIC RESULTS

Analysis has been performed on the context sensitive antenna pattern correction and side lobe compensation problem. In the previous study two characteristically different types of antenna correction processes have been identified; context-free and context-sensitive antenna pattern correction processes. Very careful analyses have been conducted so as to characterize the problem in the continuum as opposed to the discrete domain. In order to do this, BTS has developed a data interpretive technique in which exact continuum representations are used in conjunction with integral representations of cost functions, in order to establish optimum coefficients in the matrix estimation of brightness temperatures as seen through some desired "eye" window function. The technique is a generalization over that used by A. Stogryn[1] in establishing brightness temperatures from scanning radiometer data. The procedure involves many steps as indicated by the detailed analysis which is presented in Appendix A.

In this section, we attempt to illustrate the concepts of context sensitive approaches to Brightness temperature estimates and leave any new mathematical analysis to Appendix A as much as practicable.

3.1 Context-Free Versus Context-Sensitive Processes

The distinction between a context-sensitive and a context-free process of antenna pattern correction is easily seen. All context-free antenna correction processes involve the computation of a linear combination of observed antenna temperatures in estimating the brightness temperature at any point. This linear combination may be performed via matrix multiplication or other approaches such as the use of Fast Fourier Transform techniques. The important distinction is that the coefficients that are used in the linear combinations are independent of antenna

[1] IEEE transaction on antennas and propagation Volume 18-26, No. 5, September 1978.

temperature measurements or patterns that are observed in the data, nor are the coefficients dependent upon other a priori knowledge such as the location of land/water boundaries. On the other hand, a context-sensitive process depends upon a priori knowledge and is conceptually more complex, although not necessarily computationally less efficient.

Context-Free Theory

The coefficients to be used in a linear context-free process are predetermined coefficients independent of observed brightness temperatures and independent of other knowledge of the real earth brightness temperatures. This does not imply that these coefficients are independent of any a priori knowledge. Indeed, it is necessary to utilize a set of statistical assumptions (an a priori model) in deriving the desired set of coefficients to be applied in the APC process; different context-free correction philosophies will lead to different sets of coefficients. The following types of assumptions are needed for a context-free theory:

- Choice of cost functions,
  - Least squares
  - Minimum variance
  - Minimum entropy

- For the case of minimum variance, a polynomial model of brightness temperatures may be locall required
  - Mean model
  - Constant radiant
  - Higher order splines, etc.

- A priori knowledge of either the brightness temperature auto-correlation function or the auto-correlation function of the variance about a polynomial model is required
  - Zero correlation model
  - Exponential correlation model
  - Linear auto-correlation function model.

As can be seen from the above list of potential context-free models, many alternative philosophies are possible, and each philosophy will lead to a separate approach to antenna pattern corrections, yielding different sets of coefficients. In addition to the above assumptions, it is also possible to include other factors such as a penalty function of the Backus-Gilbert type which could be utilized to help suppress side lobes in exchange for minor degradation in the spatial resolution of the main beam. In the computer simulations that were performed, very specific philosophies for context-free and context-sensitive theories were chosen. The context free philosophy was oriented toward the establishment of maximum accuracy of inferred brightness temperatures values in open ocean. Here, a minimum variance approach was chosen in which the geometric model of brightness temperatures was assumed a priori to be a constant. Fluctuations in brightness temperature from this constant was assumed to have no spatial correlation whatsoever, but with a mean fluctuation signal of S. The a priori power spectra therefore was S^2 and constant independent of frequency. Also, in this model, a noise power spectra is assumed having amplitude σ^2, also independent of spatial frequency. Linear equations resulting from this model do not require the existence of a well-defined Fourier transform and is as defined in Appendix A. There are advantages and disadvantages of this context-free approach. The major advantages are:

- The theory permits a matrix multiplication approach with a fixed set of coefficients dependent only upon the antenna scan angle,
- The method does not require any additional a priori knowledge,
- The theory permits an adjustment of derived coefficients when the multiplication matrix is truncated.

In fact, the theory demands that the sum of a truncated set of coefficients should add up to one, and that the adjustment should be made additively to each of the coefficients in the array.

There are also a number of disadvantages to a context-free process:

- The theory is applicable to a single set of statistical assumptions so that a theory which might work well in open ocean will not be optimal in a situation where there may exist water/land boundary. Hence, water/land interface artifacts will be present.

- Optimization of the process to minimize land/water interface artifacts will sacrifice resolution in open ocean.

- No context-free theory can improve spatial resolution without simultaneously incurring the disadvantages of a point source beaming energy into one of the side lobes of the resultant antenna point spread function. This is the Gibb's phenomena associated with the ringing that occurs near boundaries and is unavoidable in the region of any brightness temperature discontinuity.

One of the major results of our previous analysis on context-free approaches is that avoidance of artifacts resulting from the antenna pattern correction process near land/water interfaces would require a point spread function which is not too different from the assumed model antenna point spread function. As such, a case is made for not performing any antenna pattern correction at all if one desires to avoid ringing artifacts. Applying a quadratic penalty function in the Backus-Gilbert cost function also leads to similar results.

It therefore appears that for a context-free theory we either put up with ringing artifacts near land/water boundaries and take advantage of higher spatial resolution in mid-ocean, or, we avoid artifacts caused by the antenna correction process and put up with a less than optimal spatial resolution over relatively uniform areas. The best of both worlds can only be achieved with a context-sensitive antenna pattern correction process where the influences of land in the side lobes are compensated.

Context-Sensitive Theory

A context-sensitive theory incorporates a priori knowledge of the real world into the antenna correction process. The coefficients to be utilized in an antenna pattern correction process could be adaptive based upon observed patterns in the data but more fundamentally, we propose a land/water geographic model be used to compute an a-priori antenna temperature world map. Fundamentally, a context-sensitive theory will pre-examine the array of antenna temperatures locally, and classify the scene to be one of several anticipated patterns based upon our knowledge of the real world. Once the scene is classified, a specific set of coefficients for antenna pattern corrections of any unexplained antenna temperature residuals will be applied which match the statistical character of the classified region. In such a theory, it may not be necessary to have a detailed knowledge of the locations of land/water interfaces since, to a large extent, these locations could be extracted from the observed behavior of antenna temperatures as they vary spatially. Nonetheless, it may be computationally more effective to utilize the geographic location data because no special effort would be needed for pattern recognition.

In all of our context-sensitive approaches, a spatial model of brightness temperatures is required. The brightness temperature model may be obtained in alternative ways:

- Land/water flags can be used from an earth surface map with an associated latitude-dependent brightness temperature model for both water and land.

- An a priori brightness temperature model can be created from the LAMMR antenna temperature measurements which are processed and statistically incorporated in a world brightness map.

- Brightness temperatures for water and for land can be inferred from the antenna temperature measurements on the basis of land/water flags and thereby utilized in a context-sensitive a priori parameterized model.

- A bi-modal brightness temperature model can be assumed everywhere and utilized to avoid Gibb's artifacts that occur near land/water boundaries as well as at other geophysical fronts which may occur in nature.

In each of the four aforementioned context-sensitive models, the approach to antenna pattern corrections would be to infer a priori antenna measurements from the assumed brightness temperature model. These modeled antenna temperatures are then subtracted from the observed antenna temperature measurements, yielding a variational antenna temperature measurement which is not explained by the assumed model. These unexplained antenna temperature fluctuations are then processed in a context-free spirit, utilizing a philosophy which is statistically appropriate to the prevailing conditions. One could expect that the observed fluctuations should have no a priori correlation and hence, a conservative minimum variance philosophy may be appropriate for enhancing the spatial degradations imposed by the modulation transfer function of the antenna. The inferred brightness temperature fluctuations can then be added to the brightness temperature a priori model to yield our best estimate of observed brightness temperatures. It is to be noted that many benefits can be obtained utilizing a context-sensitive approach to antenna pattern corrections. Some of the benefits are:

- Discontinuities in the a priori brightness temperature model introduce high frequencies into the interpretation of the antenna temperature measurements in a manner reminiscent of Shell's introduction of positive definite constraints in the interpretation of radio telescope data, thereby avoiding the ringing artifacts due to Gibbs' phenomena.

- Because an antenna pattern correction process is applied on the fluctuations in antenna temperatures, we can relax our concerns a bit on the statistical assumptions that have been involved in converting these fluctuations to brightness temperature's fluctuations.

- The theory could make use of a world brightness map, thereby justifying an approach which has many other side benefits especially in the area of Quality Control and Assurance.

- Such a theory directly attacks the problem of side lobe interferences due to land masses, (side lobe compensation) and thereby permits the isolation of the problem of spatial resolution enhancement which can now become a simplified process. We have shown it can be handled adequately utilizing a 5×5 or even a 3×3 matrix multiplication approach. (It is also viable not do perform any spatial enhancement of the antenna temperature fluctuations at all, thereby significantly reducing real time computational burdens of the antenna pattern correction process.)

Thus far, we have addressed our concerns on artifacts that are generated due to the sharp spatial variation of brightness temperatures over the surface of the earth which the antenna does not adequately respond to. However, there are other sources of antenna temperature misinterpretations caused by biases which may be introduced into the system from the long tails of the point spread function response which although is low in amplitude, does however, cover large spatial extent. The integrated effects of the antenna temperatures caused by the tails of the distribution are not corrected using a matrix approach to antenna pattern corrections. Experience with SMMR data has indicated such biases are related to the direction of coast lines relative to the flight path of the spacecraft. An a priori world brightness map could be utilized to compute biases caused by the tails of the antenna pattern, and these biases would then be incorporated in the a priori estimate of antenna temperatures from the world brightness map, and incorporated into the

antenna pattern correction process. Details of the four aforementioned approaches to context-sensitive processes are shown in Appendix A, Section A.11. Analysis of these four approaches was conducted during the course of this work and the following paragraphs and comments are pertinent:

Latitude Dependent Model

The latitude dependent model establishes brightness temperatures for various catagories of ocean, ice, snow and land which dependents both on latitude and seasonal (time). The use of such a model, of course, would only be approximate and local conditions would occur in which the actual brightness temperature, for example over land, might be significantly different than the global model. Under these circumstances the artifacts introduced by the land water discontinuity would not be total compensated for by our context sensitive model. The advantages, however, of the latitude dependent model is that it is parameter free and therefore not subject to errors that might occur in the datastream as might occur in any parameterized model.

Parametric Land/Water Model

In a parameterized model, the values of brightness temperatures are inferred from the actual antenna measurements over some local array. The advantages of this model are that the parameterized values are extracted directly from the datastream and hence the discontinuity of brightness tempeatures across water, land boundaries are more accurately represented. The disadvantage of this scheme is that some degree of computation are required in tracking the brightness temperature parameters over the world surface types. Methods of establishing these parameterized brightness temperatures are shown in Appendix A, Section A.11.

By-Modal Model

In the by-modal model no a priori knowledge of the world structure is required. The algorithum continuously assumes that each region is

by-modal consisting of two species. A threshold temperature is established to distinguish both species. Brightness temperature estimates are established for both species and an antenna temperature is therein computed. The disadvantage to this scheme is that it is computationally complex and not really applicable over open ocean or open land. It has however, the advantage of representing weather front discontinuities which the other techniques cannot accommodate. (Large weather fronts, however, are not really modelable as discontinuities in brightness temperatures so that this later advantage is not truly applicable).

World Brightness Map

In the world brightness map approach the a priori model of brightness temperature is obtained from an analysis of data itself and stored in a statistical data set. The antenna temperature expected from a given region is extracted and subtracted from the observed field. This approach suffers from the disadvantage that statistical fluctuations in brightness temperature over land would still yield discontinuity artifacts and also from the disadvantage that the process requires a continuous updating from a world brightness map and associated statistics. It has, however, the advantage that such a world brightness map would have other benefits to the LAMMR ground processing systems.

A tradeoff analysis was conducted for each of these four systems from the expected error point-of-view. It was determined that the parametric land/water model was most appropriate for the LAMMR processing system.

3.2 Process Overview

Figure 3.0 shows a block diagram of the context sensitive antenna pattern correction and side lobe compensation processes. Details of the APC and SLC process is shown in Figure 3.1. Here the a priori brightness

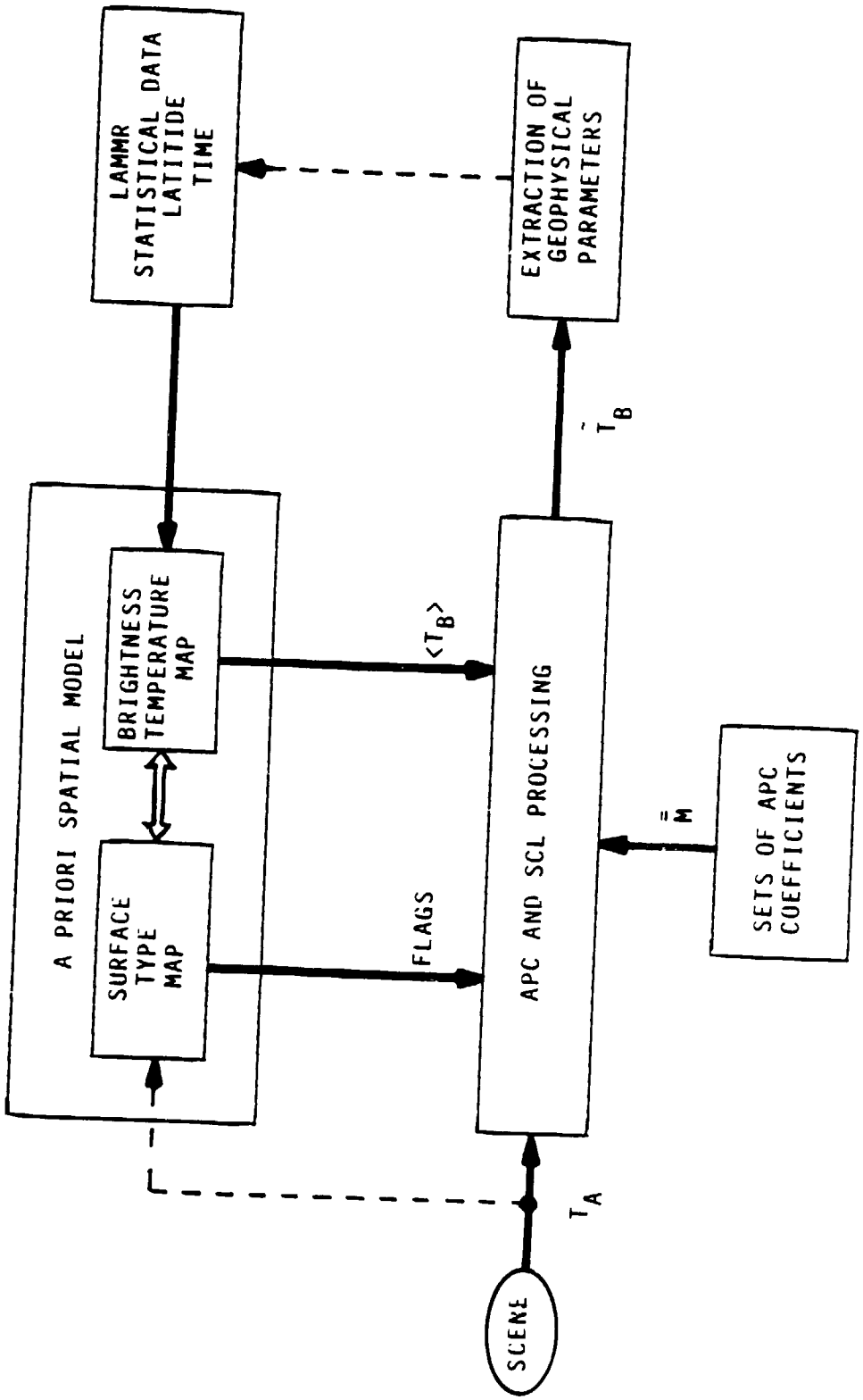

Figure 3.0 Block Diagram of Context-Sensitive APC and SLC Processes

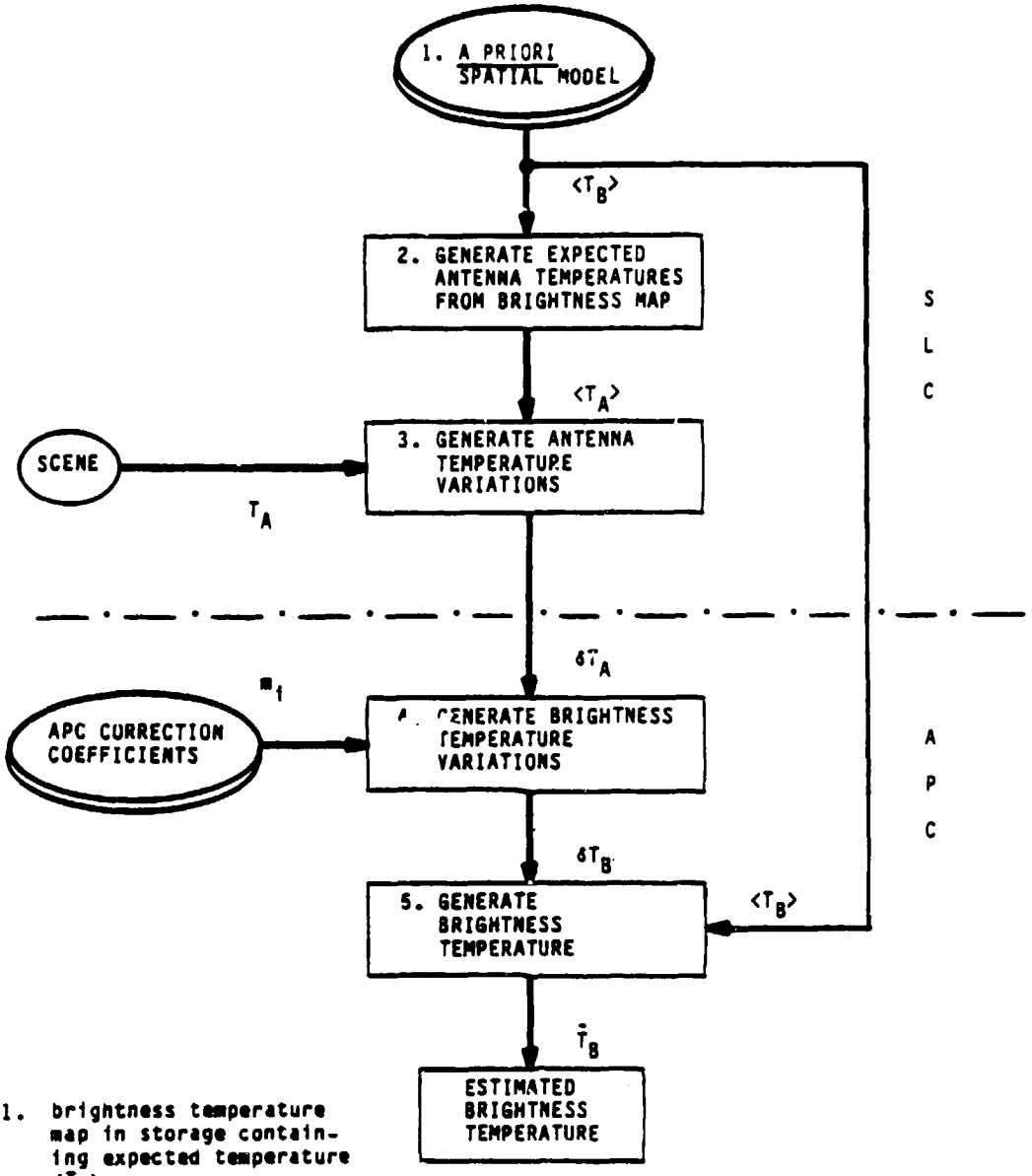

1. brightness temperature map in storage containing expected temperature $\langle T_B \rangle$

2. $\langle T_A \rangle = \int A \langle T_B \rangle \, d\bar{x}$

   where A is some antenna function

3. $\delta T_A = T_A - \langle T_A \rangle$

4. $\delta T_B = \int m_1 \delta T_A$

5. $\bar{T}_B = \langle T_B \rangle + \delta T_B$

Figure 3.1 APC and SLC Context-Sensitive Process

temperature map is shown being convolved with the antenna point spread function to generate the a priori antenna temperature (step 2). The measured antenna temperatures of the scene is modified by subtracting the expected antenna temperature from the model generating an antenna temperature variation. These three steps constitute the side lobe compensation process, in that, a priori knowledge of the Earth's geometry is incorporated so as to remove the side lobe influences of land. In step 4, brightness temperature variations are obtained through an antenna pattern correction process of the matrix variety and these are added in step 5 to the a priori brightness model generating an estimated brightness temperature. These brightness temperatures are self consistent, in that, a convolution with the antenna profile would generate the original antenna temperature as observed. An alternative approach to context-sensitive antenna pattern corrections is shown in Figure 3.2. It uses different APC processes in different circumstances. Local regions are examined to determine their homogeneities by accessing information from the a priori Spatial Model. Spatial frequency enhancement processing is applied to homogeneous regions (ocean) and side-lobe suppression processing is applied to heterogeneous regions where there are large signal fluctuations (land-ocean boundaries).

In studying the details of this approach, it was originally conceived that different APC coefficients would be utilized in a relatively few sets of circumstances, such as over ocean, over land and at land-ocean boundaries. However, it was soon realized that proper consideration at the land ocean boundaries would require a further disection according to boundary directions. Although the approach is viable, the large number of antenna pattern correction coefficients that would be required to handle the different spatial circumstances would be overwhelmingly large so that this alternative approach is not recommended.

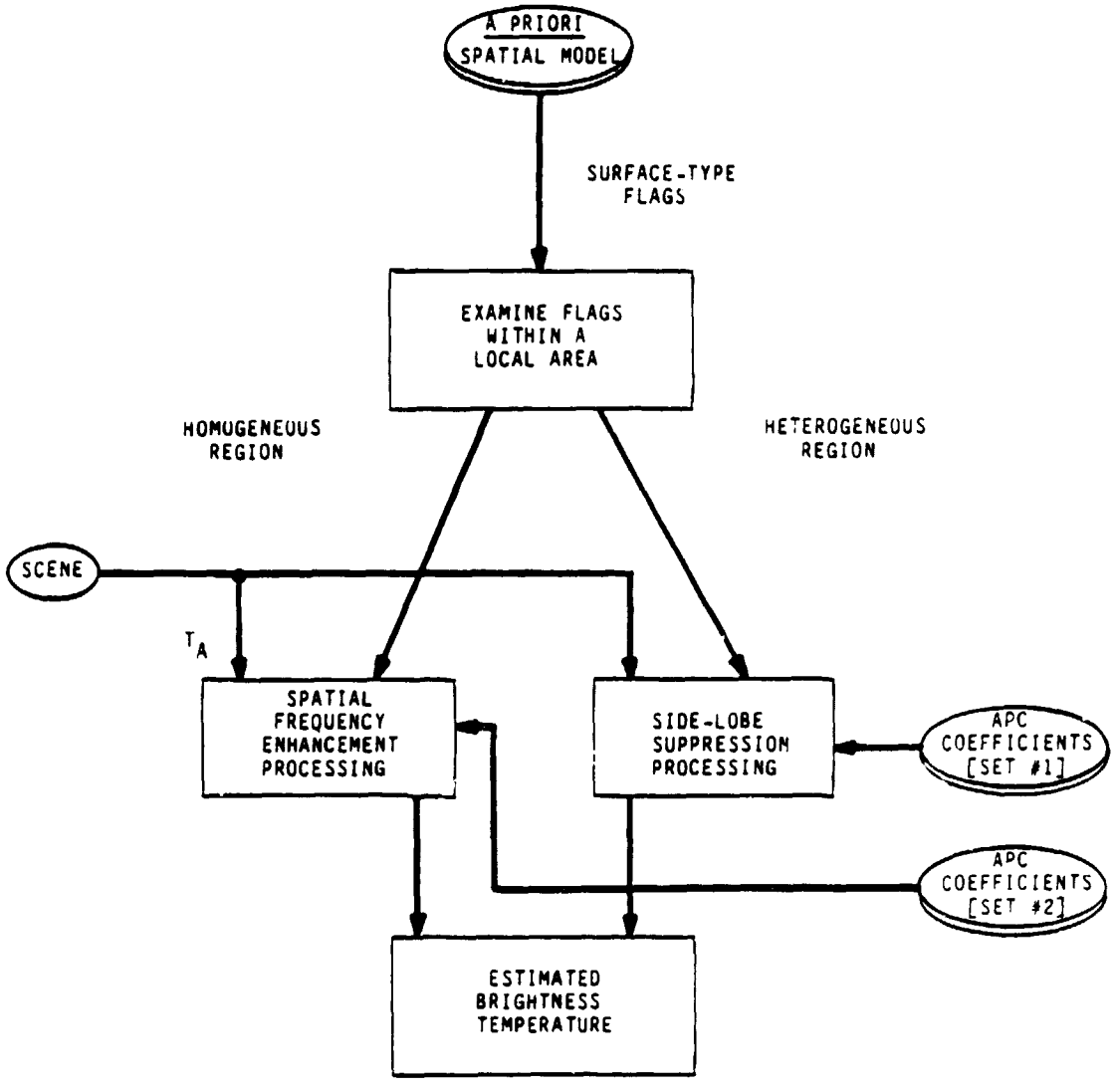

Figure 3.2 APC Context-Sensitive Process

3.3 Generation of Surface Type Map

The generation of surface type map (see Figure 3.3) involves the segmentation of various geophysical features and land masses from the ocean. It can be done by thresholding and utilizing known geographical data. An alternative approach to the generation of a surface feature map is to utilize surface feature boundary tapes and convert them to a grid of latitute/longitude surface types. A code exist at Goddard Space Flight Center for performing such a function. However, as previously mentioned, such a conversion is non-trivial and to date the conversion process leads to rather wide dispersion near the boundaries. Nonetheless, it is believed that modifications of this code is possible with relatively little effort and presents perhaps a better alternative to the thresholding procedure described above.

3.4 Our Planning Effort

Figure 3.4 shows a summary of our antenna pattern correction plan. It consists of five basic areas.

- Context-free antenna pattern correction
- Context-sensitive antenna pattern correction
- Synthetic scene simulation
- Performance evaluations
- Documentation

A brief description of this plan follows:

APC Processes

- correct side-lobe effects (SLC)
- enhance spatial frequencies (APC)

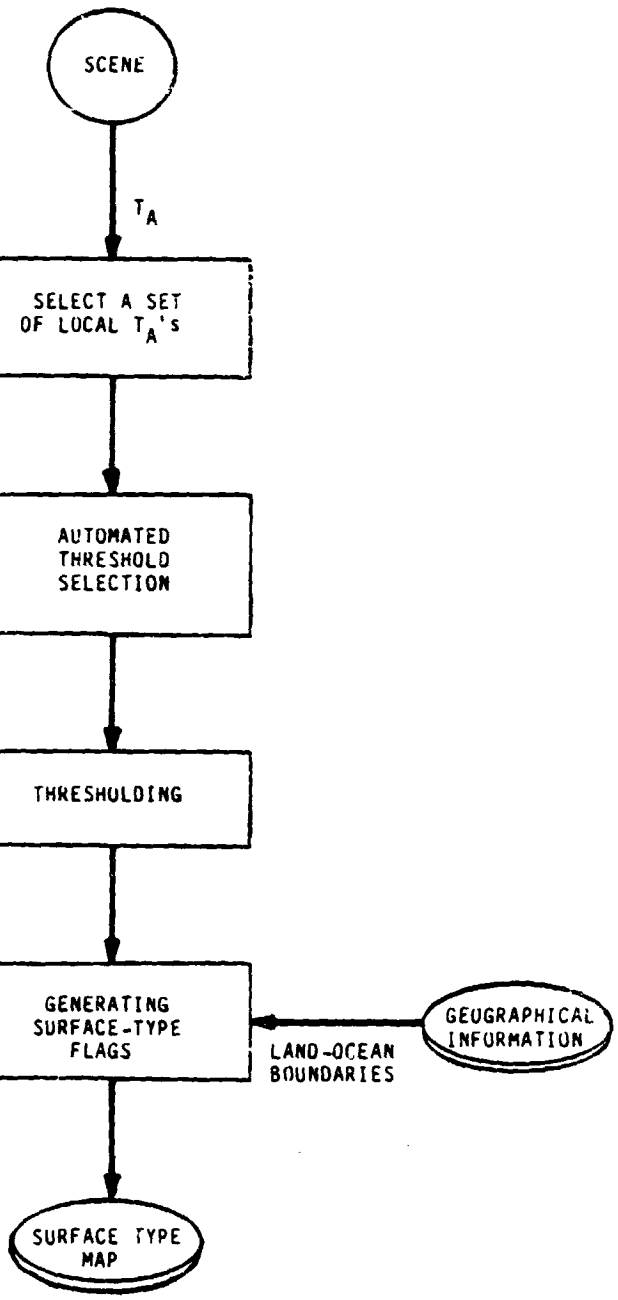

Figure 3.3 Surface Type Map

(A) Context-free APC

- Context-free APC algorithms
- Performance evaluation
- Prototype software
- Sets of correction coefficients

(B) Context-sensitive APC

- Context-sensitive APC algorithms
- Sets of correction coefficients
- Performance evaluation
- Prototype software

(C) Synthetic Scene Simulation

- Various simulated scenes
- T_A simulator software

(D) Performance Evaluations

- Context-free APC apply to simulated scenes
- Context-sensitive APC apply to simulated scenes
- Comparison/evaluation of APC responses on simulated scenes
- Context-free APC apply to SMMR data
- Context-sensitive APC apply to SMMR data
- Comparison/evaluation of APC responses of SMMR data
- Trade-off evaluation of context-free vs context-sensitive approaches

(E) Documentations

- Final report and presentation
- Monthly progress reports
- Documentation of all software nodules

Figure 3.4 Summary of APC Plan

(i) Context-free APC

A linear-filter APC algorithm based on least-square constraints has been developed and implemented. It enhances the spatial responses of the antenna pattern and at the same time ehances the Gibb's oscillations near discontinuities (example: land-ocean boundaries). This APC philosophy employs no geographical information and hence suffers from the fact that the antenna side lobes can be suppressed only at the expense of spatial resolution.

(ii) Context-sensitive APC

It is feasible to suppress the antenna side lobes as well as enhance spatial frequencies by incorporating some a priori information into the correction process. One way to achieve this is to utilize information about where land masses are situated geographically and approach the correction problem in a pattern recognition point of view. This involves the using of a-priori models of antenna temperatures and comparing these with observation.

Context-sensitive APC Development

(i) Perform analysis for context-sensitive APC processes
(ii) Define scenarios on how the context-sensitive processes are to be performed
(iii) Context-sensitive processes error evaluation and selection
(iv) Generate context-sensitive APC coefficients
(v) Software development of the APC process
- design
- coding
- testing
- documentation

Antenna Temperature Simulator

(i) Generate a synthetic scene with land/ocean boundaries and various geophysical parameters.

(ii) Generate T_B's that correspond to the given geophysical parameters.

(iii) convert the given scene of T_B's into T_A's with the effects of the side-lobes of the antenna.

(iv) Software development of the simulator
- design
- coding
- testing
- documentation

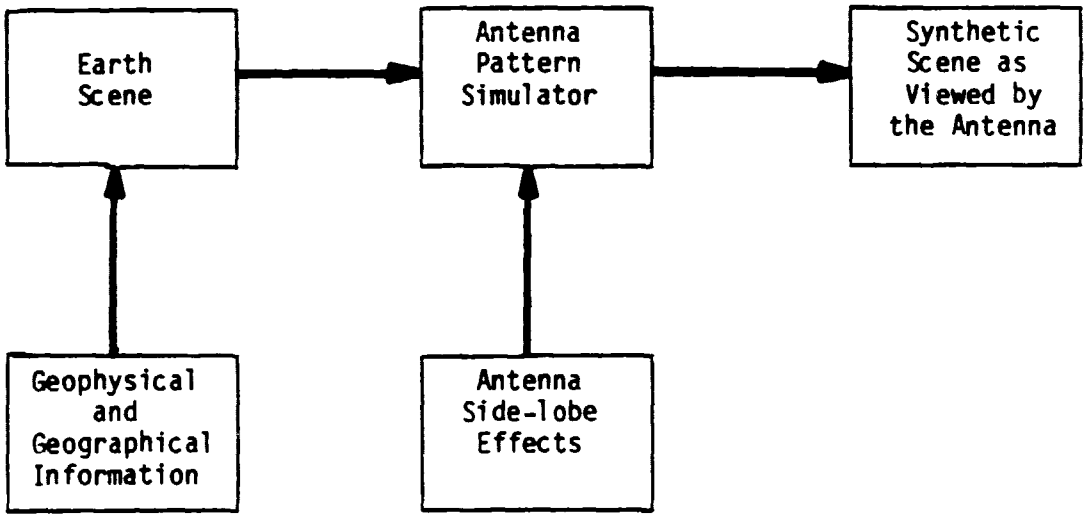

Testing and Evaluation

The software will take as input both a simulated scene and the SMMR data. Both the context-free approach and the context-sensitive approach will perform the APC to retrieve the T_B's. A trade-off analysis will be performed to evaluate the two APC approaches based on the responses of the simulated scene and of the SMMR data.

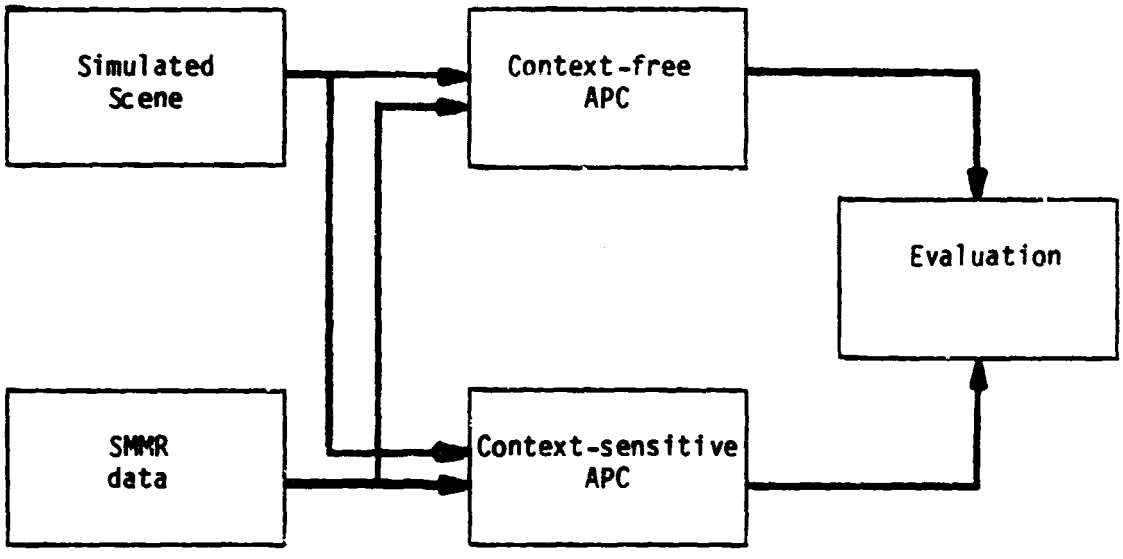

Work Performed

Most of the effort progressed on schedule as planned, except for the use of SMMR data in replacing our simulated scene. At this juncture, we had difficulties obtaining a useable surface type map which delineated land water boundaries sharply and also discovered that the SMMR data, because of the binning process, no longer revealed the point spread function characteristics of the antenna; it would not constitute a valid test for evaluation. Hence, more effort was spent on the simulated scene approach.

As a result of the evaluation, we have shown that the context-sensitive antenna pattern correction process as originally conceived indeed avoids many of the aliasing artifacts that are generated in the context-free antenna pattern correction process. Hence, it is highly recommended that LAMMR processing include the use of a brightness temperature world map for side-lobe compensation and subsequent antenna pattern correction for enhancing spatial frequencies.

3.5 Analytic and Simulated Results

The context-sensitive side lobe compensation and antenna pattern correction process was simulated on a synthetic image shown in Figure 3.5 called the rectangular island. In this figure, the brightness temperature over water was designated by a zero while the brightness temperature over land was designated by a numeric 4. These values were chosen so that the island could be represented as a single digit output. Mapping these values into realistic brightness temperatures is easily accomplished by applying a gain and an offset to the rectangular island file within the computer. The simulation plan calls for comparing the context-free antenna pattern correction process with a context-sensitive one. In achieving this end, it was decided that the k-space Fourier domain would be the most suitable space within which to do the required computations. The fast Fourier transformed algorithm was utilized, and Figure 3.6 gives a representation of the rectangular island in the k-space Fourier domain. Fourier transforms were taken with and without additive noise to the simulated antenna temperature field. This field was obtained by multiplying the ideal antenna transfer function by the Fourier transform of the rectangular island image and performing the inverse Fourier transform. Figure 3.7 shows a trace of the antenna temperature across the boundary of the island. The antenna was assumed to be a circular aperture with no tapering thereby leading to a first order Bessel function type point spread function as described in the previous report. Note how the antenna function blurs the discontinuity between water and land and that the residual side lobes cause some minor

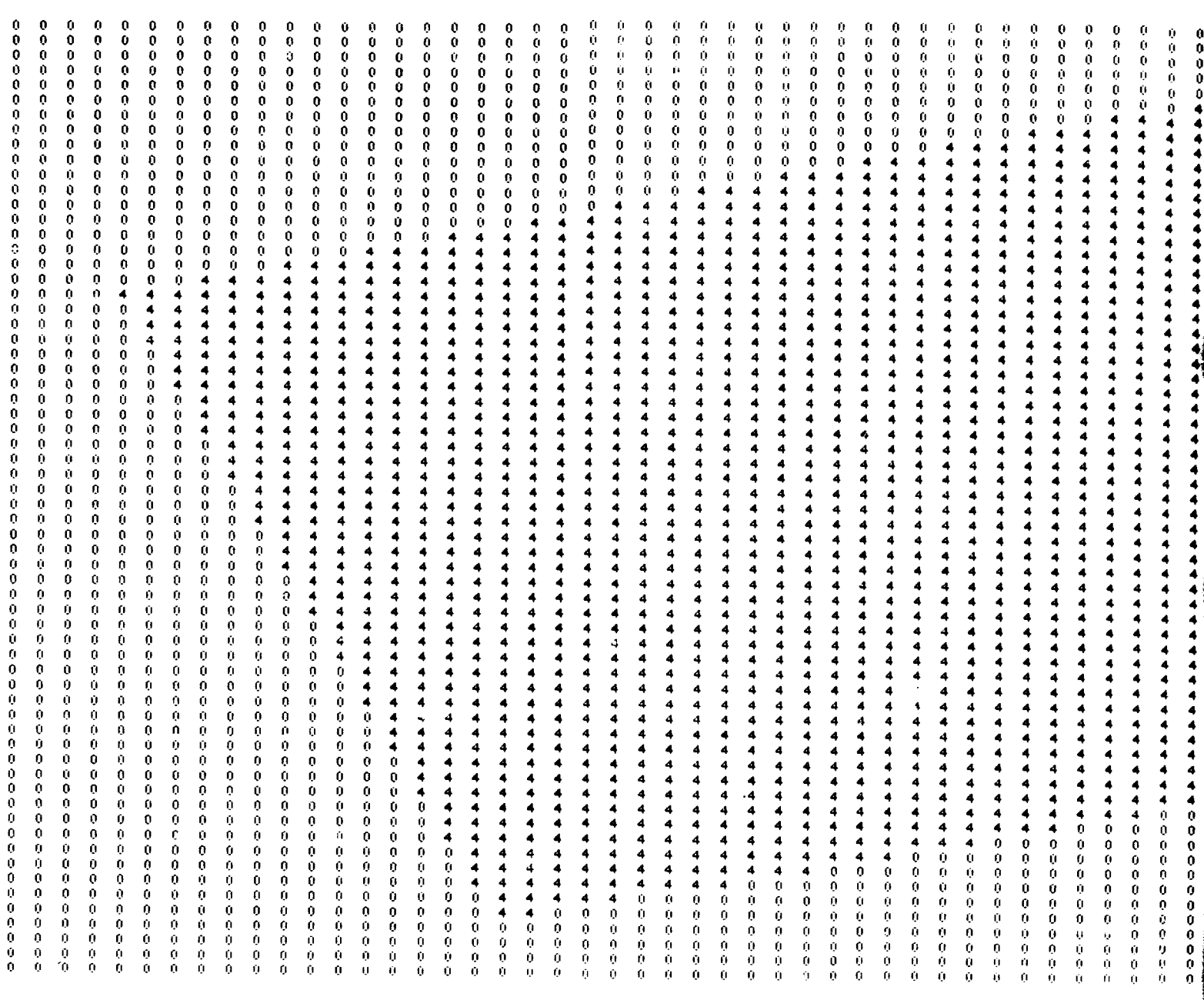

FOLDOUT FRAME

Figure 3.5 Rectangular Island Simulation

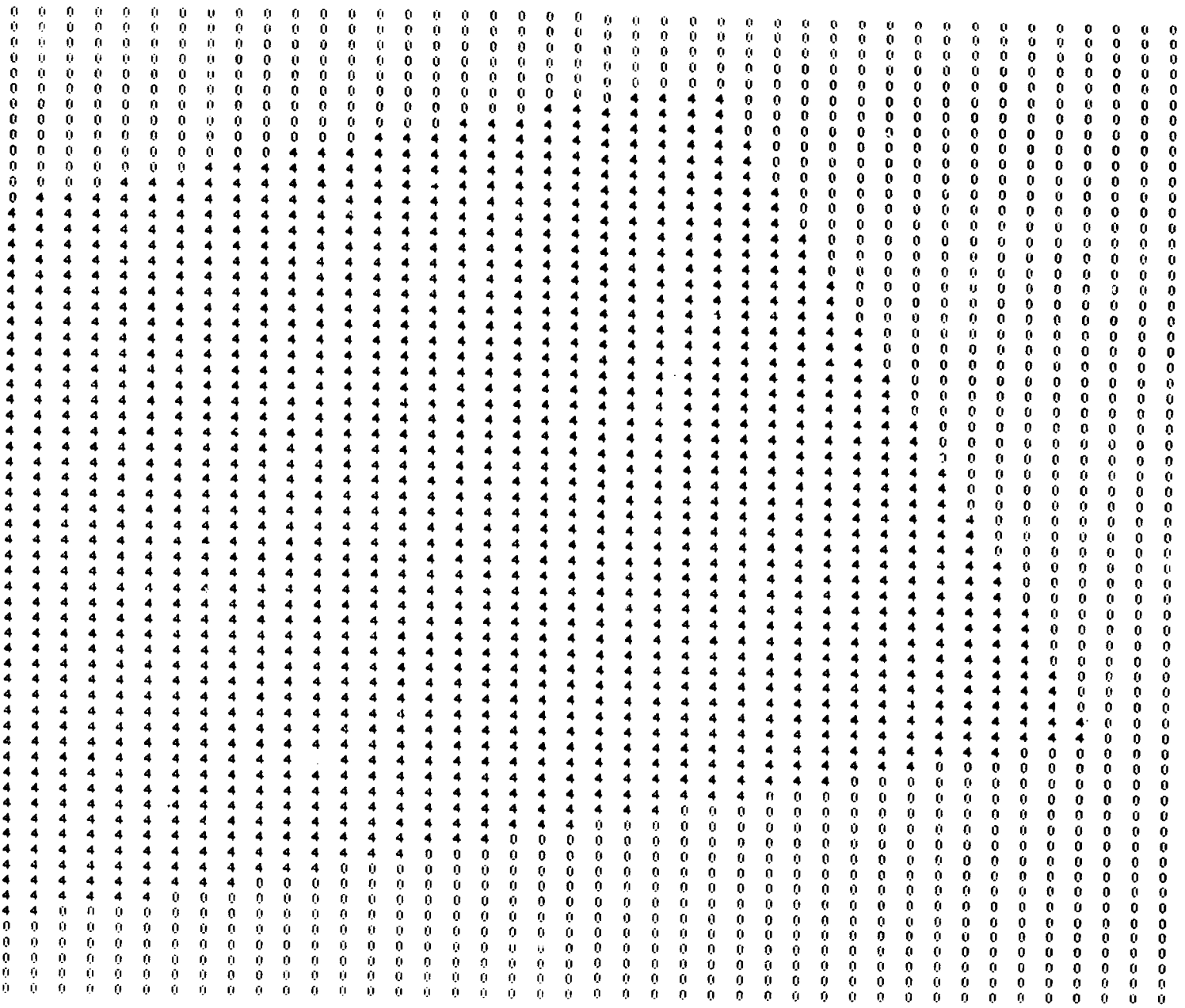

gure 3.5 Rectangular Island Simulation

FOLDOUT FRAME 2

PRINT OUT IMAGE (YES=1)

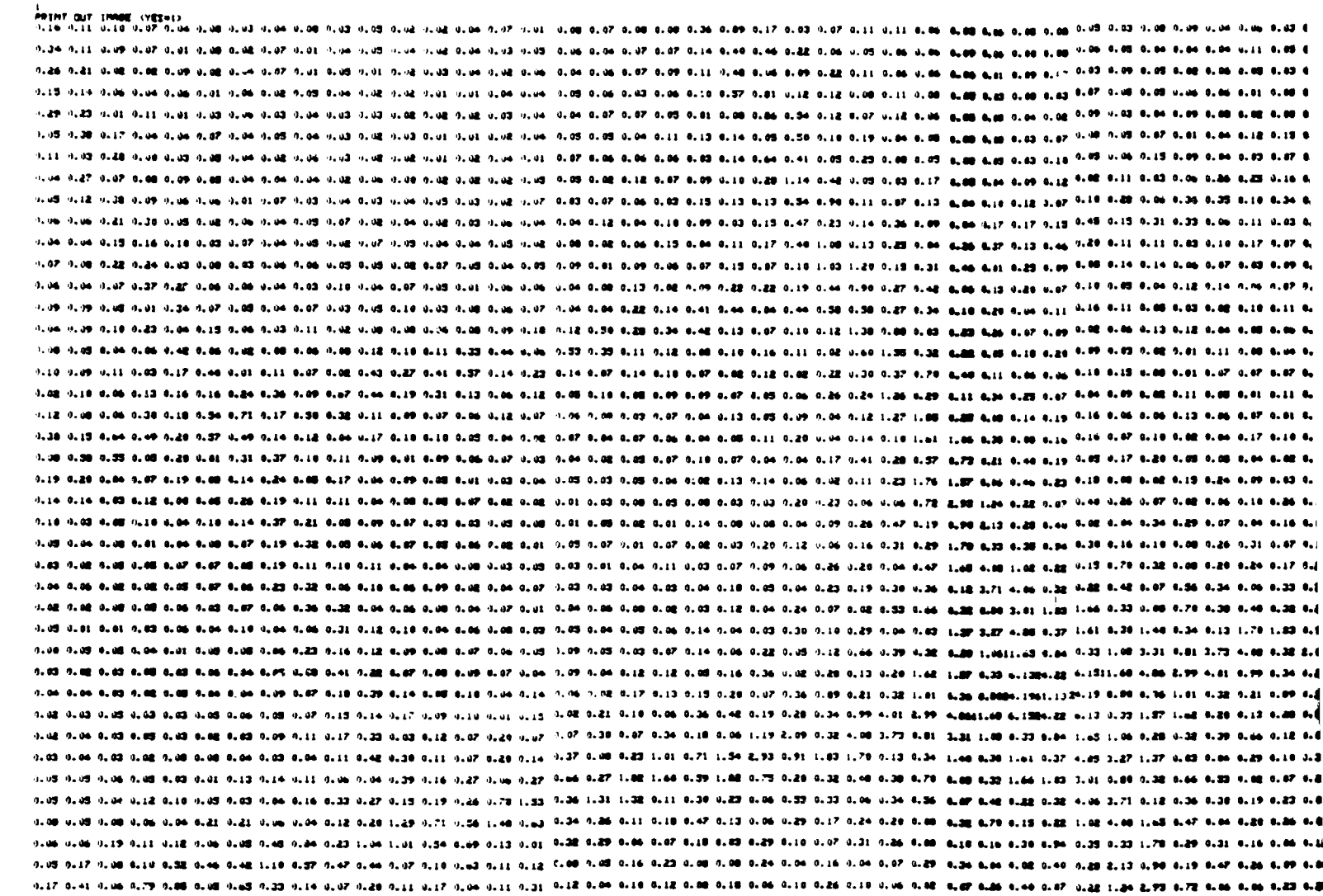

FOLDOUT FRAME

ORIGINAL PAGE IS
OF POOR QUALITY

Figure 3.6 Fourier Transform of the Rectangular

FOLDOUT FRAME 2

rier Transform of the Rectangular Island

oscillation as the antenna temperature approaches the steady state values of land and water. A 5×5 context-free antenna correction process was applied to an array of extracted antenna temperatures obtained selecting every fourth value for every fourth line. This sampling strategy corresponded to a minor amount of undersampling as in the design of the LAMMR instrument. Figure 3.8 shows the trace of the context-free antenna pattern correction process applied to the antenna temperatures for estimating brightness temperatures. Prior to the antenna correction process a realistic amount of noise was added to the antenna temperature. From the results we can see traces of the Gibb's phenomenon which in this example is a bit subdued due to the slight undersampling and therefore, inability to totally compensate frequencies up to the antenna cutoff frequency. The context-sensitive algorithm which has been previously described was applied to the same noisy array of antenna temperatures for the rectangular island. A trace across the island water boundary interface is shown in Figure 3.9. As expected, the simulation shows a reconstruction of the original brightness temperature scene with minor perturbations most probably induced by the additive noise. Many experiments were conducted, the behavior of which could be totally explained on the basis of previously developed theories. In general the results are not too startling and in some respects, many of the potential advantages of a context-sensitive implementation for brightness temperature estimates have not really been tested. In addition to 5×5 matrices, 7×7 and 3×3 arrays sizes have been tried with minor differences of the ones already presented. Figure 3.10 shows the frequency response of the antenna pattern correction arrays associated with different matrix sizes. In the higher frequency region, one can see that 5×5 array behaves as well as a 7×7 and that the 3×3 antenna pattern correction compensates for high spatial frequencies in a manner just slightly below the optimum nominal.

In conclusion, the context-sensitive antenna pattern correction and side lobe compensation processes herein described generate results which are generally superior over the context-free approaches, while simultaneously reducing the amount of real time computation albiet the need to generate a brightness temperature world data base.

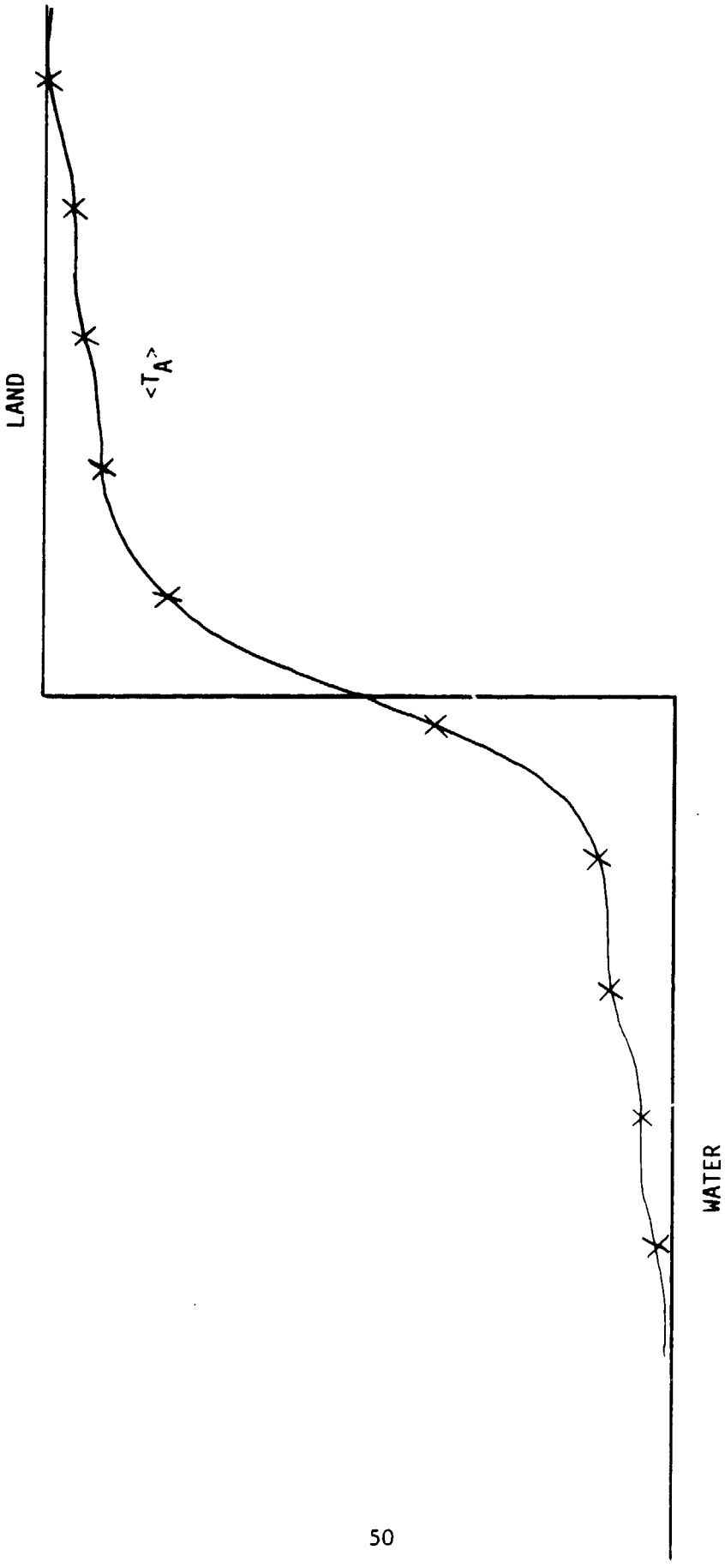

Figure 3.7 Trace of the Antenna Temperature Across the Rectangular Island Boundary

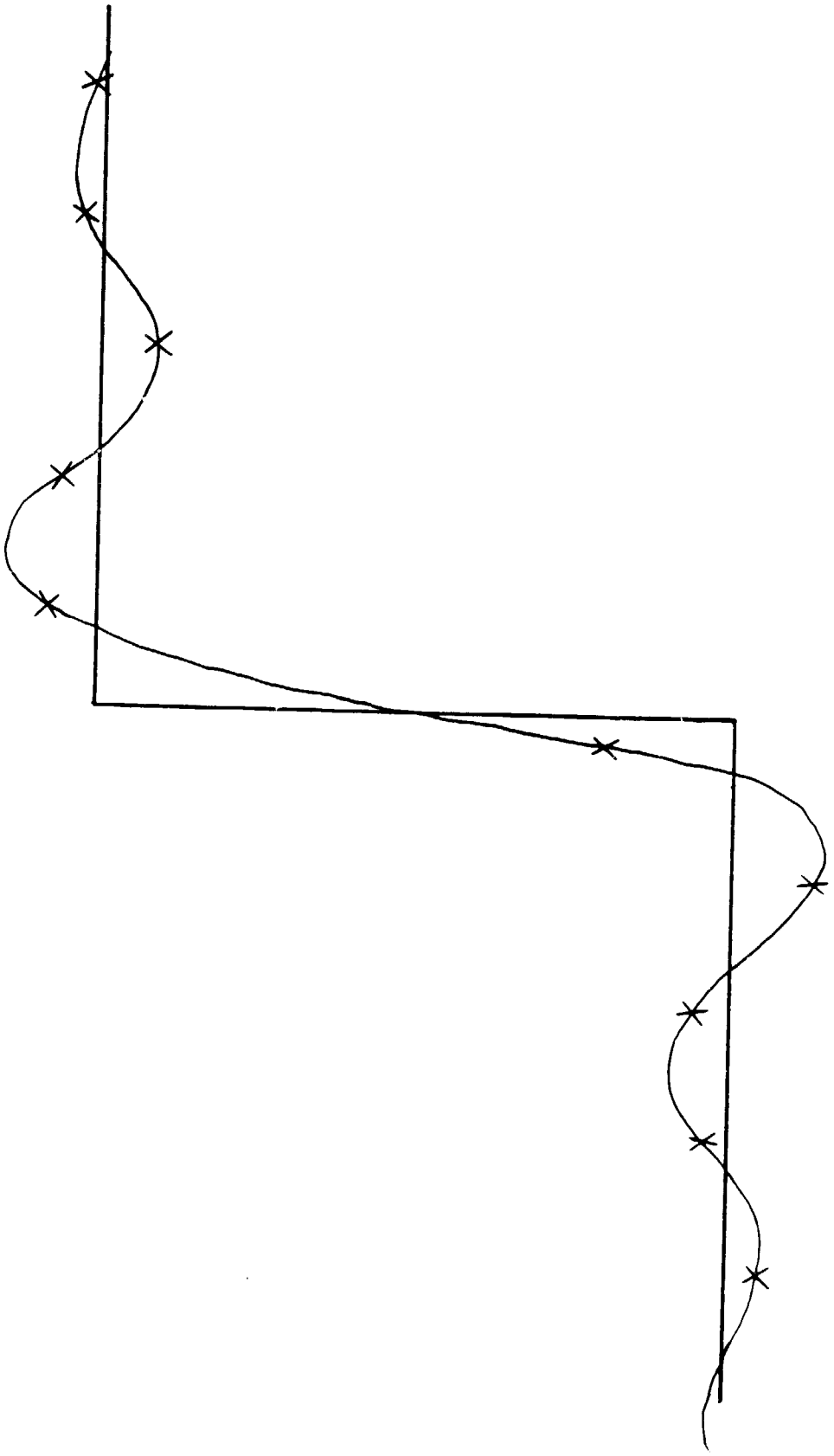

Figure 3.8 Trace of Context-Free Antenna Correction Process APC For Estimating Brightness Temperatures (5x5) with Additive Noise

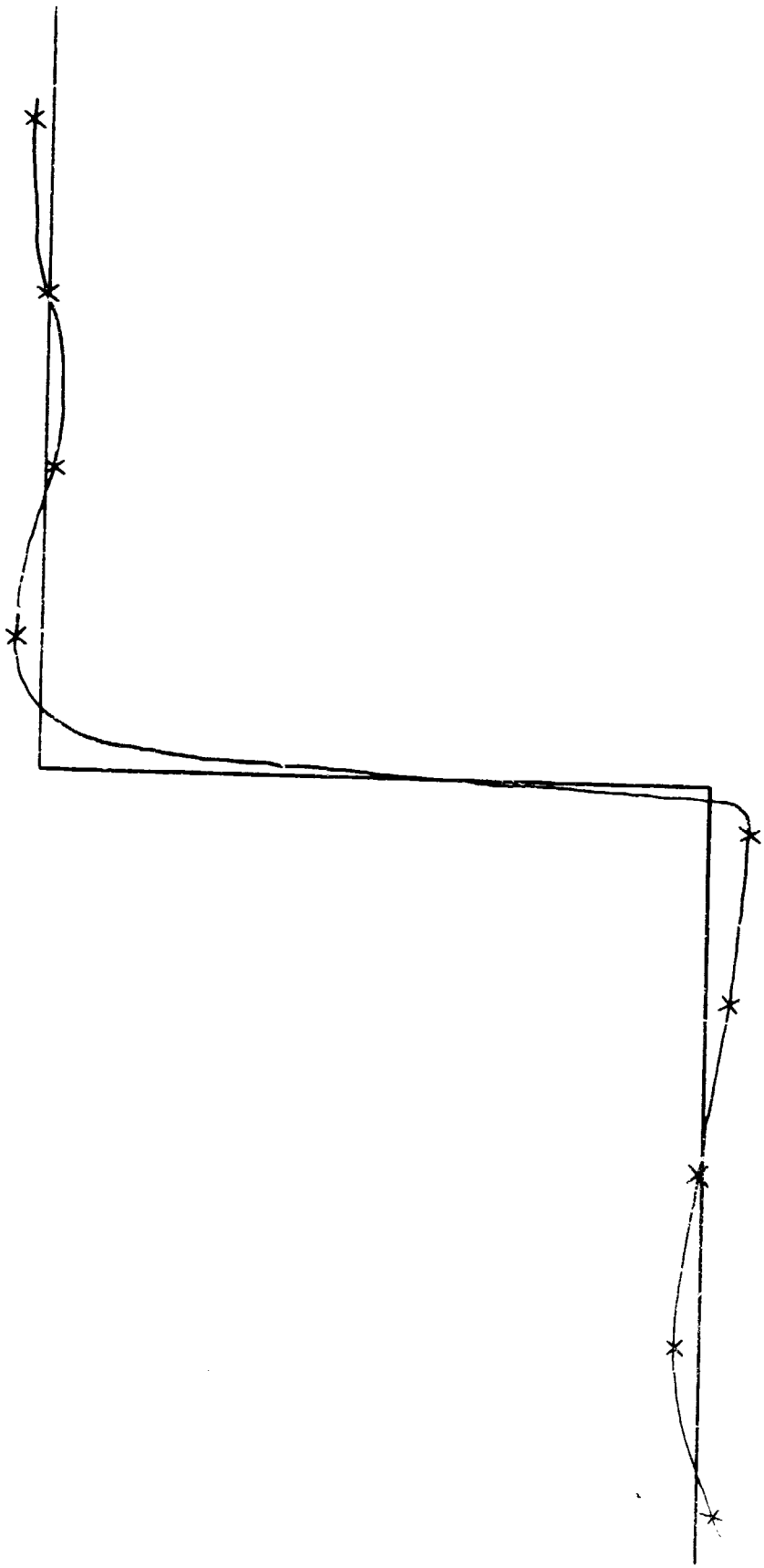

Figure 3.9 Trace of Context-Sensitive Antenna Correction Process For Estimating Brightness Temperatures (5x5 APC on δT_A) with Additive Noise

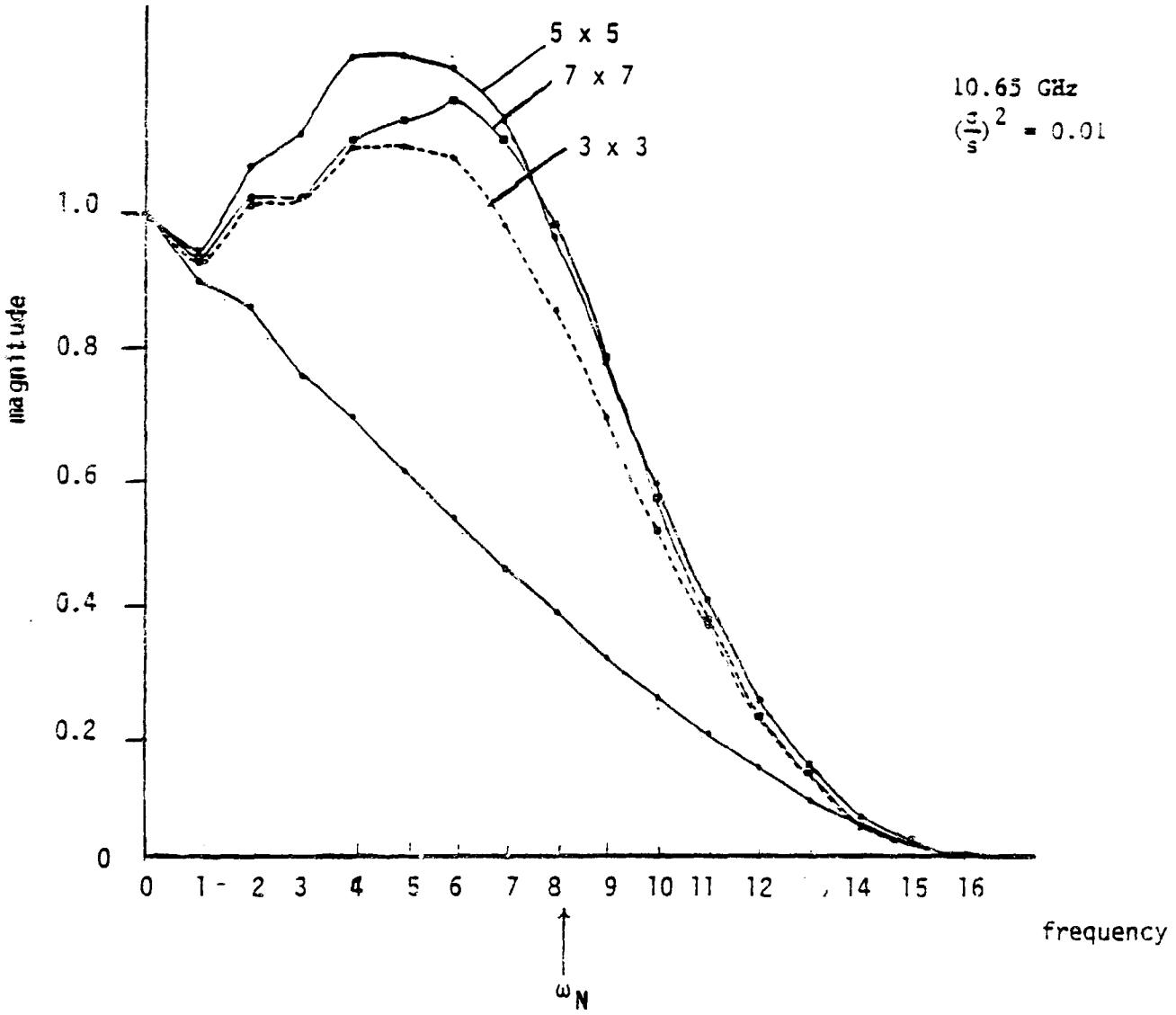

Figure 3.10 Frequency Response of Antenna Patterns Corrected by Different Matrix Sizes

PRECEDING PAGE BLANK NOT FILMED

4.0 SOFTWARE DESCRIPTION

In this chapter, the implementation of APC software and the demonstration of context dependent APC philosophies are described.

In prior work, context-free philosophies were implemented and evaluated. A model of two-dimensional power pattern was generated upon which the APC process was performed. A detailed geometric transformation was developed and coded. This transformation relates the antenna pattern as might be provided through antenna testing to the instrument coordinate system in which digital data is sampled. A system of software was developed to generate antenna pattern correction coefficients in conformance with the established context-free analysis. The system includes routines to calculate cross-correlation, to shift and rotate antenna patterns, and to solve linear equations. Software to generate effective point spread function in instrument coordinates was also developed. Another set of routines was implemented to perform Fourier analysis of the correction processes. With some enhancements, this system provides the basic tool to demonstrate and evaluate the proposed context-dependent antenna pattern correction and side lobe compensation philosophies.

The design and implementation of the APC software functions are based on top-down and modular design. This structural design will be discussed in detail in Section 4.2. The code used in this study is given in Appendix B.

4.1 Functional Organization and Overview

Figure 4.1 shows a system overview of the performed functions. The programs were written in FORTRAN and implemented on the IBM 360/91 at NASA/GSFC. The operational software consists of the following functions:

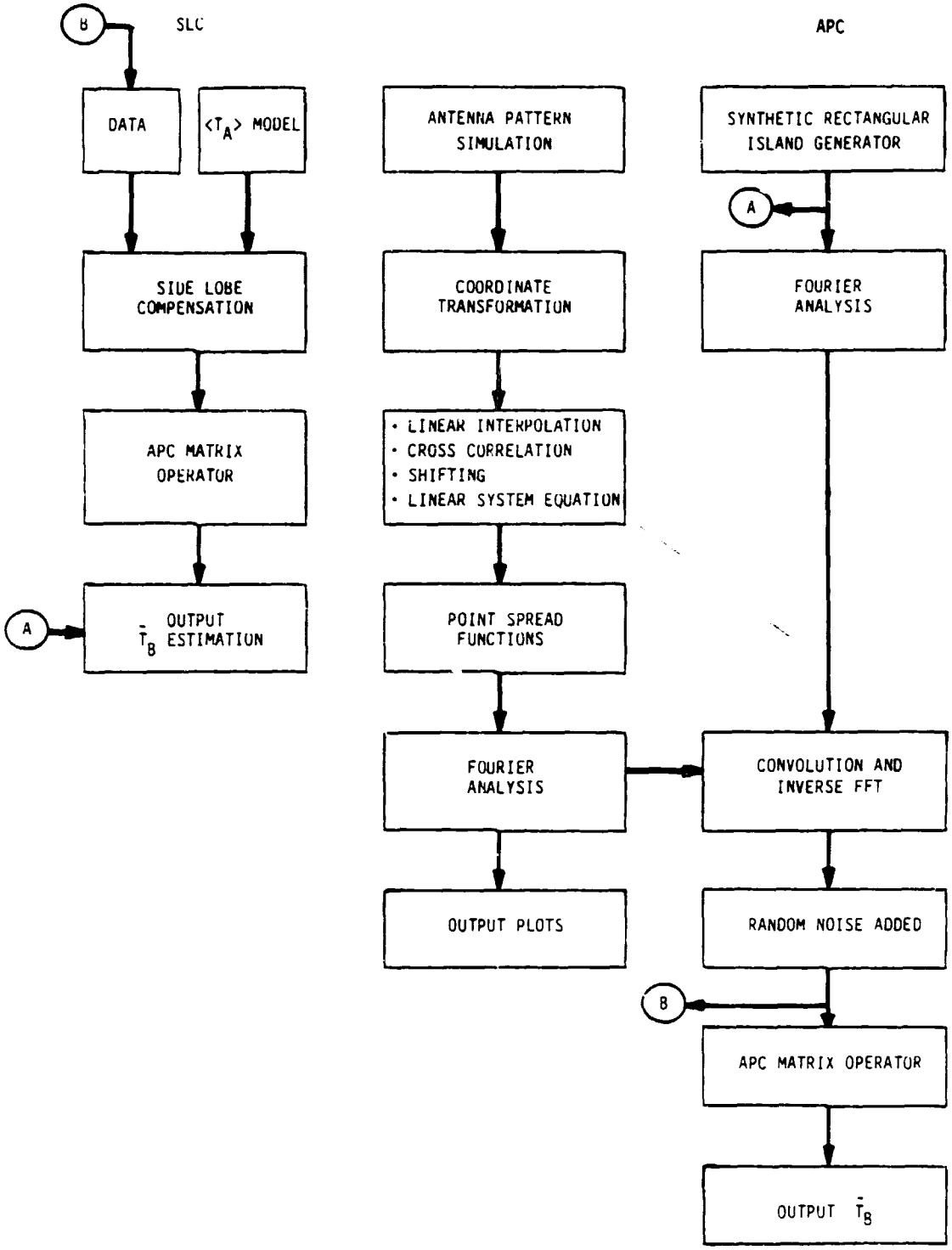

Figure 4.1 Software System Overview

(1) Simulation of an antenna power pattern on a 64×64 plane (k-space) parallel to the antenna aperture.

(2) Transformation of coordinates from the k-space to the instrument coordinates (x-space).

(3) Generation of necessary parameters required by the optimization processes. These parameters are used in the data interpretive equations and the matrix truncation approach.

(4) Determination of correction coefficients by solving the set of linear equations.

(5) Correction of antenna patterns to generate various point spread functions.

(6) Perform two-dimensional discrete Fourier transform of various point spread functions.

(7) Generate synthetic image

(8) Two-Dimensional Fourier Transform on Synthetic Image

(9) Generate antenna temperature field

(10) Add random white noise

(11) Perform matrix HPC operation

S (12) Difference simulated T_A and $\langle T_A \rangle$ model

L (13) Perform matrix APC operator

C (14) Compute brightness temperatures

(15) Generate synthetic scene

In the following subsections the above-mentioned functions are described in detail and flow diagrams are provided.

4.1.1 Simulation of Antenna Pattern

Using the concepts of linearity, the impulse response of an incoherent system due to a circular aperture with a 0-1 function having 1 in the area of the aperture and 0 elsewhere is the so-called Airy disk. In classical optics, an Airy disk is the diffraction pattern intensity for a uniformly illuminated circular aperture. The analytic solution to this pattern is the square of a first order Bessel function divided by its

argument, $[J_1(k)/k]^2$. By assuming a 0-1 real function circular antenna aperture, an antenna power pattern formed on a plane parallel to the antenna aperture will have an Airy disk characteristic.

Subroutine LENS was implemented to generate a 64×64 Airy disk which corresponds to $[J_1(k)/k]^2$. The diameter of the disk was chosen to be 32 with 64 equally-spaced intervals along its diameter. The disk contains the main lobe and more than four side lobes as shown in Figure 4.2(d). The power at each location is computed by the polynomial approximations as shown below:

$$\frac{[J_1(k)]}{k} \simeq \frac{1}{2} - 0.56249\left(\frac{k}{3}\right)^2 + 0.21093\left(\frac{k}{3}\right)^4 - 0.03954\left(\frac{k}{3}\right)^6 + 0.00443\left(\frac{k}{3}\right)^8 - 0.00031\left(\frac{k}{3}\right)^{10} + 0.00001\left(\frac{k}{3}\right)^{12}$$

for $-3 \leq k \leq 3$

wnere $k = \sqrt{k_x^2 + k_y^2}$

with $k_x , k_y = -15.5, -15.0, -14.5, \cdots 0.0, \cdots, 15.5, 16.0$

For $3 \leq k < \infty$

$$\frac{[J_1(k)]}{k} \simeq k^{-3/2} f \cos\theta$$

where

$$f = 0.79788 + 0.000001\left(\frac{3}{k}\right) + 0.1659\left(\frac{3}{k}\right)^2 + 0.00017\left(\frac{3}{k}\right)^3 - 0.00249\left(\frac{3}{k}\right)^4 + 0.00113\left(\frac{3}{k}\right)^5 - 0.00020\left(\frac{3}{k}\right)^6$$

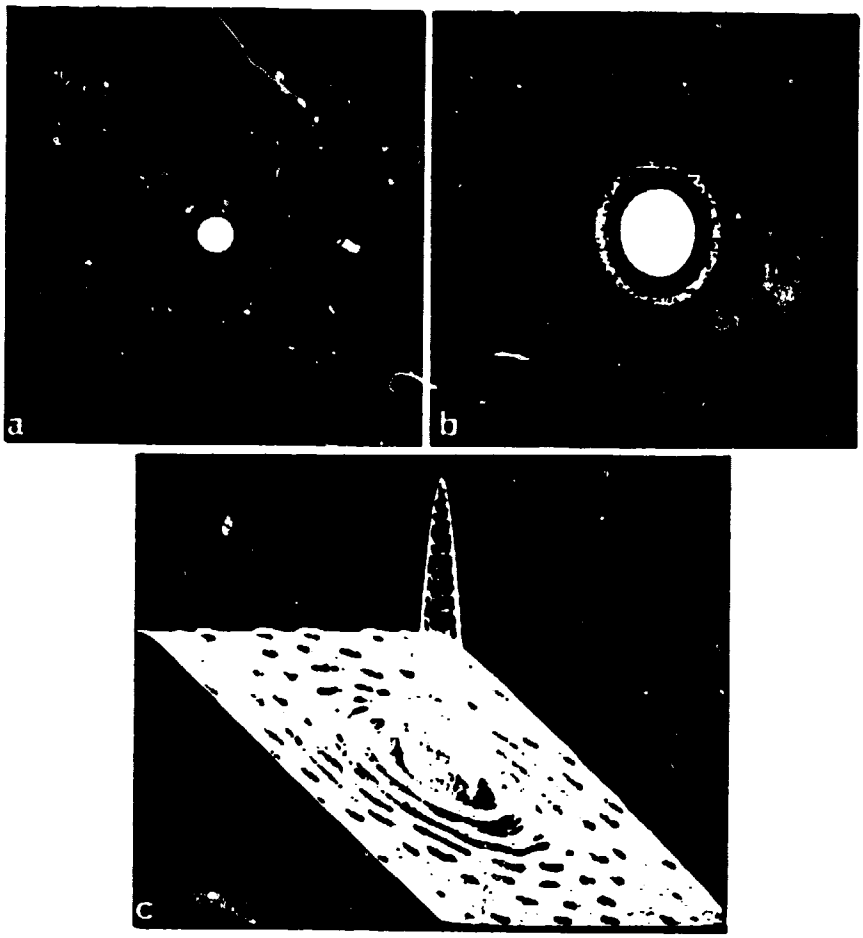

Figure 4.2 Airy disk

a. Circular antenna operture

b. Antenna power pattern, $[\frac{J_1(k)}{k}]^2$

c. Perspective of the antenna power pattern

d. One-dimensional plot of the disk pattern along its diameter

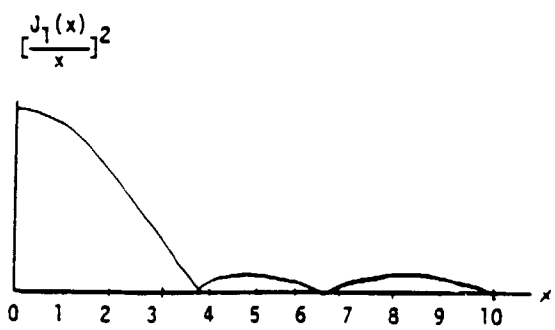

and

$$\theta = k - 2.35619 + 0.12499 \left(\frac{3}{k}\right) + 0.00005 \left(\frac{3}{k}\right)^2$$

$$- 0.00637 \left(\frac{3}{k}\right)^3 - 0.00074 \left(\frac{3}{k}\right)^4$$

$$+ 0.00079 \left(\frac{3}{k}\right)^5 - 0.00029 \left(\frac{3}{k}\right)^6$$

The generated antenna power pattern was normalized to have a total power of one and the resulting Airy disk was stored in a disk file named AIRY.DATA using I/O unit number 12 for ready access. The data flow is shown in Figure 4.3.

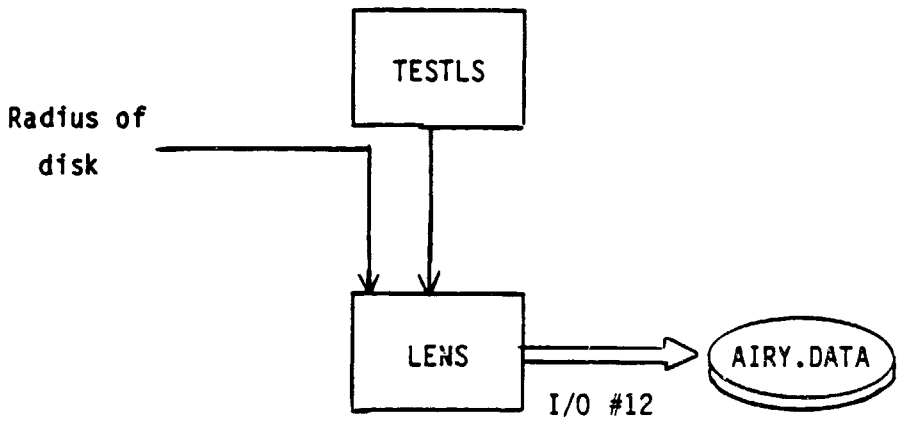

Figure 4.3 Data Flow of Subroutine LENS

TESTLS: Test program for subroutine LENS
LENS: Routine to generate the Airy disk

4.1.2 Coordinate Transformation

Our antenna power pattern is presented in a plane (k-space) orthogonal to the pointing axis of the antenna. We need to transform this coordinate system to instrument coordinates in which the grid is represented by a differential change along the scan and across the scan line.

We begin with the scan pixel i and line number j in instrument coordinates and compute the antenna power and its location in the k-space by the following transformation procedures:

(1) The antenna power pattern (the Airy disk) is retrieved. It consists of a two-dimensional array

$$G(k_x, k_y)$$

where (k_x, k_y) is the integer grid point and G is the antenna power at (k_x, k_y).

(2) Given $\hat{S}_0$, the unit vector of the boresight direction of the antenna, the position of the antenna with respect to the earth, and the instrument coordinates (i,j), the unit vectors $\hat{S}$ from the antenna to (i,j) can be computed.

(3) Then, a pointing vector $\bar{R}$ projected in the k-space orthogonal to $\hat{S}_0$ is expressed as

$$\bar{R} = \frac{\pi D}{\lambda} [(\hat{S}-\hat{S}_0) - (\hat{S}-\hat{S}_0) \cdot \hat{S}_0\hat{S}_0] \text{ where}$$

D is the antenna operture diameter and λ the wavelength.

(4) From k, we can compute the x and y components of k which permits us to interpolate the antenna power pattern $G(k_x, k_y)$ where (k_x, k_y) is closed to (x,y).

(5) The relationship between the power pattern in the k-space and the power pattern in the instrument coordinates is given by

$$A = G\, k^2 \cos\psi_0\, v_0 r_0 \Delta t \Delta\theta \cos(\theta - \theta_0) \frac{(-\hat{s}\cdot\hat{\rho})}{S^2}$$

where A is the power pattern in instrument coordinates,

v_0 is the ground velocity of the satellite subtrack which depends upon earth rotation. It is latitude dependent and assumed constant in the APC computations (v_0 = 7 km/sec.)

r_0 is a nominally constant radius of the ground trace scanned circle. It depends upon the distance from the antenna to the earth's center, the earth's radius and the instrument cone angle ψ_0.

Δt is the time between adjacent line (Δt = 1 sec)

$\Delta\theta$ is the separation in radians between adjacent pixel samples

θ_0 is the angle at which the sweep is orthogonal to the ground velocity vector. In the simplified model, we assume there is no earth rotation and hence $\theta_0 = 0$.

$\hat{s}$ is the instantaneous pointing unit vector from the antenna to the pixel sample.

$\hat{\rho}$ is the instantaneous pointing unit vector from the earth's center to the pixel sample.

$\bar{k}$ is the pointing vector projected onto the k-space

ψ_0 is the instrument pointing angle from Nadir ($\psi_0 = 43.6°$), and

G is the power pattern in k-space.

Subroutine TXFORM was implemented to transform an instrument coordinates (i,j) to (x,y). Subroutine INT3P was implemented to locate three integer grid points in the k-space which are closest to (x,y). Subroutine INTLN performs the bi-linear interpolation to obtain an interpolated power magnitude at (x,y). The main program ANTENA was implemented to link all three subroutines together to generate a file of 64 x 64 elements containing an antenna power pattern in instrument coordinates. The grid spacing is 7/4 kilometers. The generated pattern named ANT.DATA was normalized to have a total power of one and was stored in a disk file using I/O unit number 11. Figure 4.4 shows the data flow.

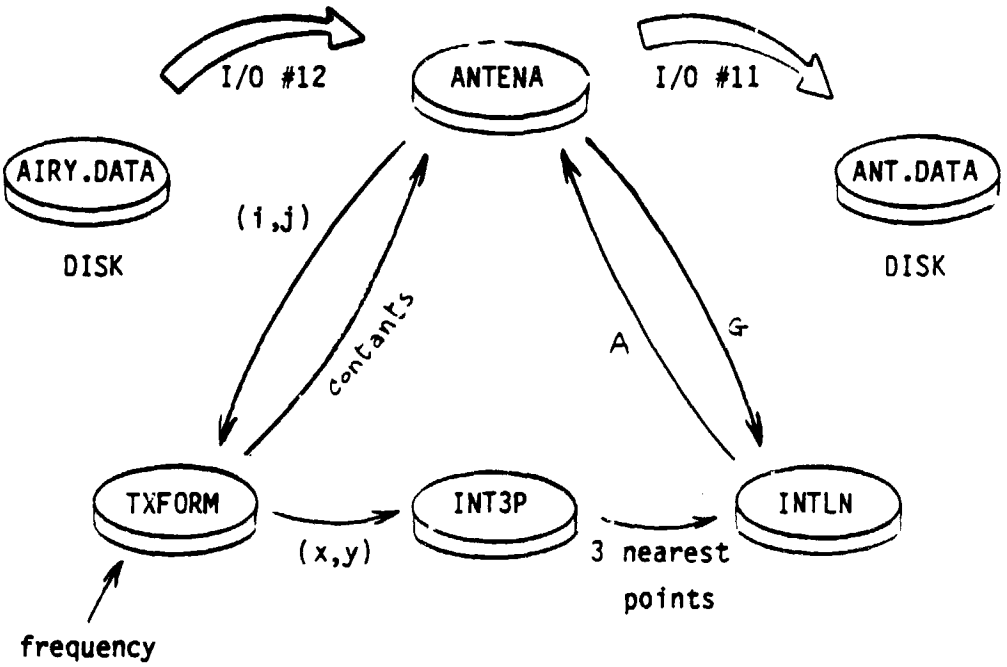

Figure 4.4

Flow diagram of the coordinate transformation and the generation of the antenna power pattern, ANT.DATA, in instrument coordinates.

(i,j) is the instrument coordinates

(x,y) is the k-space coordinates

constants = $k^2 \text{Cos}\psi_0 v_0 r_0 \Delta t \Delta\theta \text{ Cos}(\theta - \theta_0) \frac{(-\hat{s}\cdot\hat{\rho})}{s^2}$

G = power pattern in k-space

A = power pattern in instrument coordinates

INT3P and INTLN are routines to interpolate A

4.1.3 Data Interpretive Equations and Matrix Truncation

A modeled approach is used to estimate the brightness temperature. It involves the estimation of the optimum set of coefficients $\underline{\underline{M}}$ that minimizes the least squares error in the temperature fluctuations. Taking a functional variation of the variance with respect to the estimation coefficients leads to a set of normal equations. By assuming the statistical independence of the brightness temperature fluctuations and a delta function burring effects of the antenna, we simplify the set of normal equations to an expression that only involves the cross-correlation function and shifting of the antenna pattern. We further select a finite set of grid points and truncate the grid, the simplified normal equations become a simple matrix equation:

$$\underline{\underline{M}} = \underline{\underline{\Gamma}}(\underline{\underline{\Sigma}} + \sigma^2 \underline{\underline{I}})^{-1}$$

where $\underline{\underline{M}}$ is the estimation coefficients,

$\underline{\underline{\Sigma}}$ represents the cross-correlation function of the antenna pattern

$\underline{\underline{\Gamma}}$ is the shifted antenna pattern, and

σ^2 is the signal-independent noise.

An element $\Sigma_{i,j}$ of the matrix $\underline{\underline{\Sigma}}$ is approximated by

$$\Sigma_{i,j} = S^2 \sum_{n=1}^{64} \sum_{m=1}^{64} A(i_{x-m}, i_{y-n})\, A(j_{x-m}, j_{y-n})\, \Delta n \Delta m$$

where $i = (i_x, i_y)$ and $j = (j_x, j_y)$ are locations of sample pixels, (n,m) is an integer grid point of the antenna pattern, Δn, Δm are spacings of the grids ($\Delta n = \Delta m = \frac{1}{4}$), S^2 is the signal of the brightness temperature fluctuation, and A is the antenna power pattern. In estimating the 3x3 coefficient matrix, $\bar{\bar{\Sigma}}$ is a 9x9 matrix with elements arranged in a fashion as shown in Figure 4.5.

A 3x3 coefficient matrix $\bar{\bar{M}}$

A	B	C
D	E	F
G	H	I

The 9x9 cross-correlation matrix $\bar{\bar{\Sigma}}$

$$\bar{\bar{\Sigma}} = [\Sigma_{i,j}]$$

$\Sigma_{A,A}$								
$\Sigma_{A,B}$	$\Sigma_{B,B}$							
$\Sigma_{A,C}$	$\Sigma_{B,C}$	$\Sigma_{C,C}$		S	Y M	M E	T R	I C
$\Sigma_{A,D}$	$\Sigma_{B,D}$	$\Sigma_{C,D}$	$\Sigma_{D,D}$					
$\Sigma_{A,E}$	$\Sigma_{B,E}$	$\Sigma_{C,E}$	$\Sigma_{D,E}$	$\Sigma_{E,E}$				
$\Sigma_{A,F}$	$\Sigma_{B,F}$	$\Sigma_{C,F}$	$\Sigma_{D,F}$	$\Sigma_{E,F}$	$\Sigma_{F,F}$			
$\Sigma_{A,G}$	$\Sigma_{B,G}$	$\Sigma_{C,G}$	$\Sigma_{D,G}$	$\Sigma_{E,G}$	$\Sigma_{F,G}$	$\Sigma_{G,G}$		
$\Sigma_{A,H}$	$\Sigma_{B,H}$	$\Sigma_{C,H}$	$\Sigma_{D,H}$	$\Sigma_{E,H}$	$\Sigma_{F,H}$	$\Sigma_{G,H}$	$\Sigma_{H,H}$	
$\Sigma_{A,I}$	$\Sigma_{B,I}$	$\Sigma_{C,I}$	$\Sigma_{D,I}$	$\Sigma_{E,I}$	$\Sigma_{F,I}$	$\Sigma_{G,I}$	$\Sigma_{H,I}$	$\Sigma_{I,I}$

Figure 4.5

The $\bar{\bar{\Sigma}}$ matrix of a 3x3 matrix equation

The elements of the $\bar{\bar{\Gamma}}$ matrix is nothing more than the shifted antenna power pattern multiplies by S^2 given by

$$\Gamma_i = S^2 A(i_x, i_y)$$

In the 3x3 coefficient matrix problem, $\bar{\bar{\Gamma}}$ is a 9x1 column vector and can be written as $\bar{\bar{\Gamma}} = (\Gamma_A \Gamma_B \Gamma_C \ldots \Gamma_I)^T$.

The matrix equation then becomes

$$\bar{\bar{M}} = \bar{\bar{\Gamma}}' S^2 \, (\bar{\bar{\Sigma}}' S^2 + \sigma^2 \, \bar{\bar{I}})^{-1}$$

$$(\bar{\bar{\Sigma}}' + \frac{\sigma^2}{S^2} \bar{\bar{I}}) \, \bar{\bar{M}} = \bar{\bar{\Gamma}}'$$

where $\bar{\bar{\Sigma}}' S^2 = \bar{\bar{\Sigma}}$, $\bar{\bar{\Gamma}}' S^2 = \bar{\bar{\Gamma}}$ and $\frac{\sigma^2}{S^2}$ is the square of the noise to signal ratio. This equation is in the form of $\bar{\bar{A}}\bar{\bar{X}} = \bar{\bar{B}}$ linear equations where given the $\bar{\bar{A}}$ and $\bar{\bar{B}}$ matrices, $\bar{\bar{X}}$ can be solved for by Gaussian elimination with partial pivoting.

Subroutine CONVOL was implemented to compute the cross-correlation of two antenna patterns centered at i and j respectively. Both i and j are neighborhood sample pixels of the center of a 64x64 plane. The computed cross-correlation is used to generate the $\bar{\bar{\Sigma}}'$ of various sizes. The $\bar{\bar{\Sigma}}'$ matrix can be a 9x9, 25x25, or 49x49 matrix determined by the size of the matrix of correction coefficients. Figure 4.6 shows three different window sizes of $\bar{\bar{M}}$ with respect to the antenna pattern.

Subroutine GAMMA was implemented to compute the matrix $\bar{\bar{\Gamma}}'$. The generated $\bar{\bar{\Gamma}}'$ is a 9x1, 25x1, or 49x1 row vectors. Having obtained $\bar{\bar{\Sigma}}'$ and $\bar{\bar{\Gamma}}'$, subroutine COEF solve the linear equations by using the IMSL subroutine LEQT1F. The resulting $\bar{\bar{M}}$ contains correction coefficients and they are normalized to have a sum of one.

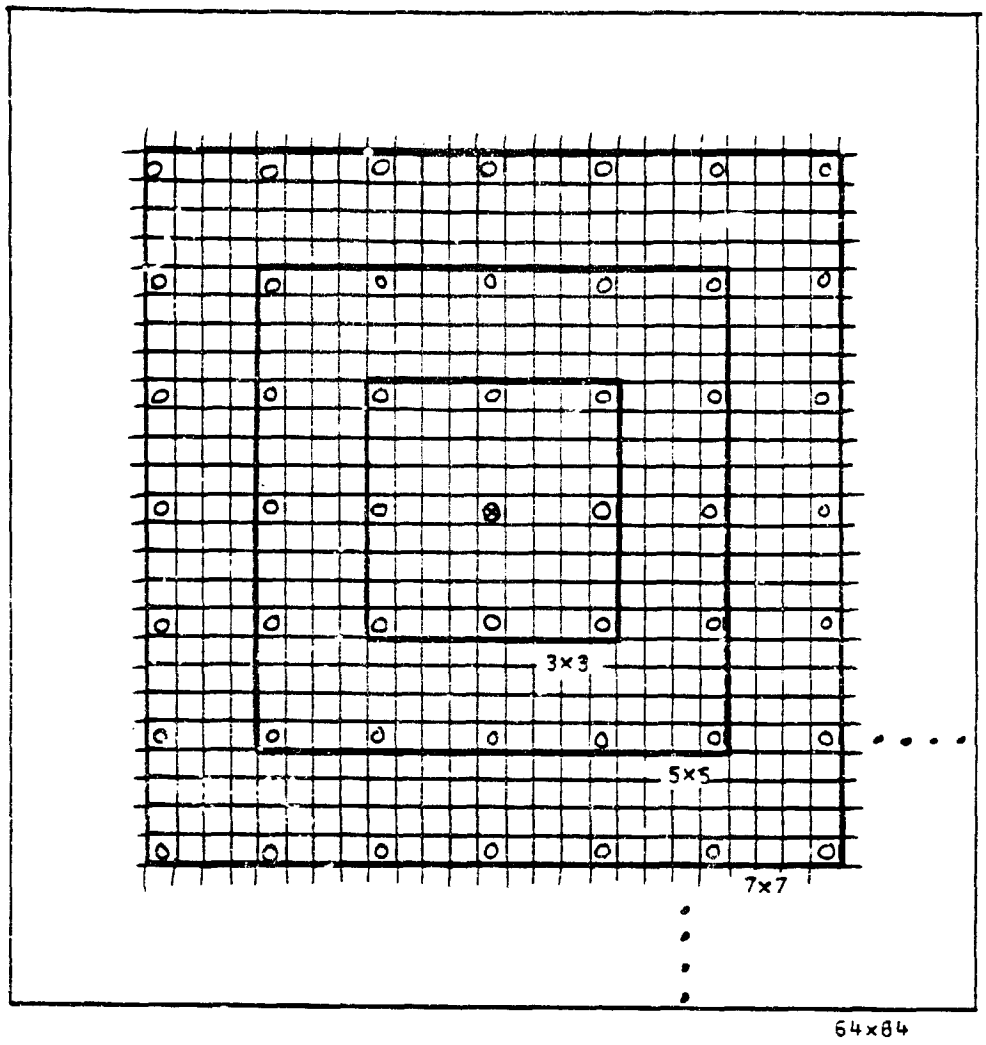

⊗ center of a 64x64 antenna pattern

○ sample pixels

grids of antenna pattern

Figure 4.6

The 3x3, 5x5, and 7x7 correction windows superimpose on a 64x64 antenna pattern.

Figure 4.7 presents three sets of coefficients generated by the above described procedures with 10.65 GHZ and a signal to noise ratio of 10.

0.066	-.713	0.066
-.440	3.046	-.440
0.070	-.726	0.070

-.005	0.001	0.211	0.001	-.005
-.044	0.051	-.921	0.051	-.044
0.087	-.479	3.198	-.479	0.087
-.043	0.060	-.941	0.060	-.043
-.005	-.008	0.225	-.008	-.005

0.001	0.010	-.042	-.104	-.042	0.010	0.001
-.006	-.003	0.040	0.298	0.040	-.003	-.006
0.008	-.034	0.040	-.966	0.040	-.034	0.008
-.020	0.095	-.459	3.252	-.459	0.095	-.020
0.009	-.034	0.052	-.989	0.052	-.034	0.009
-0.006	-.002	0.022	0.316	0.022	-.002	-.006
0.000	0.008	-0.030	-.110	-.030	0.008	0.000

Figure 4.7

Correction Coefficient Matrices $\underline{\underline{M}}$, of sizes 3x3, 5x5, and 7x7 at ω = 10.65 GHZ and $(\sigma/S)^2$ = 0.01

4.1.4 Point Spread Function of the Corrected Antenna Pattern

The optimum set of correction coefficients $\bar{\bar{M}}$ can be used to estimate the brightness temperature measurements T_B by the linear combination of $\bar{\bar{M}}$ and the antenna temperature measurements T_A. It has been recognized that the estimated T_B is associated with a specific point spread function given by

$$PSF(\bar{x}) = \sum_{\bar{i}} M_{\bar{i}} A(\bar{x} + \bar{i})$$

where $\bar{\bar{M}}$ can be thought of as a local template that operates on each and every pixel $\bar{x}$ of the antenna pattern A. The vector $\bar{i}$ points from the center of the template to pixels inside the template and $M_{\bar{i}}$ represents the coefficient at $\bar{i}$. The value of the PSF at $\bar{x}$ is then computed by the weighted sum of A at various locations $(\bar{x} + \bar{i})$.

Subroutine ANTPSF was implemented to comput the point spread function of the antenna pattern ANT.DATA. For the 3x3 coefficient matrix, 37,000 multiplications and additions are needed to generate the 64x64 PSF. The resultant point spread function is stored on a disk file named PSF.DATA using I/O unit number 13. Figure 4.8 shows the data flow and all the software modules required to generate the coefficients and point spread function.

A system of software was implemented to perform Fourier analysis of the antenna pattern correction processes. It includes routines to perform two-dimensional discrete Fourier transform, and to compute decibels, power spectrum and various output functions.

4.2 Software Structure

Top-down design and modular programming are used in the design and implementation of the APC demonstration software. All the routines are documented and listed in Appendix B.

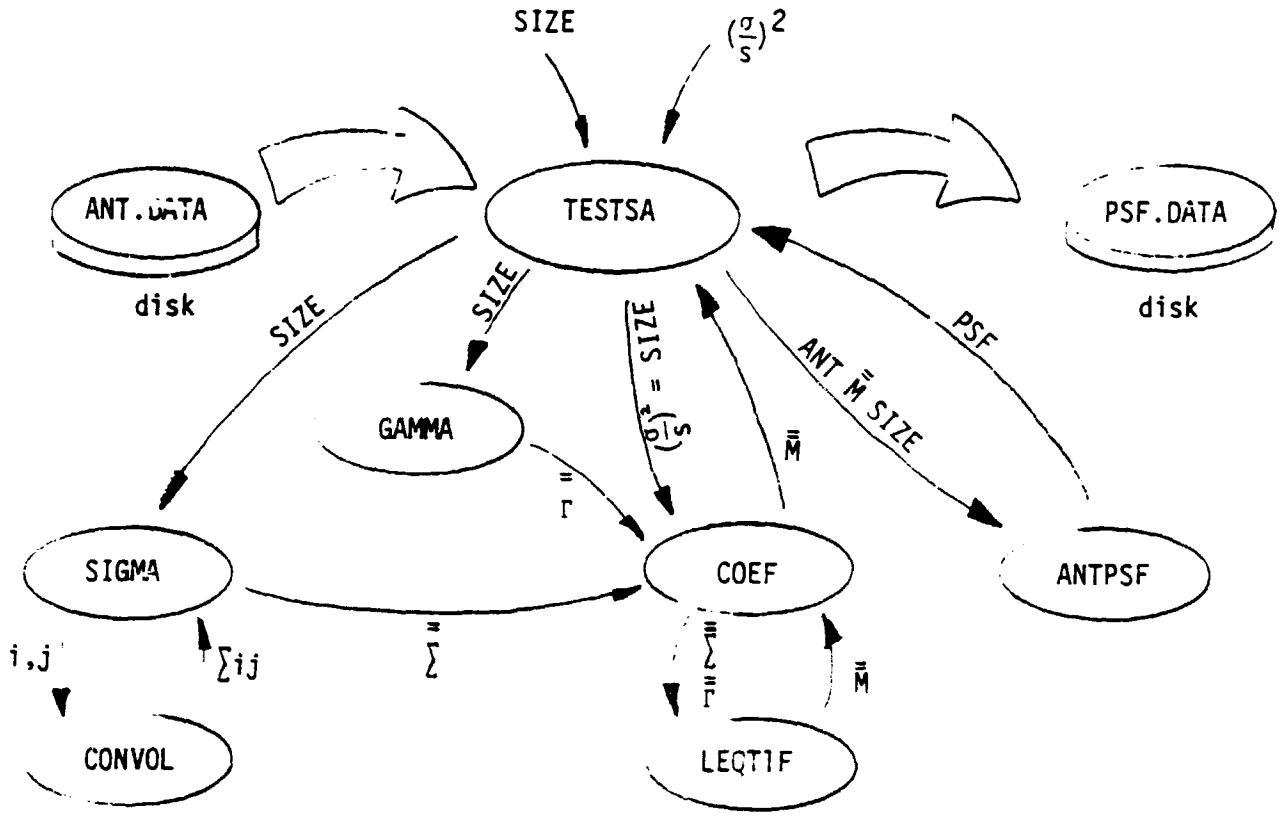

SIZE = 3, 5, or 7

$\frac{\sigma}{s}$ = noise to signal ratio

(i,j) = pixel locations

$\bar{\bar{\Sigma}}$ = cross-correlation matrix

$\bar{\bar{\Gamma}}$ = shifted antenna matrix

$\bar{\bar{M}}$ = correction coefficients

ANT = antenna power pattern

PSF = point spread function

Figure 4.8

Data Flow and Software Modules for the Generation of Coefficients and Point Spread Function

The idea of top-down design can be viewed as breaking down the problem into simpler problems and checking the relationships between them before proceeding to a more detailed specification. In programming, it involves decomposing the overall complicated program into precisely specified subprograms, so that each subprogram is solved correctly, and fitting these solutions together in a specified way. This programming method allows us to generate clean algorithms with far fewer mistakes than by the conventional line-by-line method.

Modular programming has several objectives. (1) A program module must be working correctly by itself regardless of the context of its use in building larger systems of software. (2) To realize large software systems, program modules written under different authorities must be conveniently fitted together without changes in any of the component modules. A module is joined to other modules by communication links. Each module receives data from its input links, transforms it, and outputs it to other modules over its output links. Function subprograms and subroutine subprograms can serve as program modules. The use of FORTRAN is a reasonable choice in the implementation of the APC software to test out module design.

Top-down modular analysis can be described by a graphical model in the form of a tree of the functions to be performed. Attached to each node of the tree are programs to perform specialized operations and structure tests. Each node can branch to one of the other nodes in the same level. All nodes are also modular, meaning they are completely independent of the other nodes. Programs that are designed on the basis of this method are very simple to debug or to modify. Each module can be tested separately and when it works, can be added to the system.

The tree diagram of the software system for the APC processes is shown in Figure 4.9. This graphical structure specifies the types and instances when primitive operators in terms of subroutines are used during the APC processes. The program modules below the first level are

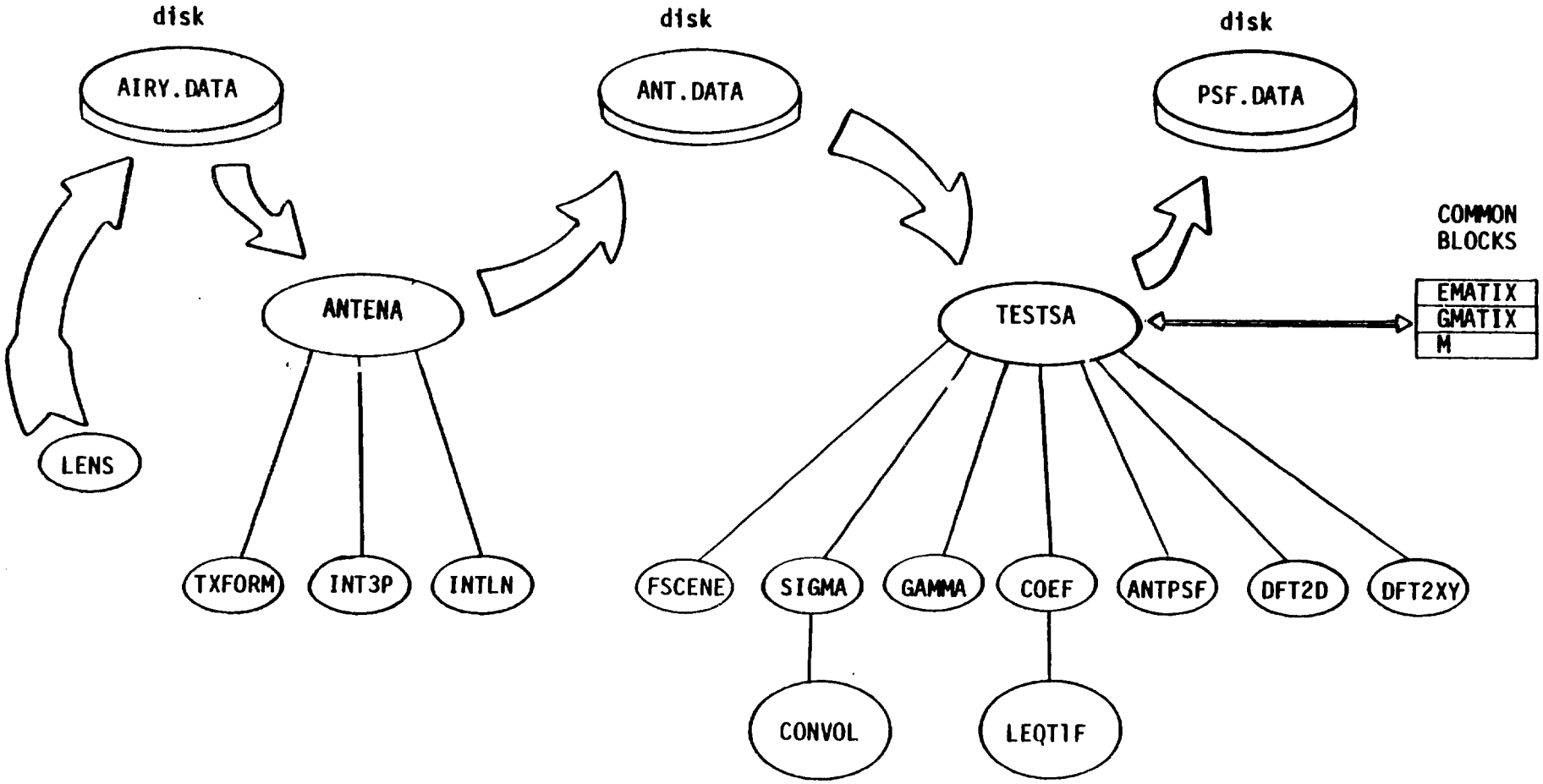

Figure 4.9 Software System and its Structure for the APC Demonstration Procedures (Descriptions of Software Modules are Listed in Section 4.2)

primitive operators that perform function described in previous sections. Attached to each module of the software tree structure are a list of program variables and common storage areas. All communication between modules is through the program variables connecting them at a higher or lower level in the tree. The modules at all levels are basically independent of each other. Hence, changes in any of the modules may only require modifications in themselves and a minimum number of changes in the nodes directly connected to them. The parent node is a supervising program. It performs the functions of linking the primitive modules together, branching to appropriate ones, testing their program variables, evaluating their performances, and outputting results.

The following summarizes the various primitive modules implemented. Each is associated with a different primitive operation, and each is stored in a disk file.

PRIMITIVE MODULE	DESCRIPTION
LENS	To generate a 64x64 Airy disk, which corresponds to the square of the first-order Bessel function divided by its argument.
	INPUTS: RADIUS (radius of the disk)
	OUTPUTS: AIRY (airy disk on disk file)
TXFORM	To transform a discrete location in the instrument coordinates to an antenna coordinate system orthogonal to the antenna pointing axis.
	INPUTS : (FJX, FJY) (Antenna Pointing Direction)
	(FIX, FIY) (pixel location on ground)
	GHZ (radiometer frequency)
	NOSPS (number of samples/scan line)
	OUTPUTS: (QX, QY) (transformed coordinates)
	CONST (transformed antenna constant)

INT3P — To locate 3 nearest neighborhood grid points

INPUTS : (QX, QY) (input point)
OUTPUTS : (AX, AY)
(BX, BY) (3 nearest grid points)
(CX, CY)

INTLN — To perform bi-linear interpolation

INPUTS : (QX, QY) (input point)
(AX, AY)
(BX, BY) (3 nearest grid points)
(CX, CY)
AIRY (Common block contains Airy disk)
OUTPUTS : VALUE (interpolated value at (QX, QY))

CONVOL — To compute the cross-correlation of two antenna power patterns centered at i and j respectively.

INPUTS : (IX1, IY1) (1st point)
(IX2, IY2) (2nd point)
OUTPUTS : EI1I2 (the cross-correlation)

SIGMA — To compute the $\bar{\bar{\Sigma}}$ matrix

INPUTS : ISIZE (window size of $\bar{\bar{M}}$)
ANT (common block contains power pattern)

OUTPUT : EMATIX (matrix $\bar{\bar{\Sigma}}$)

GAMMA — To compute the $\bar{\bar{\Gamma}}$ matrix, a windowed antenna power pattern

	INPUTS :	ISIZE	(window size of $\bar{\bar{M}}$)
		ANT	(common block contains power pattern)
	OUTPUTS :	GMATIX	(matrix $\bar{\bar{\Gamma}}$)

COEF — To solve the set of linear equations

	INPUTS :	ISIZE	(window size of $\bar{\bar{M}}$)
		SNTSR	(square of noise to signal ratio)
		EMATIX	(common block contain $\bar{\bar{\Sigma}}$)
		GMATIX	(common block contain $\bar{\bar{\Gamma}}$)
	OUTPUTS :	GMATIX	(common block contain $\bar{\bar{M}}$)

ANTPSF — To compute the point spread function associated with a specific coefficient matrix $\bar{\bar{M}}$

	INPUTS :	ISIZE	(window size of M)
		GMATIX	(common block contains M)
		ANT	(common block contain power pattern)
	OUTPUTS :	PSF	(common block contain corrected pattern)

DFT2D — To compute the two-dimensional discrete Fourier transform of an MXN image.

	INPUTS :	(M,N)	(size of the input image)
		FXY	(input image)
	OUTPUTS :	FUVRL	(transformed image, real)
		FUVIM	(transformed image, imaginary)

DFT2XY — To compute the two-dimensional discrete Fourier transform along the 2 axes of an 64x64 image, to compute their power and dB, and to output results.

INPUTS :	FXY	(input image)
OUTPUTS :	FUREAL	(2-D DFT real along V=0 axis)
	FUIMAG	(2-D DFT imaginary along V=0 axis)
	FVREAL	(2-D DFT real along U=0 axis)
	FUIMAG	(2-D DFT imaginary along U=0 axis)
	FUMAGN	(2-D power spectrum along V=0 axis)
	FVMAGN	(2-D power spectrum along U=0 axis)
	FUDB	(dB along V=0 axis)
	FVDB	(dB along U=0 axis)

FSCENE — To compute the fourier transform of an image using subroute DFT2D. The resulting real and imaginary parts are stored at FSCENER.DATA and FSCENEI.DATA with 15 and 16 as LUN's

INPUTS :	IDUM	(64×64 input image)
OUTPUTS :		Are Real and Imaginary transforms stored in LUN 15 and 16.

MAIN PROGRAM	DESCRIPTION
TESTLN	Test program for subroutine LENS and to create the Airy disk.
ANTENA	Main program to generate a simulated antenna power pattern on an instrument coordinate system.

INPUTS : AIRY (common block contains Airy disk)
GHZ (primary radiometer frequency)
OUTPUTS : ANT (common block contains antenna power pattern)

TESTSA — Main program to generate the APC correction matrix $\bar{M}$, to compute the corrected antenna point spread function, and to perform Fourier analysis.

INPUTS : ANT (common block contains antenna power pattern)
ISIZE (window size of correction matrix $\bar{M}$)
SNTSR (square of noise to signal ratio)
OUTPUTS : PSF (common block contains point spread function)

5.0 CONCLUSIONS AND RECOMMENDATIONS

The analyses and demonstrations in this report illustrate a method for processing LAMMR data so as to extract a context sensitive brightness temperature for side lobe compensation and at the same time, to modify the antenna pattern for frequency enhancements. The objectives in this processing are to suppress the influences of the side lobes and to enhance the spatial frequency responses. The influences from side lobes become a severe problem when the antenna encounters land-ocean boundaries, since the contrast between land and ocean is very high. There is, however, a serious problem in connection with the antenna patterns: there is a loss in spatial responses as a result of the finite size of the receiving antenna. In this context, the ideal antenna pattern correction processing should correct the side-lobe influences and enhance the spatial frequency responses. Both of these desires cannot be simultaneously achieved with linear processing; context sensitive processing is the answer. The antenna side lobes can be suppressed by a linear filter only at the expense of spatial resolution. On the other hand, the enhancement of the pattern also enhances Gibb's oscillations near discontinuities. There is no way to compensate the antenna frequency responses and avoid radiance from nearby land masses beaming through the antenna side lobes. However, this study shows it is feasible to suppress the Gibb's oscillations as well as enhance frequences by incorporating an a-priori model in the correction process. This can be done by using information about where land masses are situated geographically. In so doing, a process has been established to remove side-lobe influences near land-ocean interface and to simultaneously enhance spatial frequency responses everywhere. The results of this study show how to use the a-priori knowledge of location of land-ocean boundaries for antenna pattern correction.

It has been shown that no single context-free antenna pattern correction process will adequately compensate for the antenna side lobe influences, while simultaneously enhance the spatial frequency responses

modulated by the physical limitations of the antenna. It is for this reason that a context-sensitive antenna pattern correction process was developed in details and was implemented to prove its feasibility. There are several context-sensitive techniques which were applied in this application study.

- A statistically-derived world brightness map that contains a priori knowledge of expected brightness temperature over the surface of the earth was simulated to generate expected antenna temperatures and the temperature biases associated with the geographical locations of land and ocean. These biases were incorporated into the context-sensitive APC synthetic model to compensate for the side-lobe effects.

- The use of a two-model procedure in conjunction with the world brightness map was simulated for the applications of different sets of coefficients in two different situation. In the case of near land-ocean boundaries, a special set of correction coefficients was applied so as to eliminate some of the artifacts associated with Gibb's oscillations. Another general set of correction coefficients was then be used everywhere over uniform ocean to enhance spatial frequencies. The set near the boundaries, however, blured that interface and did not really meet the objectives.

- Another approach was to hypothesize the existence of land-ocean boundaries everywhere and apply a set of coefficients that suppresses side lobes to the entire scene, thereby affecting the APC performance over the ocean. Analysis proved this technique to be too complex for Real time ground processing.

Errors measurements of these different context-sensitive approaches were assessed and a trade-off analysis was conducted to make the final selection. The trade-off included performance evaluations. Computational requirements such as resolution versus side-lobe suppression and noise amplications were also studied and used in the trade-off evaluation.

The Recommended Algorithm

In general, a model of expected brightness temperatures, $\langle T_B \rangle$, must be constructed based on the geographical locations of land-ocean boundaries and the statistical data of ocean phenomena. Given this world brightness model, the expected antenna temperatures, $\langle T_A \rangle$, can be generated. The fluctuation of antenna temperature, δT_A, are then computed as the difference between expected and measured antenna temperatures. APC process matched to the statistical data base are then be applied to the fluctuation δT_A in order to generate the fluctuation brightness temperatures δT_B. The final data interpreted brightness temperature is computed as:

$$T_B = \langle T_B \rangle + \delta T_B .$$

It is recommended that this context-sensitive approaches be implemented for LAMMR ground processing. A complete evaluation of various context-sensitive approaches and context-free approaches showed it to be the most practicable.

APPENDIX A

Appendix A

Detailed Analysis

A.1 Basic Mathematical Formulation of Antenna Temperatures

In this section, we deal specifically with the problem of performing transformations on the antenna point spread functions that are viable in order to maximize the information contained in the data without being severely penalized by the influences of noise.

There are several elements of concern in the performance of the antenna pattern correction:

- The desire to limit the convolution array size needed to perform the APC.
- The formulation of the problem in the continuum domain so as to avoide complications that may result from aliasing influences.
- The desire to include alternative measures of performance as suggested by A. Stogryn.

In general, the problem that must be solved involves the inversion of a set of horizontal and vertical polarization antenna temperatures T_A (2x1 vector) that are sampled uniformly over some grid to an estimate of the brightness temperature components of polarization anywhere in the spatial field. In usual applications, the brightness temperature estimates are evaluated at the same set of grid points upon which the

measurements of antenna temperature are made. However, in general, the estimation problem also provides for estimates at points other than those sampled grid points.

We assume that the antenna temperature measurement at any instrument coordinate location $\bar{x}$ is a linear combination of brightness temperatures located in the neighborhood of $\bar{x}$ plus a random noise element denoted by ε. The antenna pattern designated by A is assumed to be an explicit 2×2 matrix function of $\bar{x}$ to account for the possibility of varying geometries and polarizations as the antenna is scanned across the field of view. Equation (1) expresses this relationship:

$$T_A(\bar{x}) = \iint d^2\bar{x}' \; A_{\bar{x}}(\bar{x}-\bar{x}') \; T_B(\bar{x}') + \varepsilon(\bar{x}) \; . \qquad (1)$$

The instrument coordinate system is defined as follows:

x_1 = direction along the scan with integer values representing the location of each sampled data point.

x_2 = direction along the ground track with integer values representing the scan line number.

Unfortunately, the antenna pattern is non-stationary in this coordinate system (it rotates with x_1 and may undergo compression/expansion as a function of x_2 depending upon S/C latitude). Antenna pattern measurements are usually performed in a space which is simply related to "Solid Angle Space", Ω. We shall strongly suggest K-space for antenna patternrepresentations in sections that follow. It is usual, however, to represent the antenna response function, G, in solid angle space, as follows:

$$\bar{T}_A(\hat{s}_0) = \int_E \bar{\bar{G}}(\hat{s}_0,\hat{s})\ \bar{T}_B(\rho,\bar{s})\ d\Omega \qquad (2)$$

where $\hat{s}$ is a unit vector from the antenna in the direction of the solid angle $d\Omega$. The region of integration E includes all directions $\hat{s}$ which intercept the portion of the earth visible from the satellite if the very small contributions from the cosmic background radiation and possible contributions from the spacecraft itself are neglected. In (2), $\bar{\bar{G}}(\hat{s}_0,\hat{s})$ is the antenna gain 2×2 matrix function (normalized so that $\int_{4\pi}$ trace $[\bar{\bar{G}}]\ d\Omega = 1$) and $\bar{T}_B(\vec{\rho},\hat{s})$ is the brightness temperature polarizatic s propagating toward the antenna. $\bar{T}_B$ depends on both the region being viewed, which is indicated by the position vector $\vec{\rho}$ from the center of the earth to the point on the earth's surface, and the direction of propagation $-\hat{s}$ to the satellite.

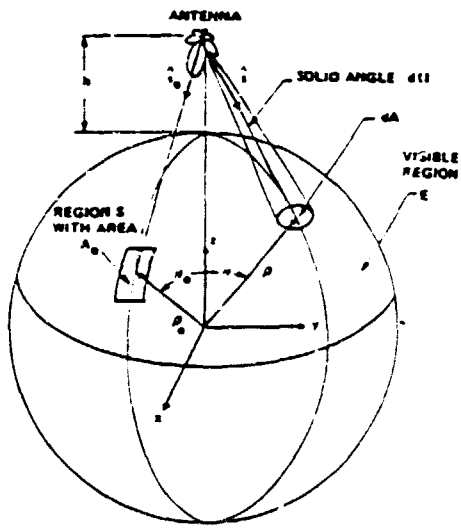

Figure A.1 Geometry for Antenna Temperature Determination

$\bar{T}_B$ corresponds to a two-vector of Horizontal and Vertical components of polarization, $\bar{T} = \begin{pmatrix} T_H \\ T_V \end{pmatrix}$.

The antenna pattern components of the 2×2 tensors consist of G_{HH}, G_{HV}, G_{VH}, and G_{VV}. As a first problem, we assume $G_{HV} = G_{VH} \equiv 0$ everywhere so that Horizontal and Vertical components do not mix. The generalization to other mixing cases is not difficult.

A.2 K-Space Representation

Our antenna representation is best expressed in k-space (pointing vector space). We consider incoming radiation at fixed frequency and hence wave vector magnitude (pointing vector in units of inverse antenna radius)

$$K^2 = k_x^2 + k_y^2 + k_z^2 = \left[\frac{\pi D}{\lambda}\right]^2$$

This is equivalent to having chosen λ in units of the antenna radius. k_z is chosen along the "look" direction of the antenna. This (k_x, k_y) space is important because in this space, the antenna electric field response function is the Fourier transform of the antenna aperture

$$E = \int_{d\bar{x}} (\text{unit source } (k_x,k_y))\ A(x)\ e^{i\bar{k}\cdot\bar{x}}$$

and $T_A(\hat{s}_0)$, the power, or antenna temperature which is the expected square value of electric field $\langle E^2 \rangle$ is the Fourier transform of the antenna aperture function $A(\bar{x})$ convolved onto itself. Likewise, if we choose $\bar{k}$-space as the spatial coordinates to represent the antenna point spread function, then the corresponding antenna frequency response will be the multiplication of $A(\bar{\omega})$ with itself. Since $A(\bar{\omega})$ has a sharp cut-off corresponding to the finite antenna at $|\bar{\omega}| \equiv \omega_c$ radius, then so will the convolution $A(\bar{\omega}) \times A(\bar{\omega})$ have a sharp cut-off at $|\bar{\omega}| = 2\omega_c$

The antenna pattern is presented in coordinates (k_x, k_y) from which

$$k_z = +\sqrt{K^2 - k_x^2 - k_y^2} \quad \text{and} \quad \sin\varphi = \sqrt{\frac{k_x^2 + k_y^2}{K}}$$

can be determined. Also, $\hat{S} = +\frac{\bar{K}}{K}$; $\hat{S}_o = +\frac{\bar{k}_o}{K}$ lies along $\hat{Z}$ (look axis of the antenna). Inversely; given $\hat{S}_o$, $\hat{S}$ we may construct

$$\bar{K} = K\,\hat{S} \; ; \; \bar{K}_o = K\,\hat{S}_o$$

and

$$\bar{q} \equiv (\bar{K} - \bar{K}_o) - (\bar{K} - \bar{K}_o) \cdot \frac{\bar{k}_o\,\bar{k}_o}{K^2}$$

which lies in a plane orthogonal to $\hat{S}_o$ permitting the computation of k-coordinates for antenna pattern computations. Now, let $\hat{a}$ be a downward directed unit vector along the LAMMR rotation axis. (See Figure A.2). Then $\frac{\hat{S}_o \times \hat{a}}{\sin\varphi_o} = \hat{x}$ is a unit vector directed in the negative scan direction, $\hat{z} = \hat{s}_o$ and $\hat{s}_o \times \hat{x} = \hat{y}$ can be computed to determine an orthogonal set of unit vectors. From this, we can compute

$$q_x = \bar{q} \cdot \hat{x} \quad \text{and} \quad q_y = \bar{q} \cdot \hat{y}$$

to give us the coordinates of the antenna pattern corresponding the $(\hat{S}_o, \hat{S})$; i.e., $G(\hat{S}_o , \hat{S}) \equiv G_{q_x,q_y}$ where G_{q_x,q_y} is the representation file in k-space.

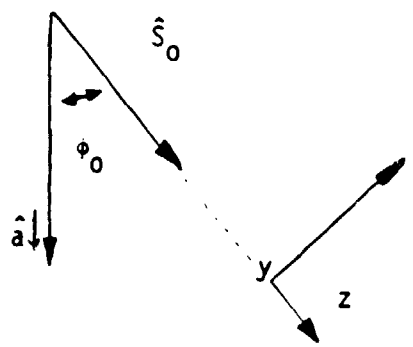

Figure A.2 LAMMR Geometry

A.3 Solid Angle to Area Integration

The transformation from solid angle integration to area integration utilizes:

$$d\Omega = \frac{(-\hat{S}\cdot\hat{\rho})}{S^2}\, dA$$

where $\hat{\rho}$ points to the area (km^2) element from the earth's center, and S is the distance to the area element from the antenna (km). Given the position vector of the S/C, $\bar{r}_{s/c}$, and the radius of the earth r_e we note that

$$\bar{S} = r\,\hat{\rho} - \bar{r}_{s/c}$$

then

$$\hat{S} = \bar{S}/S$$

where

$$S^2 = S_x^2 + S_y^2 + S_z^2$$

and

$$\hat{S}\cdot\hat{\rho} = \frac{\bar{S}\cdot\bar{\rho}}{sr_e} = r_e^2 - \bar{r}_{s/c}\cdot\bar{\rho} = r_e - r_{s/c}\, r_e \cos\phi$$

where ϕ is the cone angle between $\bar{\rho}$ and $\bar{r}_{s/c}$; this then completes the needed transformation.

A.4 Area to Instrument Coordinates

For conversion to instrument coordinates, we also need to compute the area generated by a differential change in the scan pixel (dj) and in the scan line ID (di).

If $\bar{v}_o$ is the ground track velocity (km/sec) and θ_o is the angle at which antenna scan motion on the ground $\perp$ to $\bar{v}_o$

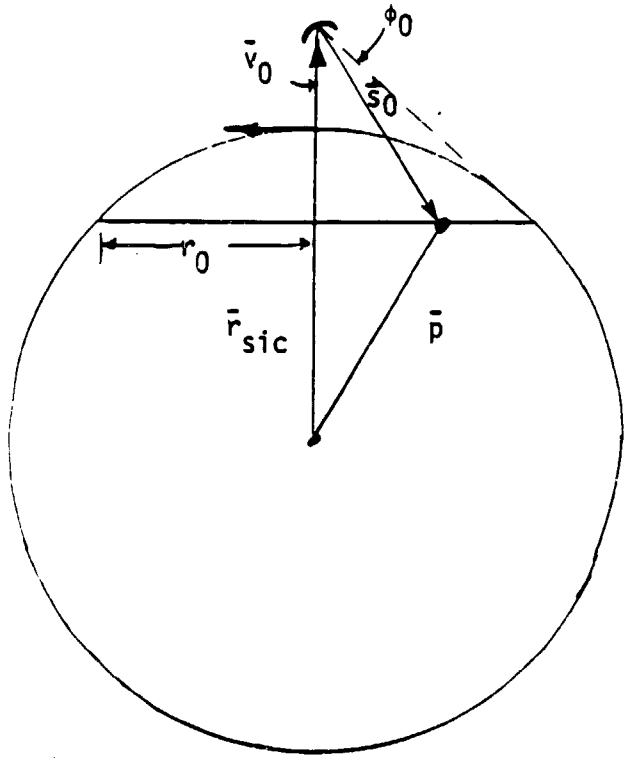

Figure A.3 Scanner Geometry Relative to Earth

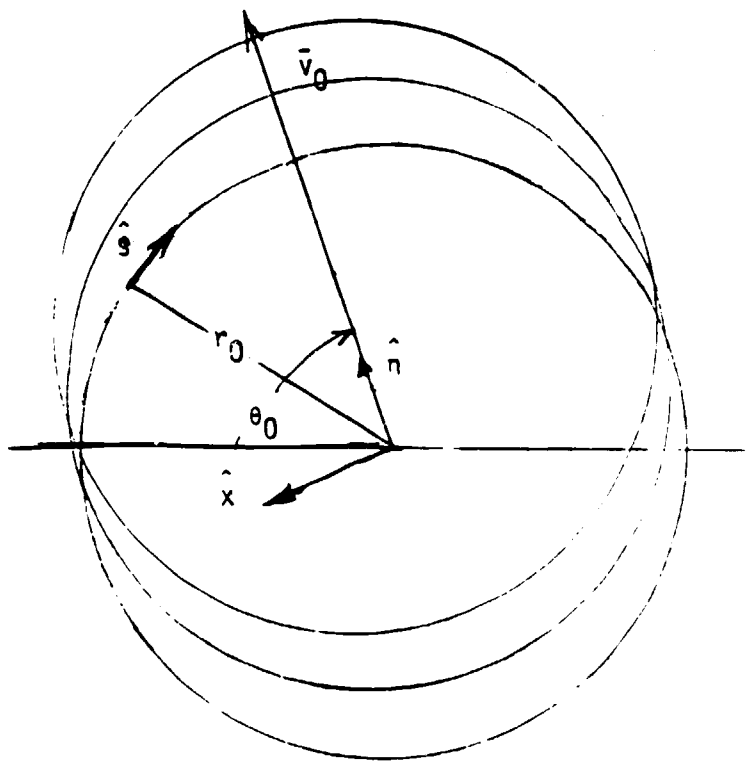

Figure A.4 LAMMR Circles on Earth's Surface

then, $r_o = S_o \sin \phi_o$ where $S_o = r_{s/c} \cos \phi_o - \sqrt{r_e^2 - r_{s/c}^2 \sin^2 \phi_o}$

i.e., $|\bar{\rho}|^2 = |\bar{r}_{s/c} + \bar{S}_o|^2 = r_e^2$ and $\bar{r}_{s/c} \cdot \bar{S}_o = r_{s/c} S_o \cos \phi_o$.

By defining a coordinte system (ground coordinates) via

$$\hat{\xi} = \frac{-\bar{r}_{s/c}}{r_{s/c}} \quad , \quad \hat{n} = \frac{\bar{v}_o}{v_o} \quad \text{and} \quad \hat{\chi} = \hat{n} \times \hat{\xi} \ .$$

then tne unit vector, $\hat{\delta}$, along the scan direction at any location θ is given by:

$$\hat{\delta} = -\hat{\chi} \cos (\theta - \theta_o) - \hat{n} \sin (\theta - \theta_o) \ .$$

The unit vector , $\hat{\ell}$, in the down track direction along the surface of the earth is orthogonal to both $\hat{\rho}$ and $\hat{\chi}$ and can be expressed as

$$\ell = \frac{\hat{\chi} \times \hat{\rho}}{|\hat{\chi} \times \hat{\rho}|} \ .$$

Here $\bar{\rho} = -\hat{\xi} \sqrt{r_e^2 - r_o^2} + r_o \hat{n} \cos (\theta - \theta_o) - r_o \hat{\chi} \sin (\theta - \theta_o)$,

then $\hat{\chi} \times \bar{\rho} = \hat{n} \sqrt{r_e^2 - r_o^2} + \hat{\xi} r_o \cos (\theta - \theta_o)$ which has magnitude $\sqrt{r_e^2 - r_o^2} \sin^2 (\theta - \theta_o)$. So

$$\hat{\ell} = \hat{n} \left\{ \frac{r_e^2 - r_o^2}{r_e^2 - r_o^2 \sin^2 (\theta - \theta_o)} \right\} 1/2 + \hat{\xi} \frac{r_o \cos (\theta - \theta_o)}{\sqrt{r_e^2 - r_o^2 \sin^2 (\theta - \theta_o)}} \ .$$

Now, the angle between $\hat{\ell}$ and $\hat{\delta}$ is obtained by computing $\hat{\ell} \times \hat{\delta}$:

$\hat{\ell} \times \hat{s}$ is

$$\begin{vmatrix} \hat{x} & \hat{n} & \hat{\xi} \\ 0 & \left[\frac{r_e^2 - r_o^2}{r_e^2 - r_o^2 \sin^2(\theta-\theta_o)}\right]^{1/2} & \frac{r_o \cos(\theta-\theta_o)}{\sqrt{r_e^2-r_o^2 \sin^2(\theta-\theta_o)}} \\ -\cos(\theta-\theta_o), & -\sin(\theta-\theta_o) & 0 \end{vmatrix}$$

$$= \hat{x} \frac{r_o \cos(\theta-\theta_o) \sin(\theta-\theta_o)}{\sqrt{r_e^2 - r_o^2 \sin^2(\theta-\theta_o)}}$$

$$- \hat{n} \frac{r_o \cos^2(\theta-\theta_o)}{\sqrt{r_e^2-r_o^2 \sin^2(\theta-\theta_o)}} + \hat{\xi} \frac{(r_e^2-r_o^2)^{1/2} \cos(\theta-\theta_o)}{\sqrt{r_e^2-r_o^2 \sin^2(\theta-\theta_o)}}$$

$$= \frac{+\cos(\theta-\theta_o)\,\bar{\rho}}{\sqrt{r_e^2-r_o^2 \sin^2(\theta-\theta_o)}}$$

which has magnitude

$$\frac{\cos(\theta-\theta_o)}{\sqrt{1-\left(\frac{r_o}{r_e}\right) \sin^2(\theta-\theta_o)}} \equiv \cos\langle \hat{\ell}, \hat{s} \rangle$$

where $\langle \hat{\ell}, \hat{s} \rangle$ denotes angle between $\hat{\ell}$ and $\hat{s}$.

(1) The element of arc length generated by dj (one pixel) is:

$$r_o \Delta\theta \quad \text{where} \quad \Delta\theta \equiv \frac{150°}{180°} \frac{\pi}{N} = \frac{5\pi}{6} \frac{1}{N},$$

with N equals to the number of scan points per line.

(2) The element of length generated by the s/c ground motion during di (one line time = one second) is:

$$v_o \sqrt{1-(\frac{r_o}{r_e})^2 \sin^2 (\theta-\theta_o)}\ \Delta t \qquad \text{where } \Delta t = 1 \text{ sec.}$$

(3) The area of (di) (dj) is therefore

$$d^2A = v_o \sqrt{1-(\frac{r_o}{r_e})^2 \sin^2 (\theta-\theta_o)}\ \Delta t\ r_o \Delta\theta \cos \langle \hat{\ell}, \hat{s} \rangle\ di\ dj$$

Finally,

$$\boxed{d^2A = v_o\ \Delta t \Delta\theta\ r_o \cos (\theta-\theta_o)\ di\ dj}$$

A.5 Transformation From Solid Angle Coordinates to Instrument Coordinates:

The transformation from Solid Angle Coordinates to instrument coordinates is done via the area representation as follows:

$$T_A (\hat{S}_o) = \int_\Omega G (\hat{S}_o, \hat{S})\ T_B (\bar{\rho}, \hat{S})\ d\Omega$$

$$= \int dA\ G\ (\frac{-\hat{S}\cdot\hat{\rho}}{S^2})\ T_B$$

$$= \int d^2X\ G \{v_o\ r_o\ \Delta t\ \Delta\theta \cos (\theta-\theta_o)\} * (\frac{-\hat{S}\cdot\hat{\rho}}{S^2})\ T_B$$

where $d^2X \equiv di\ dj$. Hence, $A_{\bar{X}_o} (\bar{X}_o-\bar{X})$

$$\equiv G (\hat{S}_o,\hat{S})\ v_o\ r_o\ \Delta t\ \Delta\theta \cos (\theta-\theta_o)\ \frac{(-\hat{S}\cdot\hat{\rho})}{S^2}$$

designates the total relationship between the antenna pattern in instrument coordinates (A) and the corresponding pattern in solid angle space, G .

A.6 The Computation Process

We begin with the antenna pointing location i_o , j_o and designate X_1 , X_2 as arbitrary location variables in instrument coordinates. We desire to compute the antenna pattern for all (X_1 , X_2) when the antenna is pointing at location (i_o , j_c) . Then

$$T_A (i_o,j_o) = \int dX_1 \, dX_2 \, A_{i_o,j_o} (i_o-X_1 \, j_o-X_2) \, T_B(X_1,X_2) .$$

Elements to be computed are

$$v_o , r_o , \Delta t , \Delta\theta , \cos (\theta-\theta_o) , \theta_c , \hat{S} , \hat{\rho} , S^2 \text{ and, } G(\hat{S}_o,\hat{S})$$

(a) v_o Computation

v_o is the ground velocity of the satellite subtrack which depends upon earth rotation. It is latitude dependent but can be assumed constant for APC coefficient computations.

(b) r_o Computation

r_o is a nominally constant radius of the LAMMR ground trace scanned circle. It depends upon s/c distance from the earth's center, and the earth's radius at subtract location. It also depends upon the instrument pointing angle ϕ_o from Nadir.

$$r_o = S_o \sin \phi_o$$

where

$$S_0 = r_{s/c} \cos \phi_0 - \sqrt{r_e^2 - r_{s/c}^2 \sin^2 \phi_0} \ .$$

This is computed by looking at $\bar{S}_0 = \bar{\rho}_0 - \bar{r}_{s/c}$ and $\bar{\rho} \cdot \bar{\rho} = r_e^2 = S_0^2 + r_{s/c}^2 + 2\, r_{s/c}^2\, S_0 \cos \phi_0$. Here ϕ_0 is the instrument cone angle.

(c) Δt Computation

Δt is the time between adjacent line samples - nominally it is $\Delta t = 1$ sec.

(d) $\Delta\theta$ Computation

$\Delta\theta$ is the separation in radians between adjacent pixel samples

$$\Delta\theta = \frac{1}{150^\circ} \underbrace{(150^\circ)}_{\substack{\text{swath} \\ \text{width}}} \times \frac{1}{N}$$

where N = Number of samples per swath. Nominally, N = 256 or 512 and is dependent on the channel frequency.

(e) θ_0 Computation

θ_0 is the angle at which the sweep is orthogonal to the ground velocity vector. Nominally, θ_0 depends on geometry and on conventions. It also depends upon the effects of earth rotations. In the absence of earth rotation we may establish a geometry for which $\theta = 0$ corresponds to forward looking; i.e., ($\theta_0 = 0$) . The effects of earth rotation can be computed using the transformation equation between inertial and body coordinates

$$\left.\frac{d}{dt}\right|_B = \left.\frac{d}{dt}\right|_\alpha - \bar{w}_\epsilon X$$

Hence, $\bar{v}_B \equiv \bar{v}_I - \bar{w}_e X \bar{r}_{s/c}$. The ground observed s/c velocity varies in both magnitude and direction dependent upon latitutde: the ground velocity magnitude is

$$\bar{v} = \bar{v}_B \left(\frac{r_e}{r_{s/c}}\right)$$

and the direction relative to $\bar{v}_I$ is

$$\sin \theta_o = \frac{|\bar{v}_I \times \bar{v}_B|}{v_B v_I}$$

$$= \frac{|v_I \times (w_e \times r_{s/c})|}{v_B v_I}$$

This computation gives

$$\frac{|\bar{w}_e(\bar{r}_{s/c} \cdot \bar{v}_I) - \bar{r}_{s/c}(\bar{v}_I \cdot \bar{w}_e)|}{v_B v_I}$$

when $\bar{r}_{s/c} \cdot \bar{v}_I = 0$ (circular orbit), then

$$\sin \theta_o = \frac{r_{s/c}}{|v_B|} \frac{v_z}{|v_I|}$$

which is latitude dependent.

(f) θ and $\cos(\theta - \theta_o)$ Computation

θ is the pixel related angle associated with j :

$$\theta = \theta_o + \Delta\theta \left(j - \frac{N}{2}\right) .$$

At scene center $j = \frac{N}{2}$ and $\theta = \theta_o$.

(g) $\bar{S}$ and $\bar{\rho}$ Computations

$\hat{S}$ and $\hat{\rho}$ are instantaneous pointings to pixels from the s/c and earth center, respectively. They are related through

$$\bar{r}_{s/c} + \bar{S} = \bar{\rho} .$$

We must compute $\bar{\rho}$ from our knowledge of i_o , j_o , X_1 and X_2 . We also assume initial conditions relative to the earth so that the position $\bar{\rho}$ corresponds to indices i_o , j_o . Then, the change from i_o to X_1 and j_o to X_2 corresponds to a rotation about the ground $\hat{x}$ coordinate axis by an angle

$$\frac{v_o \Delta t}{r_e} (X_2 - j_o) \equiv \delta_j$$

followed by a rotation about the new $\hat{\xi}'$ axis by angle

$$\Delta\theta \ (X_1 - i_o) \equiv \delta_i .$$

The transformation is:

$$\bar{\rho} = \begin{Bmatrix} \cos\delta_i & -\sin\delta_i & 0 \\ \sin\delta_i & \cos\delta_i & 0 \\ 0 & 0 & 1 \end{Bmatrix} \begin{Bmatrix} 1 & 0 & 0 \\ 0 & \cos\delta_j & -\sin\delta_j \\ 0 & +\sin\delta_j & \cos\delta_j \end{Bmatrix} \bar{\rho}_o .$$

C-2

Note: The order of these rotations are as specified since a reverse order would affect a rotation about the $\hat{x}'$ axis which would not result in a translation in the $\bar{v}$ direction for δ_j .

It is appropriate to expand the δ_j rotations for small angles while retaining finite angle (approximations for δ_i . We then note that if

$$\bar{\rho} \equiv \bar{\bar{T}}\, \bar{\rho}_o$$

then

$$\bar{\bar{T}} = \begin{Bmatrix} \cos\delta_i & -\cos\delta_j \sin\delta_i & +\sin\delta_j \sin\delta_i \\ \sin\delta_i & \cos\delta_j \cos\delta_i & -\sin\delta_j \cos\delta_i \\ 0 & +\sin\delta_j & \cos\delta_j \end{Bmatrix}$$

$$= \begin{Bmatrix} \cos\delta_i & -\sin\delta_i & +(\delta_j)\sin\delta_i \\ \sin\delta_i & \cos\delta_i & -(\delta_j)\cos\delta_i \\ 0 & +(\delta_j) & 1 \end{Bmatrix}$$

So

$$\rho_x = \rho_{x_o} \cos(\delta_i) - \rho_{y_o} \sin(\delta_i) + \rho_{z_o} (\delta_j) \sin(\delta_i)$$

$$\rho_y = \rho_{x_o} \sin(\delta_i) + \rho_{y_o} \cos(\delta_i) - \rho_{z_o} (\delta_j) \cos(\delta_i)$$

$$\rho_z = + \rho_{y_o} (\delta_j) + \rho_{z_o} .$$

Further approximations for small δ_i leads to the quadratic approximation

$$\rho_x - \rho_{x_0} = -\rho_{x_0}\left(\frac{\delta_i^2}{2}\right) - \rho_{y_0}(\delta_i) + \rho_{z_0}(\delta_j\ \delta_i)$$

$$\rho_y - \rho_{y_0} = \rho_{x_0}(\delta_i) - \rho_{y_0}\left(\frac{\delta_i^2}{2}\right) - \rho_{z_0}(\delta_j)$$

$$\rho_z - \rho_{z_0} = + \rho_{y_0}(\delta_i)$$

The relative error of neglecting quadratic terms is

$$\max\left[\left(\frac{\delta_i}{2}\right), \delta_j\right].$$

If we are concerned in the APC process only with pixels that are five (5) elements removed from the origin, then the relative displacement errors will be

$$\max\left[\frac{5}{2}\ \Delta\theta\ , 5\ \frac{v_o \Delta t}{r_e}\right]$$

$$\sim [\ .025\ ,\ .0058\ ].$$

This is a negligible fraction of a pixel displacement. Hence, a linear approximation is completely justified. Then

$$\rho_x - \rho_{x_0} = \rho_{y_0}(\delta_i)$$

$$\rho_y - \rho_{y_0} = +\rho_x\ (\delta_i) = \rho_{z_0}(\delta_j)$$

$$\rho_z - \rho_{z_0} = +\rho_{y_0}(\delta_j)$$

Computing $\bar{\rho}$ from $\bar{\rho}_o$ given δ_i and δ_j permits us to compute

$$\bar{S} = \bar{\rho} - \bar{r}_{s/c}$$

(h) $\bar{S}_o$ Computation

$$\bar{S}_o = \bar{\rho}_o - r_{s/c}$$

(i) S^2 Computation

$$S^2 = \bar{S} \cdot \bar{S}$$

(j) $[\hat{S}_o , \hat{S}]$ Computation

$$\hat{S}_o = \frac{\bar{S}_o}{|\bar{S}_o|} \qquad \hat{S} = \frac{\bar{S}}{|\bar{S}|}$$

(k) $G(\hat{S}_o , \hat{S})$ Computation

Suppose we have a file consisting of the antenna calibration data: it would consist of a two-dimensional array

$$G_{q_x q_y} .$$

Given $\hat{S}_o$, $\hat{S}$, we could construct

$$\bar{K} = K \hat{S} \qquad \bar{K}_o = K \hat{S}_o$$

where

$$K = \frac{2\pi D}{\lambda} .$$

with

D = diameter of antenna aperture, and

λ = wavelength of a particular frequency.

Then, $\bar{q} = \{(\bar{k}-\bar{k}_o) - (\bar{k}-\bar{k}_o) \cdot \hat{S}_o \hat{S}_o\}$ is an antenna related (negative) pointing vector projected in a plane orthogonal to $\hat{S}_o$. Then,

$$\hat{S}_o \times \hat{\xi} = \hat{X} \sin \phi_o$$

and

$$\hat{y} = \hat{S}_o \times \hat{X}$$

permits us to compute $q_x = \bar{q} \cdot \hat{X}$ and $q_y = \bar{q} \cdot \hat{y}$ from which the file lookup in the Gq_x, q_y tables permits us to determine $G(\hat{S}_o, \hat{S})$.

Other useful equations are:

$$\bar{\rho} - \bar{\rho}_o = \bar{\Omega} \times \bar{\rho}_o$$

where

$$\bar{\Omega} = \hat{X} \delta_j + \hat{\xi} \delta_i .$$

Also,

$$\bar{S} - \bar{S}_o \equiv \bar{\rho} - \bar{\rho}_o .$$

But,

$$\hat{S} = \frac{(\bar{S}_o + \bar{\Omega} \times \bar{\rho}_o) S_o}{S \hat{S}_o}$$

and

$$\hat{S} = \frac{S \bar{S}_o}{S \hat{S}_o}$$

So $$\hat{S} - \hat{S}_0 = \frac{\bar{\Omega} \times \bar{\rho}_0}{S} - \frac{(S^2 - S_0^2)\,\hat{S}_0}{S\,(S+S_0)} \quad .$$

Now

$$S^2 = S_0^2 + (\bar{\Omega}\times\bar{\rho}_0)^2 + 2\,\bar{S}_0 \cdot (\bar{\Omega}\times\bar{\rho}_0) \quad .$$

Hence,

$$\hat{S} - \hat{S}_0 = \frac{(\bar{\Omega}\times\bar{\rho}_0) - (\bar{\Omega}\times\bar{\rho}_0)\cdot\hat{S}_0\hat{S}_0}{S_0} \quad .$$

But,

$$\bar{S}_0 = \bar{\rho}_0 - \bar{r}_{s/c}$$

So $$(\bar{\Omega}\times\bar{\rho}_0)\cdot\bar{S}_0 \equiv + r_{s/c}\,(\bar{\Omega}\times\bar{\rho}_0)\cdot\hat{\xi} \quad .$$

A.7 A Preliminary Model of an Ideal Antenna in Instrument Coordinates

All of the analyses of the previous sections have been oriented toward the derivation of an antenna pattern as seen in instrument coordinates, the coordinate system in which data samples are uniformly distributed. In this context, the aperture function of the antenna as presented in k-space, if given, would permit one to compute the desired response of the antenna in brightness temperatures in the instrument coordinates. To accomplish this, the aperture function would be convolved onto itself, resulting in the Fourier transform of the antenna response function as projected in k-space. From there, the computation to instrument coordinates is as delineated in Sections A.1 through A.6.

In this section, we consider an ideal antenna of circular aperture, having a uniform aperture distribution up to the edge the antenna. The antenna diameter is assumed to be four meters. We can compute the electric field response of this antenna by considering a unit-point source emanating energy towards the antenna aperture with a pointing vector making an angle ϕ with respect to the bore-sight direction.

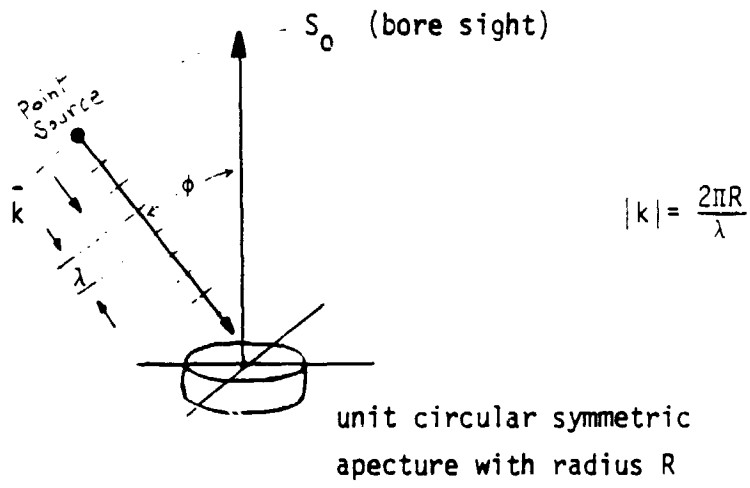

Figure A.5 Circular Aperture

For a unit source, the electric field response is:

$$E_{\bar{k}} = 2 \int_0^R r dr \int_0^{\pi} d\theta \; e^{i \bar{k} \cdot \bar{r}}.$$

$$= 2 \int_0^R r dr \int_0^{\pi} d\theta \; e^{i |k| \sin \phi \; r \cos \theta}$$

$$= a \left| \frac{2J_1(k)}{k} \right|$$

where

$$a = \text{area of the dish} = \pi R^2$$

and

$$K = 2\pi \sin \phi \frac{R}{\lambda} .$$

The power antenna response function is

$$A_{\vec{k}} = bE_{\vec{k}}^2 = b\, a^2 \left[\frac{2J_1(k)}{K}\right]^2$$

and must be normalize such that

$$\int d\Omega\, A_{\vec{k}} = 1 .$$

Hence,

$$b = \frac{1}{a^2 \int d\Omega \left(\frac{J_1(k)}{K}\right)^2}$$

we note the mathematical identity:

$$J_n(z) = \frac{i^{-n}}{\pi} \int_0^{\pi} e^{iz \cos\theta} \cos(n\theta)\, d\theta .$$

So

$$E_{\vec{k}} = (2)\pi \int_0^R rdr\, J_0 (k\, r \sin \phi) .$$

Let

$$k_{11} = k \sin \phi ,$$

then

$$E_k = 2\pi \int_0^R r dr \, J_0(k_{11} r)$$

$$= 2 \frac{\pi}{k_{11}^2} \int_0^{Rk_{11}} \xi d\xi \, J_0(\xi)$$

we also note:

$$\int_0^z t^v J_{v-1}(t) \, dt = z^v J_v(z) \quad \text{for Real } v > 0 .$$

Hence

$$\int_0^z t J_0(t) \, dt = z J_1(z) .$$

So

$$E_k = \frac{\pi}{k_{11}^2} Rk_{11}) J_1(Rk_{11}) = 2\pi R^2 \frac{J_1(Rk_{11})}{(Rk_{11})}$$

A two-dimensional file was created in k-space to represent this theoretically ideal power pattern and is the input for further transformations to instrument coordinates. It must be emphasized here that since this antenna response function has a finite band-limited Fourier transform, that an exact representation of this function could be obtained by a finite sampling in accordance with Shanon's criteria for band-limited signals. This sampling requirement corresponds to a sampling of the antenna pattern with spacing δk equal to one point every π divided by two sampling intervals. With this coarse sampling

requirement, the antenna function is exactly represented provided one does a sinc function interpolation between the established values. Since the sinc function interpolator is computationally inefficient, it was decided to sample the antenna function over a finer interval so that linear interpolation between points would be adequate.

In one dimension, the representation of a uniformly distributed band limited amplitude spectra with $w_c = 2$ gives the point spread function sinc(k) . If we sample this function at uniform intervals $k = i\Delta k$, and interpolate with a linear interpolator, we will generate an error which is easily viewed in the Fourier domain. The sampled function has an amplitude spectra which is the original "box car" spectra but repeated at uniform intervals of $\Delta w = \frac{2\pi}{\Delta k}$. The linear interpolator convolves with the comb function of the sampled data to yield a piecewise linear approximation to sinc(k) . This convolution in the spatial domain is a product function in the frequency domain. The linear interpolator Fourier transform function is:

$$\text{sinc}^2 \frac{w\Delta k}{2} .$$

The choice of Δk in the use of a linear interpolator is determined by the maximum transfer error which may be generated. There are two competing sources of error generated by a finite Δk .

- Modulation at the cutoff frequency $w_c = 2$ of the antenna
- Modulation at the first repeated zone corresponding to

$$w = \frac{2\pi}{\Delta k} - w_c .$$

This is illustrated in Figure A.6. The maximum error occurs at $w_c = 2$ and has magnitude .08 when $\Delta k = .5$. The mean RMS error can be shown to be $\frac{1}{\sqrt{5}}$ max error $\approx .035$ when $\Delta k = .5$. As a function of Δk, the maxi-

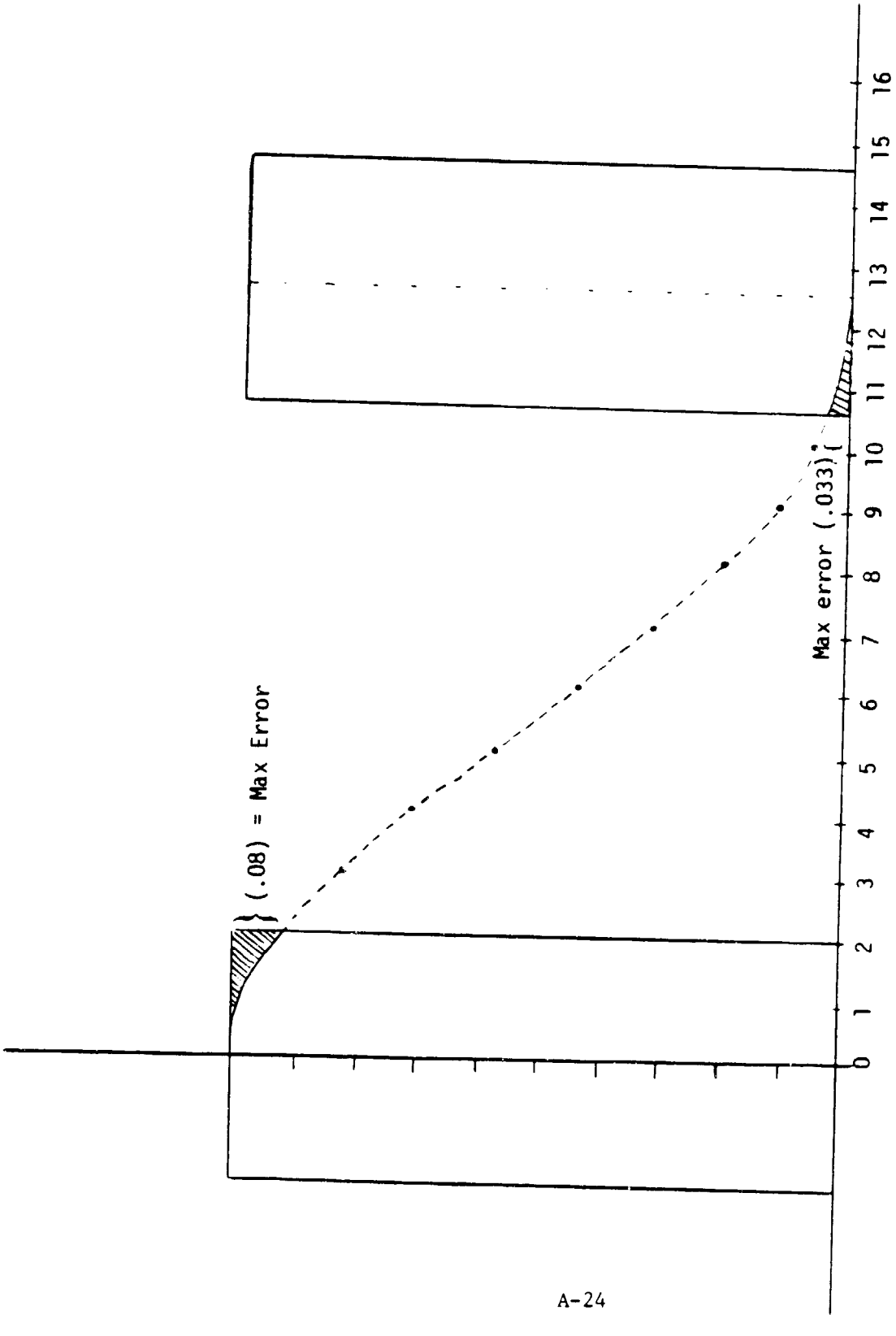

Figure A.6 Representation Error of the Antenna Pattern

mum error is $E_{max} = \frac{1}{3}(\Delta k)^2$ and the mean error is:

$$E_{mean} = \frac{1}{3\sqrt{5}}(\Delta k)^2 .$$

For initial investigations, a mean representation error of 3-1/2% was accepted and $\Delta k = .5$ was chosen. A mean error of less than 1% could have been achieved if $\Delta k = .25$ was chosen. However, this would have increased the size of the required data set by a factor of 4 without making any qualitative difference in the model and/or analysis. In future work, a cubic spline interpolator will be investigated. It is believed that the cubic spline interpolator will significantly reduce the representation error any may even permit larger values of Δk to be chosen.

A.8 Earth Rotation Effects

There are three major effects as shown in Figure A.7, caused by the rotation of the earth. First, the spacecraft groundtrack velocity varies as a result of earth rotation. Near the poles, the spacecraft may be moving in the same direction as the earth rotation, thereby causing an effective decrease and subsequent crowding of the scan line circles. At the equator, the earth velocity adds in a direction nearly orthogonal to the spacecraft velocity direction, and a skew of the scan-traced circles results thereby. Fortunately, because the scan traces are indeed circles of constant radius on the surface of the earth, the local geometry is affected in a minor way. In fact, the ground track trace becomes skewed in relationship to the instrument axis pointing in the direction of the spacecraft velocity, so that the referenced scanner angle no longer is directed along the ground track, but forms an angle relative to it, which varies with latitude.

Finally, because of this latitude-dependent rotation of the digital grid along the scan-line circle and the potential crowding of scan lines as a function also of latitude, the set of coefficients that must be applied to the data may be latitude-dependent. Fortunately, all of these

EFFECTS

- GROUND TRACK VELOCITY DECREASE CAUSES CROWDING OF THE SCAN LINES

- RELATIVE GROUND TRACK DIRECTION, θ_0, VARIES WITH LATITUDE.

- LATITUDE DEPENDENT COEFFICIENTS MAY BE REQUIRED/DESIRED.

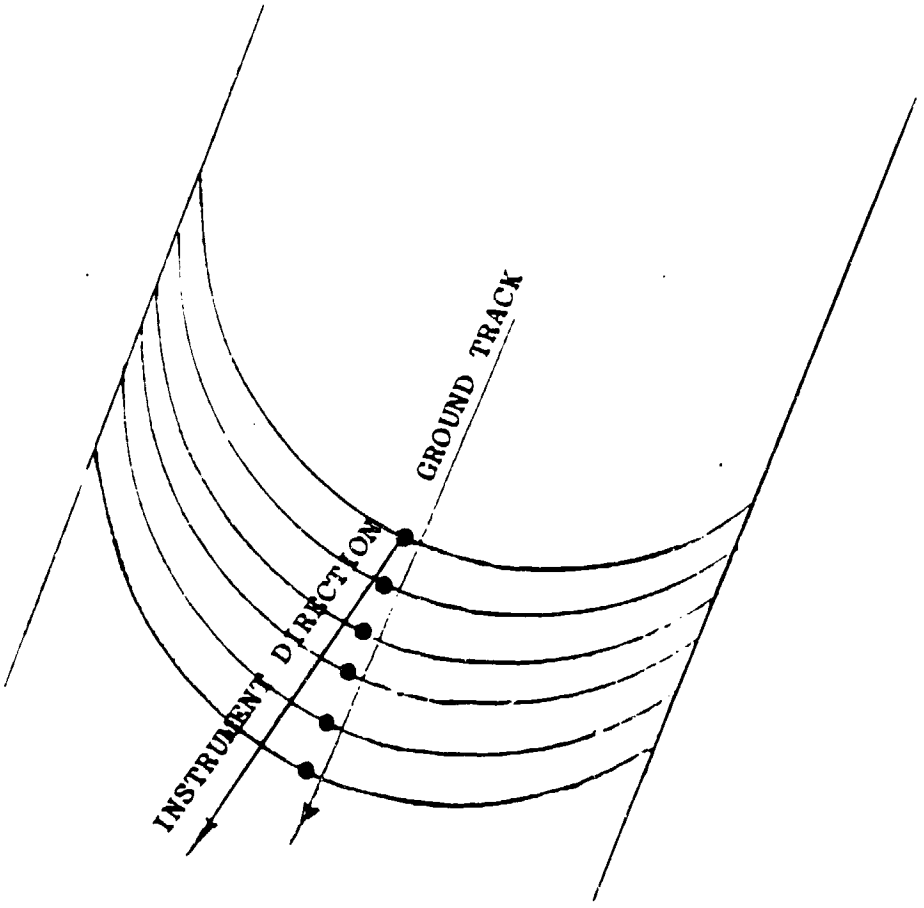

Figure A.7 EARTH ROTATION EFFECTS

effects are taken into consideration in the transformation from k-space to instrument coordinates through the variable θ_0 and its dependence on latitude. The maximum angle that θ_0 attains near the equator is approximately 4°.

A.9 Undersampling

Given the geometric parameters of the LAMMR instrument and the antenna diameter, it is possible to compute the required sampling distance in both along scan (δx) and across scan (δy) directions. For an ideal antenna without consideration of signal-to-noise, Table A.1 is a table of ideal sampling rates for each of the frequency/wave-length of the LAMMR design. It is to be noted that the ideal sampling rates are significantly higher than those rates planned for the mission. This discrepancy can in part be reconciled because the real antenna is nowhere near ideal. There are a multitude of effects which significantly deteriorate the information content of the received signal. These are:

- Effects of antenna tapering,
- Signal-to-noise ratio,
- Blur introduced by scanner motion, and
- Finite horn dimension and placement.

Except for the effects associated with the finite dimensions and placement of the individual channel horns, each of the aforementioned degradations have been taken into consideration in computing sampling rates for each of the channels that are commensurate with the signal-to-noise anticipated of the instrument. It is to be noted that the sampling distances computed in Table A.1 are based upon the ability to enhance signals that are not dominated by noise, thereby compensating for the sensor modulation transfer function. We must retain information up to that critical frequency if one intends to digitally compensate for sensor degradation effects. It is to be noted that even in the presence of tapering and sensor motion and noise, that the planned sampling rate of

$S_0 = 1020.4556$ km

$D = 400$ cm

$\frac{\sigma^2}{S^2} = .01$

$r_0 = 703.726$ km

$\Delta x = \frac{S_0 \lambda}{2D} = 1.276\lambda$ (km)

$\Delta y = \frac{\Delta x}{\sin 49.94^\circ}$

		IDEAL		NOISE CONSIDERATIONS with TAPER and BLUR	
λ_{cm}	f_{GHz}	ALONG SCAN Δx	CROSS SCAN Δy	ALONG SCAN Δx	CROSS SCAN Δy
.82	36.5	1.05 km	1.37 km	1.45	1.71
1.4	21.3	1.78	2.33	2.46	2.91
1.6	18.7	2.04	2.67	2.81	3.34
2.82	10.65	3.6	4.7	4.96	5.87
4.55	6.6	5.8	7.58	8.0	9.48
5.88	5.1	7.5	9.8	10.34	12.25
6.98	4.3	8.9	11.6	12.27	14.5

at 512 samples $\Delta x = 3.6$ km

at 256 samples $\Delta x = 7.2$ km

$\Delta = 7$ km

Table A.1 TABLE OF IDEAL SAMPLING RATES

512 samples at the three highest frequences and 256 samples at the four lowest frequencies will generate undersampling conditions in the x-direction for all but the three lowest frequencies, and the same is true for sampling in the y-direction.

Further modeling of course, could include other degradation effects to the point where this undersampling would be inconsequential. Nonetheless, it is the conclusion of this section that aliasing artifacts generated by undersampled conditions must be taken into consideration in the design of an antenna pattern correction process, and that such effects may significantly hinder our ability to adequately enhance the data with context-free matrix convolution processes. Analysis of this sort is often utilized to justify placing a low-passed filter prior to digitization, so as to avoid aliasing artifacts.

We do not recommend a purposeful degradation of the analog signal by such a low-passed filter. The only grounds for placing such a filter in the system is the ability to perfectly reconstruct the analog signal coming after the filter. But, this degraded signal is not the scene. It can be shown that a linear interpolator matched to the expected power spectra of the original signal (but one which is not necessarily a sinc function interpolator) will give an interpreted continuous image having a lower least-squares residual error than the one generated by applying the low-passed filter to the original scene. Hence, one can conclude the aliasing is not an evil that should be avoided at all costs, but is a sign that alternative interpretations of the signal are possible and that a priori knowledge of scene content can be utilized to select the best among all alternatives.

A.10 Antenna Pattern Correction Philosophy

In this section the following elements of antenna pattern correction are presented: (Figure A.8)

CONCEPTS:

- <> USED TO DESCRIBE *A PRIORI* ENSEMBLE AVERAGE
- ALTERNATIVE MEASURES OF APC PERFORMANCE

(1) LEAST SQUARES

$$L = \langle (T_B(\bar{x}) - \tilde{T}_B(\bar{x}))^2 \rangle$$

WHERE $\tilde{T}_B$ IS THE BRIGHTNESS TEMPERATURE ESTIMATE FROM ANTENNA TEMPERATURE MEASUREMENTS

(2) MINIMUM VARIANCE

$$\delta T_B = T_B(\bar{x}) - \langle T_B(\bar{x}) \rangle$$

$$L = \langle (\delta T_B(\bar{x}) - \delta \tilde{T}_B(\bar{x}))^2 \rangle$$

- $\langle T_B(\bar{x}) \rangle$ IMPLIES AN *A PRIORI* MODEL

(1) ERGODIC $\langle T_B(\bar{x}) \rangle$ = LOCAL MEAN

(2) $\langle T_B(\bar{x}) \rangle$ = MODELED *A PRIORI*

(3) $\langle T_B(\bar{x}) \rangle$ = STATISTICAL ENSEMBLE AVERAGE FROM REAL DATA

- CONCERNS

(1) TRUNCATION OF MATRIX
(2) TAILS OF THE POINT SPREAD FUNCTION DISTRIBUTION
(3) GIBBS PHENOMENA NEAR EDGES
(4) ALTERNATIVE STATISTICAL ASSUMPTIONS REQUIRED
(5) PRESERVANCE OF A CONTINUUM INTERPRETIVE THEORY

Figure A.8 APC Philosophy and Concerns

- Estimation parameters,
- Cost functions and alternative philosophies, and
- Optimization and matrix equations.

These items form the basis of all the work to follow. The incorporation of data interpretive techniques forms the basis of both context-free and context-sensitive processing philosophies for antenna pattern corrections.

Estimation Parameters

In the usual formulation of estimation theory, an estimate of $T_B(x)$, the brightness temperature, is desired. However, for LAMMR purposes, a more general estimate of the brightness temperature, as seen through the "eye" of another instrument (real estate matched $T_B(x)$) , is desired. We denote the antenna pattern of this other instrument as W , and the resulting measurement as $\bar{T}_B$. The following equation represents this measurement:

$$\bar{T}_B(\bar{x}) = \iint d^2x' \; W_{\bar{x}}(\bar{x}-\bar{x}') \; T_B(\bar{x}') \; .$$

We desire an estimate of this windowed brightness temperature as a linear combination of the antenna temperatures that were measured on the integer grid in the $\bar{x}$ space. The following equation expresses this relationship:

$$\hat{\bar{T}}_B(\bar{x}) = \sum_{\bar{i}} M_{\bar{x},\bar{i}} \; T_A(\bar{i}) \; .$$

At this point, we shall assume the existence of some a priori estimate of brightness temperatures (two polarizations) over the field of view. This assumption is made for three reasons:

- The usual formulation of minimum variance estimation filters generally account for biases separately,
- A priori knowledge of water brightness temperatures and/or land brightness temperatures can be accounted for in this way leading to a procedure for removing the influences of land in the near ocean vicinity, and
- The removal of a first-order guess does not limit the applicability of the results.

The following two equations represent the corresponding fluctuations in the windowed brightness temperature and its corresponding estimate:

$$\overline{\delta T}_B(\bar{x}) = \iint d^2\bar{x}' \; \underline{W}_{\bar{x}}(\bar{x}-\bar{x}') \; (T_B(\bar{x}') - \langle T_B(\bar{x}')\rangle)$$

$$\overline{\delta T}_B(\bar{x}) = \sum_i \underline{M}_{\bar{x},\bar{i}} \; (T_A(i) - \langle T_A(i)\rangle) \; .$$

Note that this variance approach introduces the a priori model represented by $\langle T_B(\bar{x})\rangle$.

There are alternative models that may be impled by $\langle T_B(x)\rangle$ and which stem from additional concepts and/or assumptions used in defining the cost function. Three such models are:

- Use of the Ergodic hypothesis to set

$$\langle T_B(x)\rangle = \text{Local Mean}$$

- A priori model based upon knowledge of water and land distributions on the earth and perhaps a latitude-dependent brightness temperature model for both land and water areas.

- Statistically acquired brightness temperature ensemble averages (stored in a world brightness map) used as an a priori model.

Other parametric approaches involving pattern recognition techniques also exist but are not considered to be within the scope of this section. Figure A.8 summarizes the APC philosophies and concerns with regard to estimation concept formulations and alternative cost functions.

Cost Functions/Alternative Philosophies

The optimum set of estimation coefficients M should minimize the least squares error in the unmodeled fluctuations. We, therefore, define:

$$\chi^2(\bar{x}) = \langle (\delta T_B(\bar{x}) - \overline{\delta T}_B(\bar{x}))^2 \rangle$$

where χ^2 is the variance at $\bar{x}$ and $\langle\rangle$ represents an ensemble aveage over all statistical realizations.

The cost functions introduced by Backus and Gilbert[2] do not involve ensemble averages; they recognize that $\hat{T}_B(\bar{x})$ corresponds to a specific point spread function associated with the particular linear combination of the antenna point spread functions which generate $T_A(i)$. In particular:

$$\hat{T}_B(\bar{x}) = \int\int d^2\bar{x}' \left[\sum_i M_{\bar{x},\bar{i}} A\ (\bar{i}-\bar{x}')\right] T_B(\bar{x}')$$

giving the expression in brackets, [], as the actual point spread function. Their cost function is:

[2]Backus, G. and F. Gilbert, "Uniqueness in the inversion of inaccurate gross earth data", Phil. Trans. Roy. Soc. London, Vol. A266, pp. 123-192, 1970.

$$Q_x = \iint d^2\bar{x}' \{\sum_{\bar{i}} M_{\bar{x},\bar{i}} A_{\bar{i}}(\bar{i}-\bar{x}') - F_{\bar{x}}(\bar{x}-\bar{x}')\}^2 J^2_{\bar{x}}(\bar{x}-\bar{x}')$$

where F is a desired point spread function centered at $\bar{x}$ and J^2 is an associated "penalty function".

x^2 can be related to Q_x by expressing it as:

$$x^2(\bar{x}) = \iiiint d^2\bar{x}' d^2\bar{x}''$$

$$\{\sum_{\bar{i}} M_{\bar{x},\bar{i}} A_{\bar{i}}(\bar{i}-\bar{x}') - W_{\bar{x}}(\bar{x}-\bar{x}^T)\}$$

$$*\{\sum M_{\bar{x},\bar{i}} A_{\bar{i}}(\bar{i}-\bar{x}') - W_x(\bar{x}-\bar{x}'')\}$$

$$\langle \delta T_B(\bar{x}')\ \delta T_B(\bar{x}'')\rangle \ .$$

By assuming $\langle \delta T_B(\bar{x}')\ \delta T_B(\bar{x}'')\rangle = s^2\ \delta(\bar{x}'-\bar{x}'')$ we obtain the equation for Q_x with a <u>constant</u> penalty function. A penalty function $J_{\bar{x}}(\bar{x}-\bar{x}')$ can be introduced by defining "penalized" "J-windowed" brightness variables $\delta\bar{V}_B$ and $\delta\hat{\bar{V}}_B$ such that if

$$x^2(\bar{x}) = \langle(\delta\bar{V}_B - \delta\hat{\bar{V}}_B)^2\rangle$$

is defined, then one obtains an expression similar to Q_x .

$$x^2(x) = \iiiint d^2\bar{x}' d^2\bar{x}''\ J_{\bar{x}}(\bar{x}-\bar{x}')\ J_{\bar{x}}(\bar{x}-\bar{x}'')$$

$$\{\sum M_{\bar{x},\bar{i}} A_{\bar{i}}(\bar{i}-\bar{x}') - W_{\bar{x}}(\bar{x}-\bar{x}')\}$$

$$*\{\sum_{\bar{i}} M_{\bar{x},\bar{i}} A_{\bar{i}}(\bar{i}-\bar{x}'') - W_{\bar{x}}(\bar{x}-\bar{x}'')\}\ \langle \delta T_B(\bar{x}')\ \delta T_B(\bar{x}'')\rangle \ .$$

This equation generalizes the Backus-Gilbert method so as to introduce a priori brightness temperature fluctuation statistics into the cost function and vice versa, introduce "penalty" functions into the ensemble average statistical approach.

The introduction of a penalty function is important if one wishes to penalize point spread functions having a long "tail" of side lobes. In the analysis to follow, we assume no penalty function but recognize the tool as another element of APC philosophy that may be relevant near land/water boundaries.

Optimization and Matrix Equations

Taking a functional variation of χ^2 with respect to the estimation coefficients $M_{\bar{x},\bar{i}''}$ leads to the following system of normal equations:

$$\sum_{\bar{i}} M_{\bar{x},\bar{i}} \left(\Sigma_{\bar{i},\bar{i}''} + \sigma^2 \delta_{\bar{i}\bar{i}''}\right) = \Gamma_{\bar{x},\bar{i}''}$$

where

$$\Sigma_{\bar{i},\bar{i}''} = \iiiint d^2\bar{x}\, d^2\bar{x}''\, A_{\bar{i}}(\bar{i}-\bar{x}') \langle \delta T_B(\bar{x}')\, \delta T_B(\bar{x}'')\rangle A_{\bar{i}''}(\bar{i}''-\bar{x}'')$$

and

$$\Gamma_{\bar{x},\bar{i}''} = \iiiint d^2\bar{x}' d^2\bar{x}''\, W_{\bar{x}}(\bar{x}-\bar{x}') \langle \delta T_B(\bar{x}')\, \delta T_B(\bar{x}'')\rangle A_{\bar{i}''}(\bar{i}''-\bar{x}'') \ .$$

If we now assume that the brightness temperature fluctuations are spatially independent, then these equations can be simplified by utilizing this statistical independence as:

$$\langle \delta T_B(\bar{x}')\, \delta T_B(\bar{x}'')\rangle = S^2\, \delta(\bar{x}'-\bar{x}'') \ .$$

The resulting expressions for Σ and Γ are given as follows:

$$\Sigma_{\bar{i},\bar{i}''} = S^2 \iint d^2\bar{x}' \; A_{\bar{i}}(\bar{i}-\bar{x}') \; A_{\bar{i}''}(\bar{i}''-\bar{x}')$$

$$\Gamma_{\bar{x},\bar{i}''} = S^2 \iint d^2\bar{x}' \; W_{\bar{x}}(\bar{x}-\bar{x}') \; A_{\bar{i}''}(\bar{i}''-\bar{x}')$$

Here the Σ matrix represents the auto-correlation function of the "evolving" antenna pattern in $\bar{x}$ space; it is an overlap of the antenna patterns centered at i and i'' respectively. Γ, on the other hand, represents the antenna pattern as blurred by the window function W. It is clear that these integrals can be computed given the analytic forms of A and W. If we further decide to select any finite set of sub-grid points, $\bar{x}$, and truncate the grids $\bar{i},\bar{i}''$, then the normal equation becomes a finite matrix equation which is easily inverted as shown below:

$$\bar{\bar{M}} = \bar{\bar{\Gamma}} \; (\bar{\bar{\Sigma}}+\sigma^2\bar{\bar{I}})^{-1} \; .$$

It is also noted that this solution minimizes Q for $J^2 = 1$ as previously demonstrated.

A.11 Detailed Approaches to Four Context-sensitive Processes

- Latitude Dependent Model

Given world surface map of land flags, ice flags, water flags, etc., a priori brightness temperatures will be assumed for each category which has both latitude, ϕ, and seasonal, t, dependency. For category (i), we might assume:

$$T_B^{(i)} = A^{(i)} + B^{(i)} \cos \phi + C^{(i)} \sin (\alpha t+\beta) \; .$$

Values of A, B, C, α and β can be determined statistically using SMMR data. Other terms could be included in both latitude and seasonal dependency if the SMMR data can support their need. This brightness temperature model would be used to compute a priori antenna tempera-

tures over some fine grid of points which would be stored for each orbit in a geographically-referenced world data base for access in real time operations. Actually, only sensitivity coefficients γ_i, to the model brightness temperatures $T_B^{(i)}$ need be stored since the modeled antenna temperature at each point can be computed as $\langle T_A \rangle = \sum_i \gamma_i T_B^{(i)}$ over the set of earth feature flag types (i).

- Parametric Land/Water Model

In this parametric model, the values of $T_B^{(i)}$ are inferred from the actual antenna measurements over some local array. The world surface map is used as above to compute sensitivity coefficients $\gamma^{(i)}$ for each point in the local array (a priori). Then, we compare the computation estimate $\langle T_A \rangle = \sum_i \gamma_i T_B^{(i)}$ to the actual array of antenna temperature measurements. The cost function is:

$$\sum_{\ell,m} [T_A(\ell,m) - \langle T_A(\ell,m) \rangle]^2$$

$$= \sum_{\ell,m} [T_A(\ell,m) - \sum_i \gamma_i(\ell,m) T_B^{(i)}]^2$$

Taking a variation of this cost with respect to $T_B^{(i)}$ leads to the normal equations

$$A_{i'i} T_B^{(i)} = B_{i'}$$

for each category (i) in the region. Here

$$B_{i'} = \sum_{\ell,m} T_A(\ell,m) \gamma_{i'}(\ell,m)$$

and

$$A_{i'i} = \sum_{\ell,m} \gamma_{i'}(\ell,m) \gamma_i(\ell,m)$$

and $T_B^{(i)}$ is computed as

$$\boxed{T_B^{(i)} = A_{i\,i'}^{-1} B_{i'}} \quad .$$

Note that typically, the set $\{i\}$ will consist of one species; occasionally near water/land boundaries it will consist of two species and that rarely does it consist of more than two species; e.g., land, water, and ice. An alternative process for estimating $\langle T_B^{(i)} \rangle$ is to apply a tracking filter and apply the above algorithm only over regions of a single species and over which the coefficients are constant.

- Bi-modal Model

In the bi-modal model, two species of unknown origin are assumed ($T_B^{(1)}$ and $T_B^{(2)}$) . An antenna temperature threshold value are chosen to classify each point in the array as belonging to class 1 ($T_B^{(1)}$) or to class 2 ($T_B^{(2)}$) . Bi-linear interpolation is used as a transition model between the two fields so that the modeled antenna temperature at each point can be computed . The choice of brightness temperatures $T_B^{(1)}$ and $T_B^{(2)}$ as well as the threshold temperature T_h are chosen to minimize the variance in the antenna temperatures from the model antenna temperatures. The antenna temperature can be expressed as:

$$\tilde{T}_A(i,j) = \sum_{\ell,m} A_{\ell m}\, T_B^{(1)} + \sum_{k,n} A_{kn} T_B^{(2)}$$

such that

$$(i+\ell,\ j+m) \in \{S_1\} \quad \text{and} \quad (i+k, j+n) \in \{S_2\}$$

where

$A_{\ell m}$ is the effective antenna profile

S_1, S_2 are the selected pixels classified in states 1 and 2, respectively.

Sets S_1 and S_2 are chosen to minimize

$$\sum_{i,j} (\bar{T}_A (i,j) - T_A (i,j))^2$$

- World Brightness Map

A world brightness map consists of mean brightness temperatures over the surface of the earth, possibly segmented by month. This data can be used as an a priori model of brightness temperatures to derive the associated antenna temperature needed in a context-sensitive APC process.

In each of the above models, an estimate is made of the antenna temperature $\langle T_A \rangle$ which is subtracted from the observed field.

$$\delta T_A = T_A - \langle T_A \rangle .$$

The fluctuations δT_A in antenna temperatures are then corrected for the antenna spatial degradation in concert with a minimum variance and truncated matrix correction process whose coefficients are the same as those derived in context-free APC processes. The resulting APC produces an estimate of the brightness temperature variation δT_B from the a priori model and so one can then construct the brightness temperature estimate

$$\bar{T}_B = \langle T_B \rangle + \delta T_B .$$

A.12 Matrix Truncation Approach

The system of linear equations that must be solved for deriving the antenna correction coefficient to be applied at a specific scan angle location is given by:

$$\sum_{\bar{i}}{}' M_{\bar{x},\bar{i}} \left(\Sigma_{\bar{i},\bar{i}''} + \sigma^2 \delta_{\bar{i},\bar{i}''}\right) = \Gamma_{\bar{x},\bar{i}''}$$

where the prime on $\sum'$ indicates a truncation over some array centered around $\bar{x}$. There are two assumption that are imposed in the computations that were done. The assumptions are:

$$(a) \quad \langle \delta T_B(\bar{x})\ \delta T_B(\bar{x}') \rangle = S^2\ \delta(\bar{x}-\bar{x}')$$

$$(b) \quad W_{\bar{x}}(\bar{x}-\bar{x}') = \delta(\bar{x}-\bar{x}')$$

They result in:

$$\Sigma_{\bar{i},\bar{i}''} = S^2 \iint d^2\bar{x}'\ A_{\bar{i}}(\bar{i}-\bar{x}')\ A_{\bar{i}''}(\bar{i}''-\bar{x}')$$

$$\Gamma_{\bar{x},\bar{i}''} = S^2\ A_{\bar{i}''}(i''-\bar{x})$$

with solution

$$\bar{\bar{M}} = \bar{\bar{\Gamma}}\ (\bar{\bar{\Sigma}}+\sigma^2\bar{\bar{I}})^{-1}$$

It is appropriate at this time to discuss the two assumptions for this matrix truncation approach. In assumption (a), some a priori estimate is needed for the two-point correlation function in the expected deviations of brightness temperature from some a priori model. In a context-free case, the a priori model may be chosen as the local brightness temperature mean over the truncated array, while in a context-sensitive process, a priori models may be chosen

as discussed in the previous section. Nonetheless, a reasonable choice of two-point fluctuation statistics must be assumed. In the work which has been done, it is assumed that the fluctuations in brightness temperatures from the a priori model is totally uncorrelated from one point to the next, and has fluctuation signal power given by S^2.

In addition to these assumptions, some a priori windowed function, W, must be chosen. Under the philosophy of real estate matching, W can be chosen to be any point spread function for which a smoothed brightness temperature is desired to be estimated. In the context of the LAMMR Algorithm Freeze Report, it is desirable to choose the point spread function associated with one of the lower frequency channels as the window function for W. In the work done in this report we have chosen not to follow this route in order to emphasize an alternative philosophy for brightness temperature estimates, which corresponds to brightness temperature point estimates. For this reason, assumption (b) selects for the δ function for W so that the resulting computation leads to the best least squares estimate of brightness temperatures at the point designated by $\bar{x}$. It is to be noted that a broad window function for W will, of course, lead to much smoother estimates. However, it is our contention that the process of data smoothing should be applied after the non-linear geophysical parameters are extracted so as to avoid biases which would otherwise be incurred.

Finally, the matrix equation above which has been truncated, will lead to a solution for which the sum of the antenna pattern correction coefficients may not sum to unity. This defect results from the lack of applying the appropriate constraints in the matrix equation. The constraint, however, is easily imposed by the following argument.

The derived matrix of coefficients are to be applied to antenna temperature fluctuations. Hence

$$\delta T_B = M \times \delta T_A \ .$$

Thus,

$$\tilde{T}_B = \langle T_B \rangle + M \times (T_A - \langle T_A \rangle)$$

$$= M \times T_A + \langle T_B \rangle - M \times \langle T_A \rangle \ .$$

By selecting $\langle T_B \rangle = \langle T_A \rangle$ and writing $\langle T_A \rangle \equiv \frac{1}{N}\ II \times T_A$ where II is a matrix of one's over the truncated array and N is the number of points in the array, then

$$\tilde{T}_B = M \times T_A + \frac{1}{N}(1 - \sum_{ij} M_{ij})\ II \times T_A$$

from which it is seen that the derived matrix coefficients should be modified so that the mean sum defect $\frac{1}{N}\ (1 - \sum_{ij} M_{ij})$ is uniformly <u>added</u> to each coefficient.

A.13 <u>Fourier Approach With Aliasing Consideration</u>

As previously indicated, it is erroneous to apply Fourier theory to this problem because the antenna pattern rotates in instrument coordinates as the line is scanned. Hence, there is no way to represent the antenna measurements as a strict convolution with the brightness temperatures. However, we make use of the fact that the antenna pattern is highly localized, and force a convolution-like expression as a consequence of these assumptions. The assumptions that must be made are:

- Ignore rotation dependence of the antenna pattern locally
- Ignore minor scale changes as a function of location
- Use a local antenna pattern and its corresponding Fourier transform in instrument coordinates.

With these three assumptions it is possible to convert the matrix equation to a convolution form as designated below, and to apply the Fourier transform results which convert convolutions in the spatial domain to product functions in the Fourier d[illegible]

Basic Equations:

$$\sum_{\bar{i}} M(\bar{x}-\bar{i})\{\sum(\bar{i}-\bar{i}'') + (\frac{\sigma}{S})^2 \delta_{\bar{i}-\bar{i}''}\} = \Gamma(\bar{x}-\bar{i}'')$$

Fourier Transform gives:

$$0 = \iint \frac{d^2w}{(2\pi)^2} \{M_{\bar{w}} \{A(\bar{w})A^*(\bar{w}) + (\frac{\sigma}{S})^2 \pi_{\bar{w}}\} - W(w)A^*(w)\}$$

where $\pi_{\bar{w}}$ is the 'box car' function with cut-off at the Nyquist frequency, and

$M_{\bar{w}}$ is periodic:

$$M_{\bar{w}+2\pi\bar{\ell}} = M_{\bar{w}}$$

Now, normally, each of the frequency components of the Fourier integral are independent. This frequency independence would normally be used to generate the system of equations whereby the integrand of the above expression vanishes for all frequencies. This would lead to the usual Weiner filter which optimizes the enhancement in the presence of noise. However, such is not the case in the above equations when the digitization rate is less than two points per wavelength of the maximum frequency responded to by the antenna. In such an undersampling situation, the Fourier integrals must be summed over all Nyquist zones so as to provide a set of independent frequencies so that the integrand can be set to zero. When this is done, and the resulting equation solved for the Fourier transform of the antenna pattern correction coefficient, M_{Ω}, we get the following solution which incorporates the phenomena of aliasing.

$$M_{\bar{w}} = \frac{\sum_{\bar{\ell}} W(\bar{w}+2\pi\bar{\ell})A^*(\bar{w}+2\pi\bar{\ell})}{\sum_{\bar{\ell}} (A(w+2\pi\bar{\ell})A^*(w+2\pi\bar{\ell})+(\frac{\sigma}{S})^2}$$

If $W \equiv 1$, numerator is $\sum_{\underline{\ell}} A^*(\bar{w}+2\pi\bar{\ell})$.

It is extremely important to note that the dominating terms in the denominator of the solution with aliasing at higher frequencies might never be the signal-to-noise ratio if the antenna response at the Nyquist frequency dominates the anticipated noise. A computation of the solution with aliasing is in general agreement with the power spectra obtained by the matrix truncation approach when the digitization rate is less than that required by the sampling theorem. In general, the solution with aliasing begs for slight over-enhancement over what would be anticipated for a Weiner filter where aliasing is not an issue. These results are new and are not, to the best of our knowledge, published in the open literature.

A.14 Some Antenna Pattern Correction Coefficients

Figure A.9 shows sets of coefficients that have been derived by means of the matrix truncation approach delineating in previous sections. It is to be noted that the optimum set of coefficients drops off relatively rapidly with increasing distance from the center pixel. Although simulated results have not yet performed on images having the characteristics anticipated for LAMMR, nonetheless it is anticipated that not too much improvement in the image quality will be seen by extending the set of matrices to larger arrays. In fact, frequency response curves for these antenna patterns have been computed, as shown in Figure A.10 (a case where aliasing dominates over noise), and those response curves are not significantly different. One might infer that the 3x3 frequency enhancement matrix adequately compensates for the loss of antenna response and that further enhancements with larger arrays may not be computationally worthwhile.

- 3 x 3

0.066	-.713	0.066
-.440	3.046	-.440
0.070	-.726	0.070

$$\sum_{ij} Mij = 1.0$$

- 5 x 5

-.005	0.001	0.211	0.001	-.005
-.044	0.051	-.921	0.051	-.044
0.087	-.479	3.198	-.479	0.087
-.043	0.060	-.941	0.060	-.043
-.005	-.008	0.225	-.008	-.005

- 7 x 7

0.001	0.010	-.042	-.104	-.042	0.010	0.001
-.006	-.003	0.040	0.298	0.040	-.003	-.006
0.008	-.034	0.040	-.966	0.040	-.034	0.008
-.020	0.095	-.459	3.252	-.459	0.095	-.020
0.009	-.034	0.052	-.989	0.052	-.034	0.009
-0.006	-.002	0.022	0.316	0.022	-.002	-.006
0.000	0.008	-.030	-.110	-.030	0.008	0.000

Figure A.9 Derived Sets of Coefficients

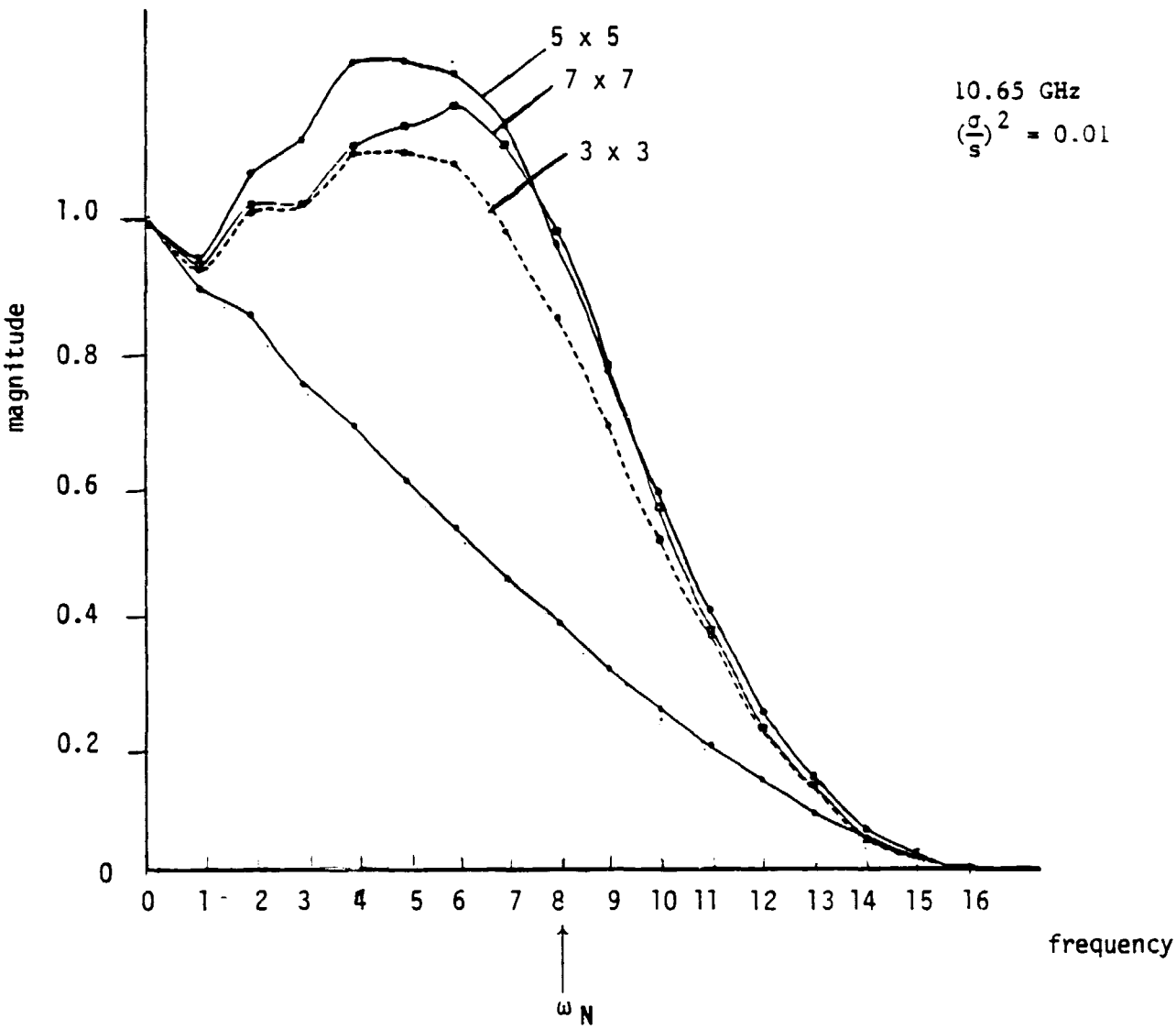

Figure A.10 Frequency Response of Antenna Patterns Corrected by Different Matrix Sizes

A.15 Various Error Measures

The following are various measures useful to the evaluation of alternative antenna pattern correction approaches:

- Noise amplification - it is well understood that any attempt to enhance higher spatial frequencies will also amplify noise. It is important that one does not amplify those frequencies for which noise dominates the signal. Weiner filtering expresses this intuitition very nicely in providing a demoninator containing the noise power to signal power ratio. In the context of a band limited response, the noise amplification factor is given by:

$$\text{Noise power amplification } (\bar{x}) = \sum_{\bar{i}} M^2_{\bar{x},\bar{i}}$$

- Model dependent error measures - if a context-free antenna pattern correction process is applied, then that process will be formulated in the context of a nominal geometric model. In practice, the spacecraft will not be in the nominal attitude nor will it be at the nominal altitude. Both attitude and altitude variations will cause a change to occur in the relationship between the antenna pattern in spherical coordinates and the instrument coordinates of the digital data. The previously derived equation gives the explicit geometric dependence of the antenna temperature measurement in relationship to the antenna pattern, A. Therefore, variations in V with respect to attitude and altitude can be explicitly evaluated and an error expression resulting from such geometric variations can be computed. The sensitivity of the antenna pattern correction process to variations in geometry has been studied and we have concluded that the effects are negligible for APC.

- Philosophy dependent error variations - alternative cost functions measuring the differences between what can be accomplished with an antenna pattern correction process in comparison to the desired point spread function (with or without penalty function) have been proposed. The cost function, Q, is a general error measure provided that the point spread function, F, and the penalty function, J^2, are normalized as:

$$\int d^2\bar{x}' \, F_{\bar{x}}(\bar{x}-\bar{x}') = 1$$

$$\int d^2\bar{x}' \, J_{\bar{x}}(\bar{x}-\bar{x}') = 1 \, .$$

  Of particular interest in the philosophy dependent error variations are changes that may occur in Q as a result of differing philosophyies such as different choices of F and different choices of a penalty function. Also of interest are the variations in Q when F is chosen to be the effective point spread function of another radiometer channel. Unfortunately, time did not permit us to evaluate alternative philosophies objectively.

- Matrix truncation errors - the affects of matrix truncation on the error generated in matching the desired point spread function can easily be determined from the expressions previously derived. In general, a simple truncation of coefficients is inadequate because the sum over all of the coefficients should add up to one in order to preserve the appropriate response at low frequencies. Therefore, it is necessary to redistribute the truncated amplitudes to interior elements of the sum and it is possible to do this in several ways:

  - add it to the center element
  - distribute it proportionately to the coefficients
  - distribute the differences uniformly over all of the elements.

As would be expected, different optimization philosophies can lead to any of the above. Within our work plan we have concluded that the third option above is appropriate for the statistical assumptions made in the derivation.

- Uncorrectable errors - it is virtually impossible to correct completely for the blur introduced by the antenna pattern. In the context-free situation, nothing can be done about frequencies that lie above the effective cut-off frequency of the sensor. This is important to understand because the sharp water/land interface is a discontinuity containing many high frequencies. The BTS proposed measures of these errors incorporate aliasing phenomena.

- Context-sensitive improvements - Section A.11 and 3.1 contains our presentation of the incorporation of a priori knowledge in brightness temperature estimates. In a context-free scheme of antenna pattern corrections, nothing can be done about spatial frequencies that are higher than the antenna cut-off frequency. In a context-sensitive antenna pattern correction process, the data which has been gathered by the antenna is analyzed and interpreted in the context of our a priori knowledge of scene variations. BTS envisions a context-sensitive processing scheme in which the high frequency content of brightness temperatures are inferred from the measurements and our knowledge of the real world. The improvement in brightness temperatures which can result from a context-sensitive process must be determined through simulation; this work requires simulation and has not yet been completed.

APPENDIX B

Appendix B

FORTRAN program listings of the APC demonstration software

```
      SUBROUTINE LENS(RADIUS)
C
C*****************************************************************
C
C     TO GENERATE A 64 X 64 AIRY DISK, WHICH CORRESPONDS TO THE
C  SQUARE OF THE FIRST-ORDER BESSEL FUNCTION DIVIDED BY ITS
C  ARGUMENT.
C     USING THE CONCEPTS OF LINEARITY, THIS IS THE IMPULSE OR POINT
C  SPREAD FUNCTION OF AN INCOHERENT SYSTEM DUE TO A CIRCULAR
C  APERTURE WITH A 0-1 REAL FUNCTION HAVING 1 IN THE AREA OF THE
C  APERTURE AND 0 ELSEWHERE.
C     THE PRINTOUT DISPLAY CONTAINS THE MAIN LOBE ONLY.
C     AIRY DISK IS STORED AT AIRY.DATA ON DISKXX USING UNIT# 12
C
C*****************************************************************
C
      DIMENSION AIRY(64,64),A(64)
C
      GRID = RADIUS/32.
      U = -RADIUS
      SUM = 0.0
      REAL = 1.0/(GRID*GRID)
C
      DO 10 J=1,64
      U = U+GRID
      V = RADIUS
      DO 10 I=1,64
      V = V - GRID
      R = SQRT(U*U+V*V)
      IF(R.LE.3.0) GO TO 33
      ANGLE = R - 2.356194 + 0.125596*3./R + 0.000056*9./(R*R)
     +          - 0.000375*27./(R*R*R) + 0.000743*81./(R*R*R*R)
      F1 = 0.797885 + 0.000047/R + 0.016567*9./(R*R)
     +   + 0.000171*27./(R*R*R) - 0.002495*81./(R*R*R*R)
      BC = F1 * COS(ANGLE)/(R**1.5)
      AIRY(I,J) = BC*BC*4.
      SUM = SUM + AIRY(I,J)
      GO TO 10
C
   33 BC = 0.5 - 0.562450*R*R/9. + 0.210936*R**4*R*R/81.
     +         - 0.039543*R*R*R*R*R*R/729. + 0.004433*(R**8)/6561.
      AIRY(I,J) = BC*BC*4.
      SUM = SUM + AIRY(I,J)
   10 CONTINUE
C
      WRITE(6,24) SUM
      SCALE = REAL/SUM
      RSUM = 0.0
      DO 22 J=1,64
      DO 23 I=1,64
      AIRY(I,J) = AIRY(I,J) * SCALE
      RSUM = RSUM + AIRY(I,J)
   23 CONTINUE
   22 CONTINUE
      WRITE(6,171)
  171 FORMAT(' PRINT POINT SPREAD FUNCTION ? (NO=0)')
      READ(5,172) IPRINT
  172 FORMAT(I1)
C
      IF(IPRINT.EQ.0) GO TO 11
C
      WRITE(6,24) RSUM
   24 FORMAT(' SUM OF AIRY = ',F5.2,//)
      DO 12 J=25,39
      DO 13 I=25,39
      A(I) = AIRY(I,J)
   13 CONTINUE
      WRITE(6,173) (A(I),I=25,39)
  173 FORMAT(15(1X,F4.2),//)
   12 CONTINUE
C
      WRITE(6,174)
  174 FORMAT(///)
C
C
   11 DO 180 J=1,64
      WRITE(12,81) (AIRY(I,J),I=1,64)
```

```
 81   FORMAT(6E12.6)
180   CONTINUE
C
      RETURN
      END
```

```
C  TEST PROGRAM FOR SUBROUTINE LENS
C
C     DIMENSION AIRY(20,20)
C
      WRITE(6,1)
 1    FORMAT(' ENTER RADIUS OF AIRY DISK')
      READ(5,2) RADIUS
 2    FORMAT(F4.1)
C
      CALL LENS(RADIUS)
C
      STOP
      END
```

```
C  MAIN PROGRAM : ANTENA
C
C*****************************************************************
C
C     TO GENERATE A FILE ANT.DATA OF 64X64 ELEMENTS CONTAINING ANTENNA
C  VALUES IN INSTRUMENT COORDINATES, THAT IS, THE X SPACE.  THE GRID
C  SPACING IS 7/4 KILOMETER.  PROGRAM TESTLS SHOULD BE EXECUTED FIRST
C  IN ORDER TO GENERATE THE IDEAL ANTENA PATTERN AIRY(64,64).  AIRY.
C  DATA IS STORED ON DISKXX BY I/O UNIT # 12.  THE RESULTING ANT.DATA
C  WILL BE STORED ON DISKXX BY I/O UNIT # 11.  ANT.DATA IS IN INSTRU-
C  MENT COORDINATES, WHILE AIRY.DATA IS IN Q SPACE, A PLANE ORTHOGONAL
C  TO THE POINTING DIRECTION.
C
C*****************************************************************
C
      COMMON AIRY(64,64), ANT(64,64)
      DIMENSION A(64)
C
      FJX=0.
      FJY=0.
      NOSPS=256
      GRID=0.25
      SUM = 0.0
      REAL = 1.0/(GRID*GRID)
C
      WRITE(6,30)
   30 FORMAT(/,' ENTER FREQUENCY (GHZ) :')
      READ(5,31) GHZ
   31 FORMAT(F6.2)
C
      DO 280 J=1,64
      READ(12,81) (AIRY(I,J),I=1,64)
  280 CONTINUE
      FIY=-8.
      DO 10 J=1,64
      FIY=FIY+GRID
      FIX=8.
      DO 11 I=1,64
      FIX=FIX-GRID
C
      CALL TXFORM(FJX,FJY,FIX,FIY,CX,CY,GHZ,NOSPS,CONST)
      CALL INT3P(QX,QY,AX,AY,BX,BY,CX,CY)
      CALL INTLN(QX,QY,AX,AY,BX,BY,CX,CY,VALUE)
C
      ANT(I,J) = VALUE * CONST
      SUM = SUM + ANT(I,J)
C
   11 CONTINUE
   10 CONTINUE
C
      WRITE(6,24) SUM
      SCALE = REAL/SUM
      RSUM = 0.0
      DO 22 J=1,64
      DO 23 I=1,64
      ANT(I,J) = ANT(I,J) * SCALE
      RSUM = RSUM + ANT(I,J)
   23 CONTINUE
   22 CONTINUE
      WRITE(6,111)
  111 FORMAT(' PRINT ANTENNA PATTERN ? (NO=1) ?')
      READ(5,112) IPRINT
  112 FORMAT(I1)
      IF(IPRINT.EQ.1) GO TO 113
C
      WRITE(6,24) RSUM
   24 FORMAT(' SUM OF ANT = ', F5.2,//)
      DO 12 J=25,35
      DO 13 I=1,64
      A(I) = ANT(I,J)
   13 CONTINUE
      WRITE(6,173) (A(I),I=25,35)
  173 FORMAT(15(F5.4),//)
   12 CONTINUE
```

ORIGINAL PAGE IS
OF POOR QUALITY

```
  113   DO 180 J=1,64
        WRITE(11,81) (ANT(I,J),I=1,64)
   81   FORMAT(64E12.6)
18MAR81 11:28:22 - VOL=SCR000, DSN=YCKJE.FCLAND.FORT
  180   CONTINUE
C
        WRITE(6,200)
  200   FORMAT(/,' THE Y-AXIS :')
        WRITE(6,201) (ANT(32,J),J=32,64)
  201   FORMAT(10F8.4)
        WRITE(6,202)
  202   FORMAT(/,' THE X-AXIS :')
        WRITE(6,201) (ANT(I,32),I=32,64)
C
        STOP
        END
```

```
C
      SUBROUTINE TXFORM(FJX,FJY,FIX,FIY,GX,GY,GHZ,NGSPS,CONST)
C
C*****************************************************************
C
C---TO TRANSFORM GROUND INSTRUMENT COORDINATES (EARTH SURFACE) TO --
C   ANTENNA COORDINATES (A PLANE PARALLEL TO ANTENNA APERTURE).
C
C   INSTRUMENT COORDINATES ARE IN PIXEL NUMBER AND SCAN LINE NUMBER.
C   (FJX,FJY) : POINTING DIRECTION
C   (FIX,FIY) : ANY NEIGHBOR POINTS
C   (GX,GY) : ANTENNA COORDINATES
C   GHZ : PRIMARY RADIOMETER FREQUENCY
C   NGSPS : NUMBER OF SAMPLES PER SCAN LINE
C   CONST : ANTENNA CONSTANT
C
C*****************************************************************
C<<<<<<<<<<<<   CONSTANTS   >>>>>>>>>>>>
C
      DIMENSION RSC(3),UP(3), PC(3),P(3),S(3),SC(3),US(3),USC(3),VK(3),
     +          VKO(3),DUP(3),XX(3),YY(3),SNAKE(3),Q(3)
C-----------------------------------------------------------------
      PI = 3.14159265
      REARTH = 6371.0
      DTIME = 1.0
      DTHETA = (PI/180.)*ISC./FLOAT(NGSPS)
      THETAO = 0.0
      VTRACK = 7.0
      ALTITU = 700.0
      PHIO = 43.6*PI/180.
      RANNT = 0.002
      C = 300000.
      THETA = DTHETA* FIX
C
C<<<<<< DEFINE SPACECRAFT POSITION, FREQUENCY, AND POINTING DIRECTION >>
C
      RSC(1) = 0.
      RSC(2) = 0.
      RSC(3) = -ALTITU-REARTH
      AESRSC = SQRT(RSC(1)*RSC(1)+RSC(2)*RSC(2)+RSC(3)*RSC(3))
      ARSCPO = ARSIN((ALTITU+REARTH)*SIN(PHIC)/REARTH)-PHIC
      PO(1) = 0.
      PO(2) = REARTH*SIN(ARSCPO)
      PO(3) = -REARTH*COS(ARSCPO)
      F = GHZ*1.0EC9
C-----------------------------------------------------------------
C<<<<<<<<<<< TRANSFORMATION >>>>>>>>>>>
C
      DI = DTHETA*(FIX-FJX)
      DJ = VTRACK*DTIME/REARTH*(FIY-FJY)
C
C
      P(1) = PO(1)-PC(2)*DI
      P(2) = PO(2)+PC(1)*DI-PO(3)*DJ
      P(3) = PO(3)+PC(2)*DJ
C-----------------------------------------------------------------
      ABSUP = SQRT(P(1)*P(1)+P(2)*P(2)+P(3)*P(3))
      UP(1) = P(1)/ABSUP
      UP(2) = P(2)/ABSUP
      UP(3) = P(3)/ABSUP
C-----------------------------------------------------------------
      S(1) = P(1)-RSC(1)
      S(2) = P(2)-RSC(2)
      S(3) = P(3)-RSC(3)
C
C
      SO(1) = PO(1)-RSC(1)
      SO(2) = PO(2)-RSC(2)
      SO(3) = PO(3)-RSC(3)
C-----------------------------------------------------------------
      ABSS = SQRT(S(1)*S(1)+S(2)*S(2)+S(3)*S(3))
      ABSSO = SQRT(SO(1)*SO(1)+SO(2)*SO(2)+SO(3)*SO(3))
C-----------------------------------------------------------------
C
      US(1) = S(1)/ABSS
      US(2) = S(2)/ABSS
      US(3) = S(3)/ABSS
C-----------------------------------------------------------------
      USO(1) = SO(1)/ABSSO
```

```
      LSO(2) = SO(2)/ABSSC
      LSO(3) = SO(3)/ABSSO
C
      WAVEL = C/F
      FK = 2.*PI*RANNT/WAVEL
C
      VK(1) = FK*LS(1)
      VK(2) = FK*US(2)
      VK(3) = FK*LS(3)
C
      VKO(1) = FK*LSO(1)
      VKO(2) = FK*LSO(2)
      VKO(3) = FK*LSO(3)
C
      DUM(1) = VK(1)-VKO(1)
      DUM(2) = VK(2)-VKO(2)
      DUM(3) = VK(3)-VKO(3)
      SODOTK = USO(1)*DUM(1)+LSO(2)*DUM(2)+LSO(3)*DUM(3)
C
      Q(1) = DUM(1)-SODOTK*LSO(1)
      Q(2) = DUM(2)-SODOTK*LSO(2)
      Q(3) = DUM(3)-SODOTK*LSO(3)
C
      SNAKE(1) = -RSC(1)/ABSRSC
      SNAKE(2) = -RSC(2)/ABSRSC
      SNAKE(3) = -RSC(3)/ABSRSC
C
      ANGLE = SIN(PHIO)
      XX(1) = (USO(2)*SNAKE(3)-USO(3)*SNAKE(2))/ANGLE
      XX(2) = (USO(3)*SNAKE(1)-LSO(1)*SNAKE(3))/ANGLE
      XX(3) = (USO(1)*SNAKE(2)-LSO(2)*SNAKE(1))/ANGLE
C
      YY(1) = USO(2)*XX(3)-LSO(3)*XX(2)
      YY(2) = USO(3)*XX(1)-LSO(1)*XX(3)
      YY(3) = USO(1)*XX(2)-LSO(2)*XX(1)
C
      QX = Q(1)*XX(1)+Q(2)*XX(2)+Q(3)*XX(3)
      QY = Q(1)*YY(1)+Q(2)*YY(2)+Q(3)*YY(3)
C
      RO = ABSSO*SIN(PHIO)
      CONST = VTRACK * RO * DTIME * DTHETA * COS(THETA-THETAO) *
     +        (US(1)*UP(1)+US(2)*UP(2)+US(3)*UP(3))/(-ABSS*ABSS)
     +      * FK * SQRT(FK*FK-VK(1)*VK(1)-VK(2)*VK(2))
C
      RETURN
      END
```

```
      SUBROUTINE INTERP(QX,QY,AX,AY,BX,BY,CX,CY)
C
C*****************************************************************
C
C     TO LOCATE 3 NEAREST POINTS TO (QX,QY) IN THE Q SPACE.  THE POINTS
C  ARE ON THE 0.5 SPACING GRID.  THESE 3 POINTS WILL BE USED TO
C  GENERATE A PLANE FOR INTERPOLATING THE VALUE AT (QX,QY).
C
C  (QX,QY)  INPUT POINTS
C  A,B,C    THREE NEAREST POINTS
C
C*****************************************************************
C
      DIMENSION PX(4),PY(4),WHICH(4)
C
      IQX = QX + SIGN(0.5,QX)
      FQX = FLOAT(IQX)
      S = QX - FQX
      QX1 = FQX + SIGN(0.5,S)
      QX2 = FQX
C
      IQY = QY + SIGN(0.5,QY)
      FQY = FLOAT(IQY)
      S  = QY - FQY
      QY1 = FQY + SIGN(0.5,S)
      QY2 = FQY
C
      PX(1)=QX1
      PY(1)=QY1
      PX(2)=QX1
      PY(2)=QY2
      PX(3)=QX2
      PY(3)=QY1
      PX(4)=QX2
      PY(4)=QY2
C
      DO 10 I=1,4
      WHICH(I) = ABS(PX(I)-QX)+ABS(PY(I)-QY)
 10   CONTINUE
C
      BIG = 0.0
      DO 11 I=1,4
      IF(WHICH(I).LE.BIG) GO TO 11
      BIG=WHICH(I)
      MAX=I
 11   CONTINUE
C
      I=1
      IF(I.EQ.MAX) I=I+1
      AX=PX(I)
      AY=PY(I)
      I=I+1
      IF(I.EQ.MAX) I=I+1
      BX=PX(I)
      BY=PY(I)
      I=I+1
      IF(I.EQ.MAX) I=I+1
      CX=PX(I)
      CY=PY(I)
C
      RETURN
      END
```

```
      SUBROUTINE INTLN(QX,QY,AX,AY,BX,BY,CX,CY,VALUE)
C
C*****************************************************************
C
C     GIVEN 3 POINTS A, B, & C, LOCATED CLOSE TO Q,  AND GIVEN F(A), F(B
C  & F(C),  THIS SUBROUTINE INTERPOLATES F(Q) LINEARLY.  VALUE = F(Q).
C  F(A), F(B), AND F(C) ARE OBTAINED FROM AIRY(X,Y).
C
C*****************************************************************
C
      COMMON AIRY(64,64)
      DIMENSION A(3),B(3),C(3),AB(3),AC(3),AEXAC(3)
C
      INDX=INT(ABS(-15.5-AX)/0.5+1.0)
      INDY=INT(ABS(-15.5-AY)/0.5+1.0)
      A(1)=AX
      A(2)=AY
      A(3)=AIRY(INDX,INDY)
C
      INDX=INT(ABS(-15.5-BX)/0.5+1.0)
      INDY=INT(ABS(-15.5-BY)/0.5+1.0)
      B(1)=BX
      B(2)=BY
      B(3)=AIRY(INDX,INDY)
C
      INDX=INT(ABS(-15.5-CX)/0.5+1.0)
      INDY=INT(ABS(-15.5-CY)/0.5+1.0)
      C(1)=CX
      C(2)=CY
      C(3)=AIRY(INDX,INDY)
C
      AB(1)=A(1)-B(1)
      AB(2)=A(2)-B(2)
      AB(3)=A(3)-B(3)
      AC(1)=A(1)-C(1)
      AC(2)=A(2)-C(2)
      AC(3)=A(3)-C(3)
C
      ABXAC(1)=AB(2)*AC(3)-AB(3)*AC(2)
      ABXAC(2)=AB(3)*AC(1)-AB(1)*AC(3)
      ABXAC(3)=AB(1)*AC(2)-AB(2)*AC(1)
C
C
C
      VALUE = (-ABXAC(1)*(QX-AX)-ABXAC(2)*(QY-AY))/ABXAC(3) + A(3)
C
      RETURN
      END
```

```
C  TEST PROGRAM FOR CONVOL AND SIGMA AND GAMMA AND COEF AND PSF
C
      COMMON ANT(64,64),EMATIX(49,49),GMATIX(49),PSF(64,64)
      DIMENSION A(49),FRLANT(64,64),FIMANT(64,64)
C
C<<<<<<<<<< READ ANTENNA PATTERN FROM I/O # 11 >>>>>>>>>>
C
      DO 280 J=1,64
      READ(11,81) (ANT(I,J),I=1,64)
   81 FORMAT(64E12.6)
  280 CONTINUE
C
C<<<<<<<<<< ENTER APC PARAMETERS >>>>>>>>>>
C
      WRITE(6,10)
   10 FORMAT(' ENTER SIZE (7, 5, OR 3) :')
      READ(5,11) ISIZE
   11 FORMAT(I1)
      WRITE(6,20)
   20 FORMAT(' ENTER SQUARE OF THE N/S RATIO (F6.4) :')
      READ(5,21) SNTSR
   21 FORMAT(F6.4)
      WRITE(6,31)
   31 FORMAT(' PRINT MATRICES ? (NO=1) : ')
      READ(5,33) IPRINT
   33 FORMAT(I1)
      MSIZE = ISIZE*ISIZE
C
C<<<<<<<<<< COMPUTE SIGMA AND GAMMA MATRICES >>>>>>>>>>
C
      CALL SIGMA(ISIZE)
C
      IF(IPRINT.EQ.1) GO TO 50
      WRITE(6,15)
      DO 12 J=1,MSIZE
      DO 13 I=1,MSIZE
      A(I)=EMATIX(I,J)
   13 CONTINUE

      WRITE(6,14) (A(I),I=1,MSIZE)
   14 FORMAT(5(1X,E8.4),/)
   12 CONTINUE
   15 FORMAT(///)
C
   50 CALL GAMMA(ISIZE)
C
      IF(IPRINT.EQ.1) GO TO 51
      DO 23 I=1,MSIZE
      A(I) = GMATIX(I)
   23 CONTINUE
      WRITE(6,14) (A(I),I=1,MSIZE)
C
C<<<<<<<<<<<< SOLVE LINEAR EQUATION FOR APC COEFFICIENTS >>>>>>>>>>>>
C
   51 CALL COEF (ISIZE,SNTSR)
C
      WRITE(6,15)
      WRITE(6,34)
   34 FORMAT(' THE APC COEFFICIENTS :')
      WRITE(6,14) (GMATIX(I),I=1,MSIZE)
      WRITE(6,15)
C
C<<<<<<<<<<<<< COMPUTE POINT SPREAD FUNCTION >>>>>>>>>>>>>>
C
      CALL ANTPSF(ISIZE)
C
      WRITE(6,41)
   41 FORMAT(/,' PRINT PSF ? (NO=1) :')
      READ(6,33) IPRINT
      IF(IPRINT.EQ.1) GO TO 42
C
      WRITE(6,35)
   35 FORMAT(' THE POINT SPREAD FUNCTION :')
      DO 32 J=25,39
      WRITE(6,173) (PSF(I,J),I=25,39)
  173 FORMAT(15F5.2,/)
   32 CONTINUE
      WRITE(6,15)
```

```
C
      WRITE(6,175)
  175 FORMAT(' THE Y-AXIS :',/)
      WRITE(6,174) (PSF(32,J),J=32,64)
  174 FORMAT(10F8.4)
      WRITE(6,176)
  176 FORMAT(' THE X-AXIS :',/)
      WRITE(6,174) (PSF(I,32),I=32,64)
C
      SUM=0.0
      DO 1 J=1,64
      DO 2 I=1,64
      SUM=PSF(I,J)+SUM
    2 CONTINUE
    1 CONTINUE
      WRITE(6,177) SUM
  177 FORMAT(' THE SUM OF PSF = ',F7.2,/)
C
C<<<<<<<<<<<< COMPLTE 2-D DFT >>>>>>>>>>>>
C
   42 CALL DFT2D(64,64,PSF,FRLANT,FIMANT)
C
      WRITE(6,43)
   43 FORMAT(/,' PRINT DFT ? (NO=1) :')
      READ(6,33) IPRINT
      IF(IPRINT.EQ.1) GO TO 144
C
      WRITE(6,44)
   44 FORMAT(/,' THE Y-AXIS (REAL) :',/)
      WRITE(6,174) (FRLANT(32,J),J=32,64)
      WRITE(6,45)
   45 FORMAT(/,' THE X-AXIS (REAL) :',/)
      WRITE(6,174) (FRLANT(I,32),I=32,64)
      WRITE(6,46)
   46 FORMAT(/,' THE Y-AXIS IMAGINARY :',/)
      WRITE(6,174) (FIMANT(32,J),J=32,64)
      WRITE(6,47)
   47 FORMAT(/,' THE X-AXIS IMAGINARY :',/)
      WRITE(6,174) (FIMANT(I,32),I=32,64)
C
      WRITE(6,48)
   48 FORMAT(/,' THE REAL DFT ',/)
      DO 150 J=25,39
      DO 151 I=25,39
      A(I)=FRLANT(I,J)*256.0
  151 CONTINUE
      WRITE(6,173) (A(I),I=25,39)
  150 CONTINUE
      WRITE(6,49)
   49 FORMAT(/,' THE IMAGINARY ',/)
      DO 52 J=25,39
      DO 53 I=25,39
      A(I)=FIMANT(I,J)*256.0
   53 CONTINUE
      WRITE(6,173) (A(I),I=25,39)
   52 CONTINUE
C
C
  144 STOP
      END
```

```
      SUBROUTINE SIGMA(ISIZE)
C
C*****************************************************************
C
C     TO COMPUTE THE E MATRIX.  E REPRESENTS THE AUTO-CORRELATION
C  FUNCTION OF THE ANTENNA PATTERN IN THE X-SPACE.  IT IS AN OVERLAP
C  OF THE PATTERNS CENTERED AT ANY 2 POINTS WITHIN A ISIZE X ISIZE
C  WINDOW, WHERE ISIZE = 7, 5, OR 3.  THE E MATRIX IS THEREFORE A
C  49X49, 25X25, OR 9X9 MATRIX.  THE ORDER OF THE ELEMENTS WITHIN E
C  IS DEFINED BY IPOINT AND JPOINT.
C
C*****************************************************************
C
      COMMON ANT(64,64),EMATIX(49,49),CMATIX(49),PSF(64,64)
      DIMENSION IPOINT(49),JPOINT(49)
C
      MSIZE=ISIZE*ISIZE
C
      II=1
      ISTX=ISIZE/2
      ISTY=-ISIZE/2
C
   11 DO 10 I=1,ISIZE
      IPOINT(II) = ISTX-I+1
      II = II+1
   10 CONTINUE
      IF(II.LE.MSIZE) GO TO 11
C
      II=0
      DO 12 J=1,ISIZE
      JJ=ISTY+J-1
      DO 13 K=1,ISIZE
      II=II+1
      JPOINT(II)=JJ
   13 CONTINUE
   12 CONTINUE
C
C
      DO 14 J=1,MSIZE
C
      IX2=IPOINT(J)
      IY2=JPOINT(J)
      DO 15 I=1,MSIZE
      IX1=IPOINT(I)
      IY1=JPOINT(I)
C
      CALL CONVOL(IX1,IY1,IX2,IY2,EIII2)
      EMATIX(I,J) = EIII2
C
   15 CONTINUE
   14 CONTINUE
C
      RETURN
      END
```

```
      SUBROUTINE CONVOL(IX1,IY1,IX2,IY2,EIII2)
C
C*****************************************************************
C
C     TO COMPUTE AN ELEMENT IN THE E MATRIX.  E REPRESENTS THE AUTO-
C  CORRELATION FUNCTION OF THE ANTENNA PATTERN IN THE X-SPACE.  IT IS
C  AN OVERLAP OF THE ANTENNA PATTERNS CENTERED AT (IX1,IY1) AND (IX2,
C  IY2).  THE ANTENNA PATTERN IS STORED AT ANT.DATA WITH 0.25 SPACING
C  AND 64X64 STORAGE ELEMENTS.  BOTH (IX1,IY1) AND (IX2,IY2) ARE
C  NEIGHBORHOOD POINTS OF XC, THE CENTER OF THE ANTENNA PATTERN.  THIS
C  ROUTINE IS CALLED BY SUBROUTINE SIGMA.
C
C*****************************************************************
C
      COMMON ANT(64,64), EMATIX(49,49),GMATIX(49),PSF(64,64)
C
      X1=FLOAT(IX1)
      Y1=FLOAT(IY1)
      X2=FLOAT(IX2)
      Y2=FLOAT(IY2)
C
      EIII2=0.0
C
      DO 10 J=1,64
C
      Y=(FLOAT(J)-32.0)*0.25
      Y1MY=-(Y1-Y)
      IF(Y1MY.LT.-7.75.OR.Y1MY.GT.8.0) GO TO 10
      Y2MY=-(Y2-Y)
      IF(Y2MY.LT.-7.75.OR.Y2MY.GT.8.0) GO TO 10
      J1=32+INT(Y1MY/0.25)
      J2=32+INT(Y2MY/0.25)
C
      DO 11 I=1,64
C
      X=(32.-FLOAT(I))*0.25
      X1MX=-(X1-X)
      IF(X1MX.LT.-8.0.OR.X1MX.GT.7.75) GO TO 11
      X2MX=-(X2-X)
      IF(X2MX.LT.-8.0.OR.X2MX.GT.7.75) GO TO 11
      I1=32-INT(X1MX/0.25)
      I2=32-INT(X2MX/0.25)
C
C
      PROD=ANT(I1,J1)*ANT(I2,J2)
      EIII2=EIII2+PROD
   11 CONTINUE
   10 CONTINUE
C
      EIII2=EIII2*0.0625
C
      RETURN
      END
```

ORIGINAL PAGE IS
OF POOR QUALITY

```
C
      SUBROUTINE GAMMA(ISIZE)
C
C*****************************************************************
C
C     TO COMPUTE THE GAMMA MATRIX.  GAMMA REPRESENTS THE ANTENNA
C  PATTERN AS SURED BY A WINDOW FUNCTION.  A DELTA FUNCTION IS USED
C  AS THE WINDOW FUNCTION AND ITS SHIFTING PROPERTY MAKES GAMMA EQUALS
C  TO THE ANTENNA PATTERN ITSELF AT (IX2,IY2).  THE GENERATED GAMMA
C  MATRIX IS A (1) X (ISIZE*ISIZE) COLUMN MATRIX.
C
C*****************************************************************
C
      COMMON ANT(64,64),EMATIX(49,49),GMATIX(49),PSF(64,64)
      DIMENSION IPOINT(49),JPOINT(49)
C
      MSIZE = ISIZE*ISIZE
C
      II=1
      ISTX=ISIZE/2
      ISTY=-ISIZE/2
C
   11 DO 10 I=1,ISIZE
      IPOINT(II)=ISTX-I+1
      II=II+1
   10 CONTINUE
      IF(II.LE.MSIZE) GO TO 11
C
      II=0
      DO 12 J=1,ISIZE
      JJ=ISTY+J-1
      DO 13 K=1,ISIZE
      II=II+1
      JPOINT(II)=JJ
   13 CONTINUE
   12 CONTINUE
C
      DO 14 I=1,MSIZE
      IX2 = 32 - INT(FLOAT(IPOINT(I)),0.25)
      IY2 = 32 + INT(FLOAT(JPOINT(I)),0.25)
      GMATIX(I) = ANT(IX2,IY2)
   14 CONTINUE
C
      RETURN
      END
```

```
C
      SUBROUTINE COEF(ISIZE,SNTSR)
C
C*****************************************************************
C
C     TO SOLVE THE LINEAR EQUATION :  EMATIX * COEF = GMATIX.
C  COEF IS THE ESTIMATION COEFFICIENTS FOR GENERATING BRIGHTNESS TEMP-
C  ERATURES IN THE APC PROCESS.  EMATIX AND GMATIX ARE COMPUTED BY
C  SUBROUTINE SIGMA AND SUBROUTINE GAMMA.   SNTSR IS THE SQUARE OF THE
C  NOISE TO SIGNAL RATIO.   THE RESULTING COEFFICIENTS ARE STORED IN
C  GMATIX REPLACING THE GAMMA.
C
C*****************************************************************
C
      COMMON ANT(64,64), EMATIX(49,49), GMATIX(49),PSF(64,64)
      DIMENSION WKAREA(49)
C
      MSIZE = ISIZE*ISIZE
C
      DO 10 I=1,MSIZE
      EMATIX(I,I) = EMATIX(I,I) + SNTSR
   10 CONTINUE
C
      N = MSIZE
      M = 1
      IA = 49
      IDGT = 4
C
      CALL LEQT1F(EMATIX,M,N,IA,GMATIX,IDGT,WKAREA,IER)
C
      SUM=0.0
      DO 11 I=1,MSIZE
      SUM=SUM+GMATIX(I)
   11 CONTINUE
      SMALL=(1.0-SUM)/MSIZE
      DO 12 I=1,MSIZE
      GMATIX(I)=GMATIX(I)+SMALL
   12 CONTINUE
C
      RETURN
      END
```

ORIGINAL PAGE IS
OF POOR QUALITY

```
      SUBROUTINE ANTPSF (ISIZE)
C
C*****************************************************************
C
C     TO COMPUTE THE POINT SPREAD FUNCTION ASSOCIATED WITH A SPECIFIC
C  LINEAR COMBINATION OF THE ANTENNA POINT SPREAD FUNCTION ANT AT X.
C  WHERE PSF(X) = SUMMATION (M * ANT(X)).   M IS THE CORRECTION COEFFI-
C  CIENT MATRIX STORED IN GMATIX AND ANT IS THE ANTENNA PATTERN.   IN
C  OTHER WORDS, THE POINT SPREAD FUNCTION, PSF, IS OBTAINED BY APPLY-
C  ING A ISIZEXISIZE LOCAL OPERATOR TO EACH AND EVERY PIXEL OF THE
C  ANTENNA PATTERN.   THE LOCAL OPERATOR IS A LINEAR COMBINATION OPER-
C  ATOR WITH GIVEN COEFFICIENTS STORED AT GMATIX.   THE RESULTING PSF
C  IS STORED ON DISK PSF.DATA (I/O UNIT # 13.)
C
C*****************************************************************
C
      COMMON ANT(64,64),EMATIX(49,49),GMATIX(49),PSF(64,64)
      DIMENSION A(49)
C
      IDIFF=ISIZE/2
      IDIFF=IDIFF*4
      MSIZE=ISIZE*ISIZE
C
      DO 10 J=1,64
      JSTART=J-IDIFF
C
      DO 11 I=1,64
      ISTART=I-IDIFF
      JNDX=JSTART-4
      K=1
C
      DO 12 JJ=1,ISIZE
      JNDX=JNDX+4
      INDX=ISTART-4
C
      DO 13 II=1,ISIZE
      INDX=INDX+4
      IF(JNDX.LE.0.OR.JNDX.GT.64) GO TO 14
      IF(INDX.LE.0.OR.INDX.GT.64) GO TO 14
      A(K)=ANT(INDX,JNDX)
      GO TO 15
   14 A(K)=0.0
   15 K=K+1
C
   13 CONTINUE
   12 CONTINUE
C
      SUM=0.0
      DO 16 M=1,MSIZE
      SUM=SUM+GMATIX(M)*A(M)
   16 CONTINUE
      PSF(I,J)=SUM
C
C
C
C
   11 CONTINUE
   10 CONTINUE
C
      DO 21 J=1,64
      WRITE(13,20) (PSF(I,J),I=1,64)
   20 FORMAT(64E12.6)
   21 CONTINUE
C
      RETURN
      END
```

```
      SUBROUTINE DFT2D(M,N,FXY,FUVRL,FUVIM)
C
C*****************************************************************
C
C     TWO DIMENSIONAL DISCRETE FOURIER TRANSFORM.
C  FXY REPRESENTS AN M X N ARRAY OF INPUTS (REAL) ON A GRID OF M X N
C  POINTS. EACH NUMBER IN THE ARRAY REPRESENTING THE VALUE OF THE
C  FUNCTION AT THE CORRESPONDING SAMPLING POINT IN THE X-Y SPACE.
C  FUVRL, AN M X N OUTPUT MATRIX, IS THE REAL COMPONENT OF THE DISCRETE
C  FOURIER TRANSFORM OF FXY.   FUVIM CONTAINS THE IMAGINARY COMPONENTS
C  OF THE TRANSFORM.
C
C*****************************************************************
C
      DIMENSION FXY(M,N),FUVRL(M,N),FUVIM(M,N)
      DATA PI/3.14159265/
C
      MN=M*N
      ISTART=-M/2
      JSTART=-N/2
C
      DO 100 J=1,N
C
      V=FLOAT(JSTART+J)
      VN=V/FLOAT(N)
C
      DO 200 I=1,M
C
      U=FLOAT(ISTART+I)
      UM=U/FLOAT(M)
      SUMRL=0.0
      SUMIM=0.0
C
      DO 10 JJ=1,N
C
      Y=FLOAT(JJ-1)
      YVN=Y*VN
C
      DO 20 II=1,M
      X=FLOAT(II-1)
      THETA=2.*PI*(X*UM+YVN)
      SUMRL=SUMRL+FXY(II,JJ)*COS(THETA)
      SUMIM=SUMIM-FXY(II,JJ)*SIN(THETA)
C
   20 CONTINUE
   10 CONTINUE
C
      FUVRL(I,J)=SUMRL/MN
      FUVIM(I,J)=SUMIM/MN
C
  200 CONTINUE
  100 CONTINUE
C
      RETURN
      END
```

ORIGINAL PAGE IS
OF POOR QUALITY

```
      SUBROUTINE DFT2XY(FXY)
C
C*****************************************************************
C
C   (1) TO COMPUTE 2-D DISCRETE FOURIER TRANSFORM OF FXY(64,64) ALONG
C       THE U-AXIS AND THE V-AXIS CENTERED AT (0,0).
C   (2) TO COMPUTE THEIR MAGNITUDES AND DB VALUES.
C   (3) TO PRINT OUT THE RESULTS.
C
C*****************************************************************
C
      DIMENSION FXY(64,64),FUREAL(64),FUIMAG(64),FVREAL(64),FVIMAG(64),
     +          FUMAGN(64),FVMAGN(64),FUDB(64),FVDB(64)
      DATA PI/3.14159265/
C
C<<<<<<<<<<< DFT ALONG (U,V) = (U,0) >>>>>>>>>>>
C
      DO 200 I=32,64
      U=FLOAT(-32+I)
      UM=U/64.
      SUMRL=0.0
      SUMIM=0.0
C
      DO 10 JJ=1,64
C
      DO 20 II=1,64
      X=FLOAT(II-1)
      THETA=2.0*PI*(X*UM)
      SUMRL=SUMRL+FXY(II,JJ)*COS(THETA)
      SUMIM=SUMIM-FXY(II,JJ)*SIN(THETA)
C
   20 CONTINUE
   10 CONTINUE
C
      FUREAL(I)=SUMRL/16.
      FUIMAG(I)=SUMIM/16.
C
  200 CONTINUE
C
C<<<<<<<<<<<< DFT ALONG (U,V) = (0,V) >>>>>>>>>>>>
C
      DO 100 J=32,64
      V=FLOAT(-32+J)
      VN=V/64.
      SUMRL=0.0
      SUMIM=0.0
C
      DO 30 JJ=1,64
      Y=FLOAT(JJ-1)
      YVN=Y*VN
C
      DO 40 II=1,64
      THETA=2.0*PI*(YVN)
```

```
      SUMRL=SUMRL+FXY(II,JJ)*COS(THETA)
      SUMIM=SUMIM+FXY(II,JJ)*SIN(THETA)
C
   40 CONTINUE
   30 CONTINUE
C
      FVREAL(J)=SUMRL/16.
      FVIMAG(J)=SUMIM/16.
C
  100 CONTINUE
C
C<<<<<<<<<<<< COMPLTE MAGNITUDE AND DB >>>>>>>>>>>>
C
      DO 300 I=32,64
      FUMAGN(I)=SQRT(FUREAL(I)*FUREAL(I)+FUIMAG(I)*FUIMAG(I))
      FVMAGN(I)=SQRT(FVREAL(I)*FVREAL(I)+FVIMAG(I)*FVIMAG(I))
      FUDB(I)=20.0*ALOG10(FUMAGN(I))
      FVDB(I)=20.0*ALOG10(FVMAGN(I))
  300 CONTINUE
C
C<<<<<<<<<<<< PRINT OUT >>>>>>>>>>>>
C
      WRITE(6,43)
   43 FORMAT(/)

 18MAR81 11.28.22 - VOL=SCR0C0. DSN=YCKJE.FCLANC.FCPT

C
      WRITE(6,44)
   44 FORMAT(/,' THE U-AXIS (REAL) :',/)
      WRITE(6,45) (FUREAL(I),I=32,64)
   45 FORMAT(7(1X,E10.3))
      WRITE(6,56)
   56 FORMAT(/,' THE U-AXIS (IMAGINARY) :',/)
      WRITE(6,45) (FUIMAG(I),I=32,64)
      WRITE(6,48)
   48 FORMAT(/,' THE U-AXIS (MAGNITUDE) :',/)
      WRITE(6,45) (FUMAGN(I),I=32,64)
      WRITE(6,49)
   49 FORMAT(/,' THE U-AXIS ( DB ) :',/)
      WRITE(6,45) (FUDB(I),I=32,64)
C
      WRITE(6,46)
   46 FORMAT(/,' THE V-AXIS (REAL) :',/)
      WRITE(6,45) (FVREAL(I),I=32,64)
      WRITE(6,47)
   47 FORMAT(/,' THE V-AXIS (IMAGINARY) :',/)
      WRITE(6,45) (FVIMAG(I),I=32,64)
      WRITE(6,50)
   50 FORMAT(/,' THE V-AXIS (MAGNITUDE) :',/)
      WRITE(6,45) (FVMAGN(I),I=32,64)
      WRITE(6,51)
   51 FORMAT(/,' THE V-AXIS ( DB ) :',/)
      WRITE(6,45) (FVDB(I),I=32,64)
C
      RETURN
      END
```

```
C  PROGRAM NAME : PLOT FOURIER TRANSFORM  (PLOTFT)
C      TO COMPUTE DFT OF ANT, PSF (AT 3X3, 5X5, 7X7), ALL AT U=0, AND V=0
C
       DIMENSION ANT(64,64),PSF(64,64)
C
       DO 230 J=1,64
       READ(11,81) (ANT(I,J),I=1,64)
       READ(13,81) (PSF(I,J),I=1,64)
   81  FORMAT(6E12.6)
  230  CONTINUE
C
       WRITE(6,90)
   90  FORMAT(/,' ************ DFT OF ANTENNA ************',/)
       CALL DFT2XY(ANT)
C
       WRITE(6,91)
   91  FORMAT(/,' ********** DFT OF POINT SPREAD FUNCTION **********',/)
       CALL DFT2XY(PSF)
C
       STOP
       END
```

```
@ED
00010 C    PROGRAM NAME = FSCENE
00020 C    TO COMPUTE THE FOURIER TRANSFORM OF AN IMAGE USING SUBROUTINE
00030 C   DFT2D.   THE ORIGINAL IMAGE IS STORED AT SCENE.DATA WITH LUN=14.
00040 C   THE RESULTING REAL AND IMAGINARY PARTS ARE STORED AT FSCENER.DATA
00050 C   AND FSCENEI.DATA, WITH 15 & 16 AS THE LUN'S.
00060 C
00070 C*****************************************************************
00080 C
00090       INTEGER*2 IDUM(64,64)
00100       DIMENSION FXY(64,64),BUFFRL(64),BUFFIM(64)
00110 C
00120       M=64
00130       N=64
00140       LUN=14
00150       LUNRL=15
00160       LUNIM=16
00170       REWIND LUN
00180 C
00190       DO 10 J=1,N
00200       READ(LUN) (IDUM(I,J),I=1,M)
00210       DO 11 I=1,M
00220       FXY(I,J)=IDUM(I,J)
00230    11 CONTINUE
00240    10 CONTINUE
00250 C
00260       CALL DFT2D(M,N,FXY,LUNRL,LUNIM)
00270 C
00280       REWIND LUNRL
00290       REWIND LUNIM
00300 C
00310 C<<<<<<<<<< READ AND PRINT OUT >>>>>>>>>>
00320 C
00330       WRITE(6,113)
00340   113 FORMAT(' PRINT OUT IMAGE (YES=1)')
00350       READ(5,114) IPRINT
00360   114 FORMAT(I1)
00370       IF(IPRINT.NE.1) GO TO 100
00380 C
00390       A=1.0
00400       IE=0
00410 C
00420       DO 13 INDX=1,4
00430       IS=IE+1
00440       IE=IS+15
00450 C
00460       DO 14 J=1,64
00470       READ(LUNRL) (BUFFRL(I),I=1,64)
00480       READ(LUNIM) (BUFFIM(I),I=1,64)
00490 C
00500       DO 15 I=IS,IE
00510       BUFFRL(I)=(SQRT(BUFFRL(I)*BUFFRL(I)+BUFFIM(I)*BUFFIM(I)))*A
00520    15 CONTINUE
00530 C
00540       WRITE(6,112) (BUFFRL(I),I=IS,IE)
00550   112 FORMAT(16F5.2,1)
00560 C
00570    14 CONTINUE
00580       REWIND LUNRL
00590       REWIND LUNIM
00600       WRITE(6,123)
00610   123 FORMAT(///)
00620 C
00630    13 CONTINUE
00640 C
00650   100 STOP
00660       END
```